Studies of Thin Liquid Films Confined between Hydrophobic Surfaces

Zuoli Li

Dissertation submitted to the faculty of Virginia Polytechnic Institute and State University in partial fulfillment of the requirements for the degree of

Doctor of Philosophy

In

Mining Engineering

Roe-Hoan Yoon, Chair
Alan R. Esker
Gerald H. Luttrell
Richard D. Gandour
William Ducker

September 05, 2012
Blacksburg, Virginia

Keywords: surface force, hydrophobic force, extended DLVO, thermodynamic analysis, thin water film, thin liquid film

Studies of Thin Liquid Films Confined between Hydrophobic Surfaces

Zuoli Li

Abstract

Surface force measurements previously conducted with thiolated gold surfaces showed a decrease in excess film entropy (ΔS^f), suggesting that hydrophobic force originates from changes in the structure of the medium (water) confined between hydrophobic surfaces[1]. As a follow-up to the previous study, surface force measurements have been conducted using an atomic force microscope (AFM) with hydrophobic silica surfaces at temperatures in the range of 10 to 40°C. The silica sphere and silica plate were treated by both chemisorption of octadecyltrichlorosilane (OTS) and physical adsorption of octadecyltrimethylammonium chloride (C_{18}TACl). A thermodynamic analysis of the results show similar results for both of the samples, that both ΔS^f and excess film enthalpy (ΔH^f) become more negative with decreasing thickness of the water layer between the hydrophobic surfaces and decreasing temperature. $|\Delta H^f| > |T\Delta S^f|$ represents a necessary condition for the excess free energy change (ΔG^f) to be negative and the hydrophobic interaction to be attractive. Thus, the results obtained with both the silylated and C_{18}TACl-adosrbed silica surfaces in the present work and the thiolated gold suefaces reported before show hydrophobic forces originate from structural changes in the medium. Thermodynamic analysis of SFA force measurements obtained at various temperatures[2] revealed that ΔS^f were much more negative in the shorter hydrophobic force ranges than in the longer ranges, indicating a more significant degree of structuring in the water film when the two hydrophobic surfaces are closer together.

It is believed that the water molecules in the thin liquid films (TLFs) of water form clusters as a means to reduce their free energy when they cannot form *H*-bonds to neighboring hydrophobic surfaces. Dissolved gas molecules should enhance the stability of structured cluster due to the van der Waals force between the entrapped gas molecules and the surrounding water molecules[1], which may enhance the strength of the hydrophobic force. Weaker long-range attractive forces detected in degassed water than in air-equilibrated water was found in the present work by means of AFM force measurements, supporting the effect of dissolved gas on the structuring of water. At last, temperature effects on hydrophobic interactions measured in ethanol and the thermodynamic analysis revealed similar results as those found in water, indicating that the hydrophobic force originates from *H*-bond propagated structuring in the mediums.

References:

(1) Wang, J.; Yoon, R.-H.; Eriksson, J. C. *J. Colloid Interface Sci.* **2011**, *364*, 257.
(2) Tsao, Y. H.; Yang, S. X.; Evans, D. F.; Wennerstrom, H. *Langmuir* **1991**, *7*, 3154.

Acknowledgements

First and foremost, I would like to express my sincere gratitude to my respected advisor, Dr. Roe-Hoan Yoon, for his guidance, inspiration and continuous support throughout the course of this doctoral work.

In addition to my advisor, I would like to thank the remainder of my thesis committee: Dr. Gerald Luttrell, Dr. Alan Esker, Dr. Richard Gandour, Dr. William Ducker and Dr. John Walz for their encouragement, insightful comments and penetrating questions.

I am also deeply grateful to Dr. John Morris and Dr. Sean Corcoran for their generosity in allowing me to use their equipment.

Sincere appreciation is extended to Jialin Wang for training on AFM force measurements, as well as inspiration for aspects of this scientific research. I warmly thank Lei Pan for his generous help in repairing essential experimental equipment, and for the stimulating discussions about my research. I also wish to thank Juan Ma for her suggestions on my thesis, and Yafen Zhang who helped me on the characterization of sample by FTIR. This work couldn't have been done without their help.

I also acknowledge the many contributions from my fellow labmates and the staff at the CAST Center—both for their help and for all the fun we have had in the last four years—particularly Ruijia Wang, Jing Niu, Riddhika Jain, Gaurav Soni, Seungwoo Park, Chris Hull, Kathy Flint and Kirsten Titland.

Last but not least, I owe my loving thanks to my family for their encouragement and understanding.

Contents

List of Figures

List of Tables

CHAPTER 1

Introduction

1.1 General

The term "hydrophobic force" was used first by Blake and Kitchener[1] in 1972 to describe the metastability of the wetting films of water formed on the hydrophobic surfaces. These investigators found that thin liquid films (TLFs) of water breaks readily when contact angle is greater than zero despite the fact that both the disjoining pressures due to double-layer and van der Waals forces are repulsive. When an air bubble adheres on a hydrophobic surface with a finite contact angle of θ, the TLF must be broken (or rupture). According to the Frumkin-Derjaguin isotherm[2,3], it is necessary that the disjoining pressure in the TLF must be negative as suggested first by Laskowski and Kitchener[4] in 1969. In this regard, the credit should go to these two investigators for recognizing the presence of the hydrophobic force in wetting films. More recently, Derjaguin and Churaev[5] calculated the contact angles of quartz at different surface potentials using the Frumkin-Derjaguin isotherm. The results showed that the potential differences alone cannot create contact angles larger than 15-16°, and higher contact angles can only be obtained in the presence of negative disjoining pressure (or hydrophobic force)[5-7].

In 1982, Israelachvili and Pashley[8] conducted the first direct measurements of hydrophobic forces between two hydrophobic mica surfaces in surfactant solutions using the surface force apparatus (SFA) technique. They showed that the TLF ruptures at film thicknesses larger than predicted by the classical DLVO theory, which was attributed to the presence of hydrophobic force. The hydrophobic force decayed exponentially with the separation distance between the two hydrophobic surfaces with a decay length of approximately 1 nm. This exponential dependence correlates well with predictions calculated for solvation force[9]. Several follow-up investigations confirmed the presence of hydrophobic forces of even longer ranges by means of SFA[10] and atomic force microscope (AFM)[11-13]. The measured hydrophobic forces are often represented by a single exponential force law:[14,15]

$$\frac{F}{R} = -C \exp\left(-\frac{h}{D}\right) \qquad [1.1]$$

where h is the closest distance between two hydrophobic surfaces, fitting parameters C and D represent the magnitude and the decay length of the force, respectively. When the measured hydrophobic forces are longer range, a double exponential force law are frequently used,[16]

$$F / R = C_1 \exp(-h / D_1) + C_2 \exp(-h / D_2) \qquad [1.2]$$

where the fitting parameters C_1, and D_1 represent the short-range hydrophobic force, while C_2, and D_2 correspond to the long-range component of the hydrophobic force. Normally, D_1 is in the range of 1-2.8 nm at h < 10 nm, while D_2 in the range of 4.5-50 nm at longer separations[10,11,16].

It has also been shown that the measured hydrophobic forces can be represented by a power law[17,18],

$$F / R = K / 6h^2 \qquad [1.3]$$

where K represents the only fitting parameter. Eq. [1.3] is of the same form as the der Waals force.

Various theoretical models have been developed to explain the hydrophobic forces measured in experiment. In 1989, Eriksson *et al.*[19] developed a statistical thermodynamic model assuming that water becomes increasingly ordered with decreasing film thickness. This model attributed the hydrophobic attraction to the surface-induced structuring of water film. Wang *et al.*[20] determined the thermodynamic functions of the hydrophobic interactions by conducting surface force measurements at several different temperatures. The results showed that macroscopic hydrophobic interactions entail decreases in both the excess entropy (S^f) and the excess enthalpy (H^f) of the thin liquid films (TLF) of water confined between hydrophobic surfaces. Based on these results, it was suggested that macroscopic hydrophobic interactions may involve building structures of water in the vicinity of hydrophobic surfaces.

Other investigators proposed, on the other hand, that long-range attractive forces may be due to the electrostatic attraction between mobile charged[21-23] patches and unoccupied[24] domains on opposing surfaces. In yet other studies, researchers have provided evidence to support that hydrophobic force is due to pre-existing nanobubbles on the surface[25,26]. The "nanobubbles theory" is supported by three important observations: 1) the presence of discontinuities (or "steps") on force curves, 2) the disappearance of attractive forces once the medium has been degassed, and mostly notably, 3) the detection of nanobubbles on hydrophobic surfaces by means of AFM imaging. However, more recent reports have indicated the presence of long-range attraction even in degassed aqueous solutions[27,28]. Additionally, Wang and Yoon showed that previously-observed steps on force curves could be eliminated by adjusting experimental conditions and procedures[29].

Molecular dynamic (MD) simulations showed indeed that the structure of water in the vicinity of hydrophobic surfaces is different from that of the bulk. However, the water structuring is limited to only a few layers from the surface, while long-range hydrophobic forces have been measured at h as large as 80 nm. Eriksson *et al.*[19] attributed this discrepancy to the fact that *ab-initio* calculations are not sensitive enough to detect the changes in H-bonding energy in the range of 10^{-5}-10^{-3} kT that are responsible for the long-range attractions.

Most recently, Hammer *et al.*[30] showed that the hydrophobic forces measured to date can be classified into three classes. The short-range forces measured in the range of 10-20 nm to 100 nm can be linked to electrostatic attractions and/or bridging vapor cavities. The forces measured in the range of 1.5-15 nm are the "pure" attractive forces that can be attributed to the enhanced Hamaker constant, while the attractions measured below 1.5 nm can be ascribed to changes in the H-bonded water structure.

The objective of the present work is to better understand the mechanisms of the hydrophobic interaction at the macroscopic scale by experimentally determining the changes in entropy, enthalpy, and free energies. The results will be useful hopefully for studying the origin(s) of hydrophobic force.

1.2 Literature Review

1.2.1 Origins of Hydrophobic Force

a. Electrostatic Force

Miklavic[31] proposed a charged-patch model to describe the forces between heterogeneously charged surfaces. Specifically, he based his findings on the fact that the horizontal mobility of the charged patches would be a positive indicator of attractive force. Similarly, as Christenson stated in 1997[32], "Either a shift of the adsorption/desorption equilibrium on approach of two surfaces, or rearrangement or lateral diffusion of the surface groups is the condition for long-range attraction" (p. 67). Research has also shown that correlations between patches of charges[33] or dipoles[34] on hydrophobic surfaces generate long-

range attractive electrostatic force. One study noted that the forces of electrostatic origin are likely to decay exponentially, with a decay length equal to half the Debye screening length[34]. As a result, attractive force should be affected by added electrolytes of various types and concentrations. On the other hand, Zhang *et al*. showed that the lattice patch size back calculated from measured force[35] was much larger than those estimated from the aggregation numbers reported by Fan *et al.*[36], with the latter one close to the value obtained by means of the scanning tunneling microscopic (STM) imaging for the dodecanethiol coated gold surfaces. In other words, to obtain the strong attractive force as detected in the force measurements, the charged patch model[31] ask for patches of significantly greater size than those actually observed with self-assembled monolayers.

b. Nanobubbles

It has long been known that thin water films confined by two hydrophobic surfaces are metastable[37]. More recently, the existence of nano-scale, flat bubbles on very hydrophobic surfaces was described[25,38]. In response to these findings, some attributed the long-range attractive force or the large jump distance (5-75 nm)—which could not be explained by van der Waals forces[39]—to gas bridging between nanobubbles or cavities[40]. When long-range attractive forces have been attributed to cavities, they typically appear between surfaces with contact angles greater than 90°, since formation of a water-vapor cavity is thermodynamically favored only when the contact angle is greater than 90°[32]. For contact angles less than 90°, however, measurable attractive forces have been found to be short-range (1.3 nm)[40]. Another study linked force curves with discontinuities or steps to the presence of bridging nanobubbles[41]. Specifically, hydrophobic surfaces initiate the formation of bubbles. In contrast, smooth surfaces (either hydrophilic or hydrophobic) do not generate *in vitro* gas bubble formation. In other words, the surface roughness and heterogeneity of a hydrophobic surface are important factors affecting the formation of submicroscopic gas bubbles in water,[42] and in so doing impact attractive force.

c. Water Structure

Small, nonpolar solute molecules have been shown to prompt the formation of cage-like structures, or "clathrates," in water films[15]. Accordingly, hydrophobic interactions between solute molecules tend to be of much greater magnitude in comparison to van der Waals interactions[15]. In a concurrent study, Eriksson *et al.*[43] suggested that the long-range hydrophobic attraction between macroscopic hydrophobic surfaces represents a special type of solvation force that originates from the enhanced hydrogen bonding of the water molecules in the vicinity of a hydrophobic surface. Based on a square-gradient assumption, the authors used mean-field theory to account for the hydrophobic force and showed that solvation layers overlap as two solvated surfaces become in closer proximity. A subsequent study reported how the total energy of the system begins to change as a function of separation distance between two surfaces, thereby producing attractive force between the surfaces[44]. Unlike hydration repulsion that results from *H*-bond ordering—which typically extends to only about 10 layers of water molecules[45]—the range of the hydrophobic force of over 80 nm or more[35] is inconsistent with the region predicted by molecular dynamic simulations on the orientation of water molecules[46]. Most recently, Wang *et al.*[20] conducted a thermodynamic analysis of hydrophobic interactions. Utilizing AFM force measurement results conducted at various temperatures, the researchers were able to provide more detailed information on the structuring of water films, whose results can be extended to a range similar to that of experimentally-detected hydrophobic forces.

1.2.2 Various Types of Hydrophobic Surfaces

In their 2001 study, Christenson and Claesson[47] made a review on the direct measurements designed to determine the force between hydrophobic surfaces—with a particular emphasis on the type of preparation method. In general, the particular preparation method can give rise to specialized surface

features, as indicated by direct surface force measurements. For this study, four types of hydrophobic surfaces were investigated, as follows:

a. Xanthate Adsorbed on Gold and Silver

Although most ionic collectors utilized in the flotation of oxide and silicate minerals have alkyl chains longer than C_{12}, ethyl xanthate, with a chain length as short as $C_{2,}$ has been shown to be efficient for the flotation of sulfide minerals[48]. As such, the possible interactions between ethyl xanthate and sulfides or metals have been examined by many investigators[49-53]. As is well known, the adsorption of ethyl xanthate is controlled by a mixed potential mechanism[51,54], which includes two independent electrochemical processes: 1) the anodic oxidation of xanthate ion (X^-),

$$X^- \rightarrow X^2 + 2e \qquad [1.4]$$

and 2) the cathodic reduction of dissolved oxygen (O_2),

$$1/2O_2 + 2H^+ + 2e \rightarrow H_2O \qquad [1.5]$$

where X_2 is dixanthogen. The oxidation product can also be a metal xanthate (MX or MX_2). Both of X_2 and MX (or MX_2) are insoluble in water and considered hydrophobic; therefore, they remain on the surface and render the mineral hosting the electrochemical reactions hydrophobic. These two reactions are related through the potential that makes the oxidation and reduction occur at equal rates. Flotation conditions under various potentials can be monitored by controlling the potential of the external circuit in a deoxygenated solution[55] .

Xanthate adsorption in the bulk phase can normally be predicted using the Nernst equation, which neglects the thermodynamically more favorable surface process,

$$E_r = E^0 + \frac{RT}{nF}\ln\left[EX^-\right]^{-2} \qquad [1.6]$$

where E^0 is the standard potential of Reaction [1.4]. One obtains the reversible potential (E_r) of Reaction [1.4] from Eq. [1.6]. The surface process was not well understood until Woods[51] confirmed the chemisorption of ethyl xanthate on platinum more than 40 years ago. Woods and coworkers noted that chemisorption exists as a prewave before the appearance of a large peak starting from the position of reversible potential (E_r) as shown by voltammetry[56,57]. This so-called "under-potential deposition"[49] involves the formation of chemical bonds between xanthate radicals and metal atoms. By retaining the position of the metal atoms in a metal lattice, chemisorption is restricted to a single monolayer[58]. It has been experimentally verified that chemisorption occurs on copper[58-60], galena[61,62] and chalcocite[59,63,64]. Above E_r, the products of potassium ethyl xanthate (KEX) adsorption can be dixanthogen or metal xanthate.

Accordingly, knowledge of the hydrophobicity of each product is especially valuable for the application of KEX as a surfactant in flotation. The hydrophobicity of the chemisorption layer has been described by several researchers[56,62]. Studies have also confirmed that dixanthogen is a prerequisite for gold flotation[55]. However, controversy persists regarding the hydrophobicity of metal xanthate. Early in 1976, Poling recognized the hydrophobic nature of metal-xanthate precipitates[65]. Some 10 years later, metal xanthate was recognized as hydrophobic, which resulted in the selective hydrophobicity of the sulfide minerals[66]. In contrast, some studies claimed that the presence of silver ethyl xanthate did not alter the contact angles or the hydrophobicity of the surface[56,57]. Unlike the single monolayer chemisorption of

xanthate, the formation of a multilayer of metal xanthate species is due to the removal of metal atoms[58]. Spectroscopic studies showed that metal xanthates (MX_2) adsorb on the top of a monolayer of chemisorbed xanthate, forming multilayers. The reason for the attraction of hydrophobic metal xanthate[65,67] to the hydrocarbon tails of the chemisorbed xanthate is the hydrophobic interaction. Some researchers believe that the multilayer formation effectively increases the chain length of xanthates and hence increases the hydrophobicity[65], while others argue that multilayers of lead ethyl xanthate are not hydrophobic[51]. Nor do such multilayers result in good flotation for copper[52]. Given these differing viewpoints, a systematic study of the hydrophobicity of each product formed during the adsorption of xanthate on gold is especially useful.

In open circuit voltammetry testing, xanthates have been reported to chemisorb on sulfide minerals or noble metals in a manner similar to thiols[68]. Studies have also described how xanthate adsorbed on gold substrates from aqueous solution are coordinated to the surface through two sulfur atoms[69,70]. Reports confirm that the adsorption of short-chain alkyl xanthates (C_2-C_5) is electrochemical in nature and the resulting products are very stable under ambient conditions[68]. Conversely, adsorbed xanthate is sensitive to temperature due to the thermal decomposition of xanthate molecules.

b. Silylated Silica or Mica Surfaces

The silanation reaction described by Morrall and Leyden[71] is comprised of two steps. First, octadecyltrichlorosilane (OTS) molecules hydrolyze as follows:

$$RSiCl_3 + 3H_2O \rightarrow RSi(OH)_3 + 3HCl \qquad [1.7]$$

Second, the hydrolyzed OTS molecules may or may not polymerize in solution before adsorbing on silica surfaces via strong chemical bonds—and this is largely dependent on the amount of water in the solution. OTS-adsorbed silica surfaces prepared in a glove box at room temperature were characterized by means of contact angle measurements, AFM force measurements and FT-IR spectra[72]. In keeping with literature reports, the rapid adsorption of OTS started from patches[72], while a complete self-assembled OTS monolayer turned out to be homogeneous. The tridecafluoro-1,1,2,2,-tetrahydro-octyl-1-dimethylchlorosilane-coated monolayer was estimated to be 1.0 (+-0.5) nm thick by means of interferometry[73], which is in accordance with the extended length of the molecule. The thickness of the OTS monolayer (*i.e.*, 2.5 nm)[74,75] was close to the chain length of C_{18} as well.

Electrostatic origin faces some difficulty on explaining the measured force between silylated surfaces. The smooth and well-defined silylated mica surfaces suggested that the resulting smooth force curve was not due to any instability of the surfactant layer; therefore, these surfaces were considered to be ideal for studying the origin of surface forces[73]. As research has shown, even though an adsorbed monolayer of fluorocarbon silane decreases the Hamaker constant of the surface at low separation distance, there is not much difference between the surface potentials of bare and silylated mica[73]. The surface force measured between those fluorocarbon silane-coated mica surfaces featured an additional exponentially-decaying attraction with a decay length of 8 nm[73]. In 1994, Parker and Claesson[76] also confirmed the existence of a pure attractive force between fluorocarbon silane-treated mica surfaces, which was nearly uncharged at a pH of 2. The much larger decay length of 5.6 nm for the measured attraction in comparison to the electrostatic Debye length of 3 nm precluded the possibility of electrostatic origin.

Researchers have attributed the measured attractive force between silylated surfaces to the bridging of nanobubbles, depending either on the presence of steps or discontinuities on the force

curves[41,77,78], or on the sudden onset of attraction in the range of 20-200nm following an initial steep repulsion[79]. On the other hand, these reports did not agree on whether the bubbles existed at the onset, or whether they were generated after the initial contact of the two hydrophobic surfaces. In order to solve this disagreement, Ishida *et al*.[80] conducted a comparison of force measurement results between two types of prepared surfaces. The type-I surface was exposed to air to dry after silanation while the type-II surface was hydrophobized in an AFM liquid cell without exposure to air. The tapping mode image of the type-1 surface revealed bubble-like domains with a diameter of 650 nm and a height of 40 nm or less. In comparison, there were no such domains associated with the type-II surfaces. The authors concluded that nanosized bubbles existed at the outset and could not be eliminated by immersing the plate into water. Rabinovich and Derjaguin[81], however, measured the attractive force between silica filaments exposed to dimethyl dichlorosilane (DMDCS) vapor and found that bubble formation occurred only after the two surfaces came into contact with each other. This finding means that the long-range attractive force that was present prior to contact could be explained by structural changes in the water that were induced by the hydrophobic surfaces. Moreover, a good correlation between surface contact angle and the attractive force in the absence of discontinuities or steps on the force curves, as reported by Rabinovich *et al*.[11,82], seems to be unrelated to the bridging of nanobubbles as well.

Since the chemical heterogeneity of treated surfaces, as indicated by contact angle hysteresis, helps anchor gas bubbles[39], the relative roughness of prepared surfaces may account for the discrepancies in force measurement results among the different samples. Therefore, care must be taken when preparing high- quality monolayer adsorbed surfaces for force measurements.

c. Adsorption of Cationic Surfactant on Surfaces with Opposing Charges

The adsorption of surfactants to a surface with an opposite charge is widely used in industry. For example, the adsorption on chromium-containing leather waste[83], on layered double hydroxide (LDH)[84] or on alumina[85] all represent efficient ways to remove anionic surfactants from wastewater. Other industrial applications that utilize the self-assembly of ionic surfactants to solid surfaces include detergency[86], flotation[86,87] wetting and enhanced oil recovery[88-91].

Cationic alkylammonium ions adsorb to negatively charged mica[14] or silica[35] surfaces due to the electrostatic attraction between them. The first direct force measurement was reported in 1982 by Israelachvili and Pashley[14]. The authors used hexadecyltrimethylammonium bromide (CTAB) adsorbed mica surfaces to confirm that the hydrophobic interactions between these surfaces was not only in the same range as the van de Waals force, but actually an order of magnitude stronger. Moreover, the exponential dependence of the interactions had more common characteristics with solvation forces than with van der Waals forces. Follow-up studies[34,92,93] demonstrated that exponentially decaying is a common feature of the long-range attraction detected between alkylammonium adsorbed surfaces.

As indicated in the literature, surfaces treated by means of the Langmuir-Blodgett (LB) deposition technique normally display longer-range attraction (80-90 nm) in comparison to surfaces hydrophobized by *in-situ* adsorption from aqueous solution—with the latter method showing an equally strong attractive force by ensuring optimal adsorption on the surfaces[15]. Adsorption is regulated by altering the concentration of surfactants. Specifically, surface charge undergoes a decrease with increasing surfactant concentration until it reaches charge neutralization at a specific concentration (*i.e.*, point of charge neutralization or p.c.n.); beyond that point, a surface begins to recharge due to additional surfactants adsorbed. For the cetyltrimethylammonium bromide (CTAB) adsorbed mica surfaces, p.c.n. occurred at a concentration of about 3.3×10^{-6} M[94]. When additional surfactant is included, results have shown that it inversely adsorbs to the surface of silica and glass above p.c.n.[27]. In accordance with the adsorption of surfactant, attractive force initially increased as the concentration increased, however, after

a maximum value was reached, the force then began to decrease until a pure repulsive force was detected[95].

As reported by Attard[34], hydrophobic attraction decays exponentially with the decay length equal to half the Debye length, suggesting an electrostatic response to account for the hydrophobic interaction. However, numerous studies have shown that the measured attractive force is not sensitive to electrolytes[96], even at concentrations as high as 10^{-2} M[93]. Similarly, the bridging of nanobubbles and the creation of cavities are inconsistent with smooth force curves without visible discontinuities as measured between surfaces with a contact angle significantly lower than 90°[27]. As reported by Sakamoto *et al*., surface force measured in a solution of octadecyltrimethylammonium chloride (C_{18}TACl) changed with surfactant concentration and agreed well with surface contact angle measurements[95]. Correspondingly, the dependence of hydrophobic force on surface hydrophobicity has been shown to be related to surface-induced water structuring[92,93]. The fact that the decay length of hydrophobic force has been reported to decrease linearly with increasing concentrations of CH_2/CH_3 groups in the surfactant solution[35] is actually in accordance with Eriksson *et al.*, regarding the change of water ordering[43].

d. Chemisorption of Alkanethiol on Gold Surfaces

Studies have confirmed that alkanethiols chemisorbed on gold surfaces give rise to monolayers[97-99]. However, the kinetic mechanisms associated with this two-step adsorption process may be different for alkanethiols of differing chain lengths. In the first step, 80% and 50% coverage were obtained for longer-chain thiols (C_{12}, C_{16}) and shorter-chain one (C_6), respectively. The second step involves the slow rearrangement of the adsorbed thiols for the formation of a homogeneous monolayer[100]. Full coverage was obtained after 3 minutes or longer[101] from a concentration of 10^{-5} M. The thickness of the formed film increased with chain length (C_4, C_8 and C_{12}) from 0.8nm to 2.3 nm. As studies have shown, a monolayer of long-chain alkanethiols adsorbed on gold may be densely packed, crystalline, or liquid-crystalline[102,103], with the ordering of adsorbed thiols highly dependent on their chain length. The free energy (19 mJ/m^2) of a hydrophobic gold surface treated in this way is lower in comparison to an analogous surface treated with other kinds of hydrocarbons. Moreover, a thiol monolayer on gold is stable at room temperature; no desorption occurs until the monolayer adsorbed gold is heated to 80°C in hexadecane[97]. It should also be noted that the stability of long-chain thiols is typically higher than short-chain thiols[97]. However, this difference becomes negligible when the chain lengths are longer than C_{10}.

Ederth *et al.*[104] demonstrated that a hexadecanethiol film can be an excellent substrate for investigating the long-range interactions between hydrophobic surfaces due to its high stability. Specifically, the mobility of adsorbed patches can be avoided due to the strong covalent bonds formed involved in chemisorption. Thus, the observed attractive force with steps can be attributed to cavity formation rather than to electrostatic force. Another study has shown that attractive force with steps decreases with increasing ethanol concentrations up to 20%[105]. In fact, the attraction completely disappeared after adding ethanol to the water, which lowered the surface contact angle to less than 90°. Therefore, attractive force measured in water was attributed to the coalescence of bubbles. However, a more systematic study[106] of surface force measured in an ethanol/water mixture (from low to high mole fractions) found that even though attractive force decreased initially with an increase in ethanol concentration, passed through a broad minimum (around mole fractions in the range of 0.15-0.20), the attractive force began to increase when the mole fraction of the mixture was further increased. Moreover, despite the fact that the contact angle of the surface as measured via a sessile drop of pure ethanol was much lower than 90°, the attractive force measured in pure ethanol was comparable to that measured in pure water. It should also be noted that the steps that typically signify the presence of nanobubbles were also avoided by using a lower concentration and a shorter reaction time[20]. Wang *et al.*[20] also conducted force measurement studies between thiolated gold surfaces in water at various temperatures and found that attractive force decreases with increasing temperature, accompanied by a less negative change in

excess film entropy (ΔS^f)for the thin water films. This finding suggests that hydrophobic force may originate from the structuring of water induced by the hydrophobic surfaces.

1.2.3 Factors Affecting the Hydrophobic Force

a. Effect of Salt

A model proposed by Eriksson *et al.*[43] for the origin of long-range hydrophobic force states that long-range attraction is due to *H*-bond-induced ordering in water films, which is confined by two hydrophobic surfaces. The model predicts that increasing concentrations of non-adsorbing electrolytes decrease the decay length of the force, while increasing its magnitude. As reported by Claesson *et al.*[93], the presence of electrolytes are also believed to affect forces of electrostatic origin, while the negligible dependence of the force on salt at concentrations up to 10^{-2} M negated the possibility that the attractive force measured between LB-deposited mica surfaces was of electrostatic origin. Instead, the researchers offered the alternative that the dynamic reorganization of water molecules in the surrounding area of hydrophobic surfaces may be responsible. Moreover, the surface-induced orientation of water molecules was believed to propagate several nanometers away from the surface[93].

Attard[34] attributed the unusually strong long-range attraction between hydrophobic surfaces to an electrostatic response of water to the neighboring hydrophobic surfaces. Furthermore, this force is likely to be shielded by electrolytes in aqueous solution, which was confirmed by Tsao[107] who reported that long-range attractive force between ammonium-adsorbed mica surfaces decreased in the presence of electrolytes in water. Additionally, the screening effect was shown to be more significant for a 2:2 electrolyte/$MgSO_4$ solution in comparison to a 1:1 electrolyte/NaCl solution. A decrease in attractive force in a C_{18}TACl solution upon the addition of NaCl was then presented by Zhang *et al.*[27]. Nevertheless, the effect of electrolyte addition on hydrophobic interaction tends to be much weaker for more stable surfaces. In a related study, a minor decrease in attraction was detected between fluorocarbon silylated mica or LB-deposited mica surfaces in an aqueous solution containing 0.1 M electrolytes[108]. The presence of 1 M NaCl in the liquid medium failed to impact the attractive force between polypropylene surfaces[12].

As reported by Parker *et al.*, the magnitude of the attractive force between glass surfaces silylated by fluorocarbon silane was shown to undergo a somewhat minor increase with the addition of electrolytes[109]. The authors attributed the increase in force to the measurable increase in water surface tension due to the presence of electrolytes in concentrations greater than 1 M. In this regard, the lack of response of the hydrophobic attraction towards salt at lower concentrations was linked to nanobubble bridging[109]. It should be noted, however, that the electrolyte effect may not only be confined to aqueous solutions; it may also extend to surface hydrophobicity as measured by contact angle—despite the fact that Parker and coworkers did not observe any significant difference between the contact angles of silylated surfaces[109] measured by a drop of 5 M NaCl solution and those measured by a drop of pure water. In an earlier study, Christenson *et al.* reported that the contact angles of equally stable LB-deposited mica surfaces decreased with increasing electrolyte concentration[15]. They also correlated the effect of greater concentrations of electrolytes on contact angle by noting that the decrease in attractive force with increasing electrolyte concentration agreed well with the change in contact angle[15].

b. Chain Length of Surfactants

In 2002, Sakamoto *et al.*[95] conducted force measurement studies between silica surfaces in trimethylammonium chloride solution with six different chain lengths. Their results confirmed that the contact angle of the hydrophobic silica surfaces was found to increase when the surfactant chain length was increased. The values of the contact angles for C_8 and C_{18} were 35° and 80°, respectively. Attractive force also becomes stronger between surfaces adsorbed with longer chain length surfactants, which is

consistent with hydrophobic interactions between dialkyldimethylammonium surfactant-adsorbed surfaces[110] and with thiolated gold surfaces treated by alkanethiols[20]. Similarly, as described by Zhang and coworkers[35], the exponentially-decaying attractive force between hydrophobic silica surfaces immersed in C_nTACl solutions was shown to have an increasing decay length of from 3 to 32 nm as the chain length of the surfactants increased from 12 to 18. The authors concluded that the decay lengths were related to the inverse square root of the real CH_2/CH_3 concentration in solution[35], which supports the model for hydrophobic interactions that originate from water structuring[43]. Due to the fact that more monomers of short-chain surfactant is left in solution compared to the long-chain ones to obtain the same surface, furthermore, the structure of water is interrupted by any kind of foreign species added to water films—including surfactant monomers—as suggested by Eriksson *et al.*[43], it is reasonable that short-chain surfactants result in weaker hydrophobic interactions in comparison to long-chain ones.

c. Effect of Temperature

Baldwin *et al.* proposed a model to explain the effect of temperature on the hydrophobic interactions involved in protein folding[111]. The authors showed that hydrophobic interactions change from being entropy-driven at 22°C to being enthalpy-driven at 113°C. Some 20 years later, researchers conducted AFM surface force measurements between trichloro(1H, 1H, 2H, 2H-perfluorooctyl)silane self-assembled monolayer glass surfaces at temperatures ranging from 20 to 40°C[112]. They reported that the jump-in distance during the approach of the two surfaces decreased linearly with increasing temperature, which they attributed to a reduction in bubble size at elevated temperatures. In a similar study, force measurements between similarly prepared surfaces showed that the range of attractive force increased with increasing temperature[109]. This trend was attributed to an increase in bubble size due to the fact that the solubility of gas decreases at higher temperatures. It should be noted, however, that researchers do not agree on the dependence of the bubble size on temperatures. Therefore, it is controversial that the hydrophobic force is necessarily linked to bridging nanobubbles.

Dynamic simulations of water films confined between two thiolated gold surfaces have confirmed that even though the hydrophobicity-induced structural effects on water films do not extend very far, lowering the temperature can significantly enhance this effect[113]. In fact, a decrease in attractive force was reported by Tsao *et al.*[10] when the temperature was increased from 25°C to 50°C. Although this decrease corresponds to the enhanced structuring at lower temperatures, the author attributed the change in force to the nature of the surfactant. Wang *et al.*[20] measured AFM surface force between thiolated gold surfaces at different temperatures; their results showed a decrease in attractive force with increasing temperature. Thermodynamic analysis has shown that changes in temperature can affect a variety of indicators, such as change of excess film entropy (ΔS^f), change of excess film enthalpy (ΔH^f) and change of Gibbs free energy (ΔG^f) per unit area. For example, ΔS^f was found to be increasingly negative at low temperatures, demonstrating the more structured water film at low temperatures. The measured attractive force was therefore attributed to the structuring of water induced by hydrophobic surfaces.

d. Effect of Degassing

Direct degassing of a surfactant solution has been difficult to achieve due to the stabilization of bubbles with the presence of the surfactants[95]; in contrast, adding surfactant to frozen water in a vacuum has been found to be more effective. Long-range attractive force measured between silica surfaces in a C_{18}TACl solution was attributed to the presence of a gas bridge, since long-rang attraction disappeared in a completely air-free surfactant solution[95]. Systematic studies on the effect of degassing on the attraction between methylated surfaces and dehydroxylated surfaces has revealed a significant decrease in the jump-in distance, as reported by Mahnke *et al.*[39]. Hydrophobic interactions between polypropylene surfaces were also found to be shorter ranged in a degassed NaCl solution than in an untreated NaCl solution[12]. Conversely, a model on structured water in the form of clathrates proposed by Wang *et al.*[20] indicated that

the decrease of hydrophobic force in degassed water may due to other mechanisms. These investigators proposed that dissolved gas molecules may enhance the stability of the clathrate structures due to the van der Waals effect between them and the neighboring water molecules, thereby increasing the hydrophobic force. While most studies have indicated a negative effect on measured attractive force as a result of degassing the liquid medium, Zhang *et al.*[27] described an even stronger attractive force in a degassed surfactant solution of a specific concentration. The authors attributed the increase to a change in pH rather than to the presence of adsorbed bubbles.

1.3 Research Objectives

In summary, although the existence of long-range hydrophobic forces has been widely described and accepted, researchers remain at odds as to their origin. No single explanation has been able to reconcile the differing reports—in part because the origin of long-range hydrophobic force has been elusive due to inconsistent force measurement results between different types of hydrophobic surfaces. The present work, therefore, correlates surface force measurement between four types of hydrophobic surfaces: 1) xanthate-coated gold surfaces, 2) silylated silica surfaces, 3) cationic surfactant in-situ adsorbed silica surfaces, and 4) thiolated gold surfaces. The properties of the measured force were investigated under various conditions (electrolytes added to water, temperature, degassing of water, *etc.*), and the resulting changes in measured force are described in order to analyze the origin of the hydrophobic force. The objectives of the present work were as follows:

1. *To adjust the adsorption of KEX on gold and silver under controlled electrochemical potentials*. The results of our force measurement assays were consistent with contact angle and voltammetry experiments, indicating that the long-range attractions were, indeed, hydrophobic force in nature.

2. *To conduct AFM surface force measurements between gold surfaces treated with xanthate, which is a commonly-used collector in flotation of sulfide minerals and precious metals.* The kinetics of the adsorption of xanthate on gold was studied by varying the concentration and chain length of the surfactant and the immersion time. Force measurement results in the presence of salt provided important information that elucidated the origin of the hydrophobic interactions.

3. *To undertake force measurement experiments between very stable OTS-coated silica surfaces at a temperature range of 10 to 40°C and conduct a thermodynamic analysis of the resulting hydrophobic interactions.* The long-range attractive forces with absence of visible steps on the force curves were found to be related to the contact angles of the surfaces. When stronger force results were obtained at lower temperatures, they were accompanied by a more negative ΔS^f, indicating more structured water films under otherwise identical experimental conditions.

4. *To carry out a follow-up study on the effect of temperature on hydrophobic force between less stable surfaces such as silica surfaces with in-situ adsorption of C_{18}TACl.* Our results showed that attractive force remained very stable at the same temperature and under long immersion times. The decrease in attraction with increasing temperature corresponds to results obtained for the OTS-coated silica surfaces. A thermodynamic analysis of the hydrophobic interaction data from Tsao *et al.*[10] revealed that ΔS^f was significantly more negative at the short-range in comparison to the long-range . These results support the supposition that the structuring of water serves as the origin of hydrophobic force.

5. *To ascertain the effect of degassing on the hydrophobic force between thiolated gold surfaces and the effect of dissolved gas on the hydrophobic force between KEX-coated gold surfaces*. The existing form of dissolved gas in structured water films was discussed.

6. *To determine the effect of temperature on surface force between thiolated gold surfaces in ethanol*. Observed changes in force with temperature changes were found to be the same in ethanol and in water. The thermodynamic properties associated with hydrophobic interactions in ethanol were found to be similar to those in water, suggesting that the structuring of liquid is due to the *H*-bonds present in *H*-bonding liquids.

1.4 References

(1) Blake, T. D.; Kitchener, J. A. *J. Chem. Soc., Faraday Trans. 1* **1972**, *68*, 1435.
(2) Derjaguin, B. V. *Zh. Fiz. Khim.* **1940**, *14*, 137.
(3) Frumkin, A. *Zh. Fiz. Khim.* **1938**, *12*, 337.
(4) Laskowski, J.; Kitchener, J. A. *J. Colloid Interface Sci.* **1969**, *29*, 670.
(5) Derjaguin, B. V.; Churaev, N. V. *Langmuir* **1987**, *3*, 607.
(6) Churaev, N. V.; Derjaguin, B. V. *J. Colloid Interface Sci.* **1985**, *103*, 542.
(7) Churaev, N. V. *J. Colloid Interface Sci.* **1995**, *172*, 479.
(8) Israelachvili, J.; Pashley, R. *Nature* **1982**, *300*, 341.
(9) Marcelja, S.; Mitchell, D. J.; Ninham, B. W.; Sculley, M. J. *J. Chem. Soc., Faraday Trans. 2* **1977**, *73*, 630.
(10) Tsao, Y. H.; Yang, S. X.; Evans, D. F.; Wennerstrom, H. *Langmuir* **1991**, *7*, 3154.
(11) Rabinovich, Y. I.; Yoon, R. H. *Langmuir* **1994**, *10*, 1903.
(12) Meagher, L.; Craig, V. S. J. *Langmuir* **1994**, *10*, 2736.
(13) Wang, J. L.; Yoon, R. H. *Langmuir* **2008**, *24*, 7889.
(14) Israelachvili, J.; Pashley, R. *Nature* **1982**, *300*, 341.
(15) Christenson, H. K.; Claesson, P. M.; Berg, J.; Herder, P. C. *J. Phys. Chem.* **1989**, *93*, 1472.
(16) Claesson, P. M.; Blom, C. E.; Herder, P. C.; Ninham, B. W. *J. Colloid Interface Sci.* **1986**, *114*, 234.
(17) Yoon, R.-H.; Flinn, D. H.; Rabinovich, Y. I. *J. Colloid Interface Sci.* **1997**, *185*, 363.
(18) Ohnishi, S.; Yaminsky, V. V.; Christenson, H. K. *Langmuir* **2000**, *16*, 8360.
(19) Eriksson, J. C.; Ljunggren, S.; Claesson, P. M. *J. Chem. Soc., Faraday Trans. 2* **1989**, *85*, 163.
(20) Wang, J.; Yoon, R.-H.; Eriksson, J. C. *J. Colloid Interface Sci.* **2011**, *364*, 257.
(21) Meyer, E. E.; Lin, Q.; Hassenkam, T.; Oroudjev, E.; Israelachvili, J. N. *Proc. Natl. Acad. Sci. U. S. A.* **2005**, *102*, 6839.
(22) Tsao, Y.; Evans, D.; Wennerstrom, H. *Science* **1993**, *262*, 547.
(23) Miklavic, S. J.; Chan, D. Y. C.; White, L. R.; Healy, T. W. *J. Phys. Chem.* **1994**, *98*, 9022.
(24) Pazhianur, R.; Yoon, R. H. *Miner. Metall. Process.* **2003**, *20*, 178.
(25) Tyrrell, J. W. G.; Attard, P. *Phys. Rev. Lett.* **2001**, *87*, 176104.
(26) Ishida, N.; Inoue, T.; Miyahara, M.; Higashitani, K. *Langmuir* **2000**, *16*, 6377.
(27) Zhang, J. H.; Yoon, R. H.; Mao, M.; Ducker, W. A. *Langmuir* **2005**, *21*, 5831.
(28) Meyer, E. E.; Lin, Q.; Israelachvili, J. N. *Langmuir* **2004**, *21*, 256.
(29) Wang, J.; Yoon, R.-H. *Langmuir* **2008**, *24*, 7889.
(30) Hammer, M. U.; Anderson, T. H.; Chaimovich, A.; Shell, M. S.; Israelachvili, J. *Faraday Discuss.* **2010**, *146*, 299.
(31) Miklavic, S. J.; Chan, D. Y. C.; White, L. R.; Healy, T. W. *J. Phys. Chem.* **1994**, *98*, 9022.
(32) Christenson, H. K.; Yaminsky, V. V. *Colloid Surf., A* **1997**, *130*, 67.
(33) Podgornik, R. *J. Chem. Phys.* **1989**, *91*, 5840.
(34) Attard, P. *J. Phys. Chem.* **1989**, *93*, 6441.
(35) Zhang, J. H.; Yoon, R. H.; Eriksson, J. C. *Colloid Surf., A* **2007**, *300*, 335.
(36) Fan, A.; Somasundaran, P.; Turro, N. J. *Langmuir* **1997**, *13*, 506.

(37) Yushchenko, V. S.; Yaminsky, V. V.; Shchukin, E. D. *J. Colloid Interface Sci.* **1983**, *96*, 307.
(38) Yang, J.; Duan, J.; Fornasiero, D.; Ralston, J. *The Journal of Physical Chemistry B* **2003**, *107*, 6139.
(39) Mahnke, J.; Stearnes, J.; Hayes, R. A.; Fornasiero, D.; Ralston, J. *Phys. Chem. Chem. Phys.* **1999**, *1*, 2793.
(40) Yoon, R. H.; Ravishankar, S. A. *J. Colloid Interface Sci.* **1996**, *179*, 391.
(41) Ishida, N.; Kinoshita, N.; Miyahara, M.; Higashitani, K. *J. Colloid Interface Sci.* **1999**, *216*, 387.
(42) Ryan, W. L.; Hemmingsen, E. A. *J. Colloid Interface Sci.* **1993**, *157*, 312.
(43) Eriksson, J. C.; Ljunggren, S.; Claesson, P. M. *J. Chem. Soc., Faraday Trans. II* **1989**, *85*, 163.
(44) Horn, R. G. *J. Am. Ceram. Soc.* **1990**, *73*, 1117.
(45) Marčelja, S.; Radić, N. *Chem. Phys. Lett.* **1976**, *42*, 129.
(46) Lee, C. Y.; Mccammon, J. A.; Rossky, P. J. *J. Chem. Phys.* **1984**, *80*, 4448.
(47) Christenson, H. K.; Claesson, P. M. *Adv. Colloid Interface Sci.* **2001**, *91*, 391.
(48) Hamilton, I. C.; Woods, R. *Int. J. Miner. Process.* **1986**, *17*, 113.
(49) Woods, R.; Hope, G. A.; Brown, G. M. *Colloid Surf., A* **1998**, *137*, 329.
(50) Buckley, A. N.; Parks, T. J.; Vassallo, A. M.; Woods, R. *Int. J. Miner. Process.* **1997**, *51*, 303.
(51) Woods, R. *J. Phys. Chem.* **1971**, *75*, 354.
(52) Mielczarski, J. *J. Colloid Interface Sci.* **1987**, *120*, 201.
(53) Woods, R.; Hope, G. A.; Brown, G. M. *Colloid Surf., A* **1998**, *137*, 339.
(54) Salamy, S.; Nixon, J. *Aust. J. Chem.* **1954**, *7*, 146.
(55) Gardner, J.; Woods, R. *Aust. J. Chem.* **1974**, *27*, 2139.
(56) Woods, R.; Basilio, C. I.; Kim, D. S.; Yoon, R. H. *Colloids Surf., A* **1994**, *83*, 1.
(57) Woods, R.; Basilio, C. I.; Kim, D. S.; Yoon, R. H. *J. Electroanal. Chem.* **1992**, *328*, 179.
(58) Woods, R.; Basilio, C. I.; Kim, D. S.; Yoon, R. H. *Int. J. Miner. Process.* **1994**, *42*, 215.
(59) Woods, R.; Young, C. A.; Yoon, R. H. *Int. J. Miner. Process.* **1990**, *30*, 17.
(60) Bozkurt, V.; Xu, Z.; Brienne, S. H. R.; Butler, I. S.; Finch, J. A. *J. Electroanal. Chem.* **1999**, *475*, 124.
(61) Buckley, A. N.; Woods, R. *Colloids Surf.* **1991**, *53*, 33.
(62) Gardner, J. R.; Woods, R. *Aust. J. Chem.* **1977**, *30*, 981.
(63) Leppinen, J. O.; Basilio, C. I.; Yoon, R. H. *Int. J. Miner. Process.* **1989**, *26*, 259.
(64) Pihlajamäki, S. V.; Kankare, J. J. *Journal of Electroanalytical Chemistry and Interfacial Electrochemistry* **1984**, *170*, 213.
(65) Leja, J. *Surface Chemistry of Froth Flotation*; Plenum: New York, 1982.
(66) Mielczarski, J. A. *J. Phys. Chem.* **1993**, *97*, 2649.
(67) Walker, G. W.; Walters, C. P.; Richardson, P. E. *Int. J. Miner. Process.* **1986**, *18*, 119.
(68) Tzhayik, O.; Sawant, P.; Efrima, S.; Kovalev, E.; Klug, J. T. *Langmuir* **2002**, *18*, 3364.
(69) Persson, N.; Uvdal, K.; Liedberg, B.; Hellsten, M.; Sjöblom, J., Lindman, B., Stenius, P., Eds.; Springer Berlin / Heidelberg: 1992; Vol. 88, p 100.
(70) Ihs, A.; Uvdal, K.; Liedberg, B. *Langmuir* **1993**, *9*, 733.
(71) Morrall, S. W.; Leyden, D. E. In *Silanes, Surfaces, and Interfaces*; Leyden, D. E., Ed.; Gordon and Breach: New York, 1985, p 501.
(72) Flinn, D. H.; Guzonas, D. A.; Yoon, R. H. *Colloid Surf., A* **1994**, *87*, 163.
(73) Parker, J. L.; Cho, D. L.; Claesson, P. M. *J. Phys. Chem.* **1989**, *93*, 6121.
(74) Mao, M.; Zhang, J. H.; Yoon, R. H.; Ducker, W. A. *Langmuir* **2004**, *20*, 4310.
(75) Tillman, N.; Ulman, A.; Schildkraut, J. S.; Penner, T. L. *J. Am. Chem. Soc.* **1988**, *110*, 6136.
(76) Parker, J. L.; Claesson, P. M. *Langmuir* **1994**, *10*, 635.
(77) Nguyen, A. V.; Nalaskowski, J.; Miller, J. D.; Butt, H. J. *Int. J. Miner. Process.* **2003**, *72*, 215.
(78) Nalaskowski, J.; Veeramasuneni, S.; Hupka, J.; Miller, J. D. *J. Adhes. Sci. Technol.* **1999**, *13*, 1519.
(79) Carambassis, A.; Jonker, L. C.; Attard, P.; Rutland, M. W. *Phys. Rev. Lett.* **1998**, *80*, 5357.
(80) Ishida, N.; Sakamoto, M.; Miyahara, M.; Higashitani, K. *Langmuir* **2000**, *16*, 5681.

(81) Rabinovich, Y. I.; Derjaguin, B. V. *Colloids Surf.* **1988**, *30*, 243.
(82) Yoon, R. H.; Flinn, D. H.; Rabinovich, Y. I. *J. Colloid Interface Sci.* **1997**, *185*, 363.
(83) Zhang, M. N.; Liao, X. P.; Shi, B. *J. Soc. Leather Technol. Chem.* **2006**, *90*, 1.
(84) Pavan, P. C.; Crepaldi, E. L.; Valim, J. B. *J. Colloid Interface Sci.* **2000**, *229*, 346.
(85) Vanjara, A. K.; Dixit, S. G. *Langmuir* **1995**, *11*, 2504.
(86) Paria, S.; Khilar, K. C. *Adv. Colloid Interface Sci.* **2004**, *110*, 75.
(87) Scamehorn, J. F. H. *Surfactants in Chemical/Process Engineering* New York, 1988.
(88) Standnes, D. C.; Austad, T. *Colloid Surf., A* **2003**, *216*, 243.
(89) Aoudia, M.; Al-Maamari, R. S.; Nabipour, M.; Al-Bemani, A. S.; Ayatollahi, S. *Energy Fuels* **2010**, *24*, 3655.
(90) Wu, Y. F.; Shuler, P. J.; Blanco, M.; Tang, Y. C.; Goddard, W. A. *Spe J* **2008**, *13*, 26.
(91) Ziegler, V. M.; Handy, L. L. *Soc Petrol Eng J* **1981**, *21*, 218.
(92) Pashley, R. M.; Mcguiggan, P. M.; Ninham, B. W.; Evans, D. F. *Science* **1985**, *229*, 1088.
(93) Claesson, P. M.; Blom, C. E.; Herder, P. C.; Ninham, B. W. *J. Colloid Interface Sci.* **1986**, *114*, 234.
(94) Kékicheff, P.; Christenson, H. K.; Ninham, B. W. *Colloids Surf.* **1989**, *40*, 31.
(95) Sakamoto, M.; Kanda, Y.; Miyahara, M.; Higashitani, K. *Langmuir* **2002**, *18*, 5713.
(96) Israelachvili, J. N.; Pashley, R. M. *J. Colloid Interface Sci.* **1984**, *98*, 500.
(97) Bain, C. D.; Troughton, E. B.; Tao, Y. T.; Evall, J.; Whitesides, G. M.; Nuzzo, R. G. *J. Am. Chem. Soc.* **1989**, *111*, 321.
(98) Evans, S. D.; Urankar, E.; Ulman, A.; Ferris, N. *J. Am. Chem. Soc.* **1991**, *113*, 4121.
(99) Nuzzo, R. G.; Dubois, L. H.; Allara, D. L. *J. Am. Chem. Soc.* **1990**, *112*, 558.
(100) DeBono, R. F.; Loucks, G. D.; DellaManna, D.; Krull, U. J. *Canadian Journal of Chemistry-Revue Canadienne De Chimie* **1996**, *74*, 677.
(101) Tamada, K.; Hara, M.; Sasabe, H.; Knoll, W. *Langmuir* **1997**, *13*, 1558.
(102) Porter, M. D.; Bright, T. B.; Allara, D. L.; Chidsey, C. E. D. *J. Am. Chem. Soc.* **1987**, *109*, 3559.
(103) Strong, L.; Whitesides, G. M. *Langmuir* **1988**, *4*, 546.
(104) Ederth, T.; Claesson, P.; Liedberg, B. *Langmuir* **1998**, *14*, 4782.
(105) Ederth, T. *J. Phys. Chem. B* **2000**, *104*, 9704.
(106) Wang, J.; Li, Z.; Yoon, R.-H.; Eriksson, J. C. *J. Colloid Interface Sci.* **2012**, *379*, 114.
(107) Tsao, Y. H.; Evans, D. F.; Wennerstrom, H. *Langmuir* **1993**, *9*, 779.
(108) Christenson, H. K.; Fang, J. F.; Ninham, B. W.; Parker, J. L. *J. Phys. Chem.* **1990**, *94*, 8004.
(109) Parker, J. L.; Claesson, P. M.; Attard, P. *J. Phys. Chem.* **1994**, *98*, 8468.
(110) Tsao, Y. H.; Evans, D. F.; Wennerstrom, H. *Science* **1993**, *262*, 547.
(111) Baldwin, R. L. *Proc. Natl. Acad. Sci. U. S. A.* **1986**, *83*, 8069.
(112) Thormann, E.; Simonsen, A. C.; Hansen, P. L.; Mouritsen, O. G. *ACS Nano* **2008**, *2*, 1817.
(113) Layfield, J. P.; Troya, D. *J. Phys. Chem. B* **2011**, *115*, 4662.

CHAPTER 2

AFM Force Measurements between Gold and Silver Surfaces Treated in Ethyl Xanthate Solutions: *Effect of Applied Potentials*

2.1 Abstract

Many investigators measured surface forces between hydrophobic macroscopic surfaces using atomic force microscope (AFM). Some investigators observed long-range attractions and attributed them to the presence of hydrophobic forces, while others suggested that they are artifacts of the nano-bubbles and cavities associated with the hydrophobic surfaces. Still others suggested that the long-range attractions are due to the electrostatic interactions between charged patches present on opposing surfaces and hence are unrelated to surface hydrophobicity. In the present work, we have measured long-range attractions between gold- (or silver-) coated surfaces hydrophobized in potassium ethyl xanthate (KEX) solutions at pH 9.2 under controlled potential conditions. The results of our AFM force measurements are consistent with those of the contact angle and voltammetry experiments, indicating that the long-range attractions are hydrophobic forces.

2.2 Introduction

Flotation is the most widely used method of separating minerals from one another. Of the various parameters affecting the process, particle hydrophobicity is most important and xanthate has been the most commonly used hydrophobizing agent for conducting minerals such as sulfide and precious metals. The mechanism by which xanthate renders a mineral hydrophobic is controlled by a pair of electrochemical reactions, involving oxidation of the xanthate ion (X^-),

$$X^- \rightarrow X_2 + 2e \qquad [2.1]$$

and the reduction of dissolved oxygen (O_2),

$$1/2O_2 + 2H^+ + 2e \rightarrow H_2O \qquad [2.2]$$

where X_2 is dixanthogen. The oxidation product can also be a metal xanthate (MX or MX_2). Both X_2 and MX (or MX_2) are insoluble in water and considered hydrophobic; therefore, they remain on the surface and render the mineral hosting the electrochemical reactions hydrophobic. The potential at which a xanthate is oxidized varies from one mineral to another and varies with collector concentration, pH, and dissolved species, all of which providing means to achieve selective flotation.

Thermodynamically, xanthate adsorption should occur only at potentials above the reversible potential (E_r) for xanthate oxidation (or adsorption). However, Woods *et al.*[1,2] showed that xanthate adsorption can occur at potentials considerably below thermodynamic potentials – a phenomenon known as under-potential deposition or "chemisorption". The term chemisorption was introduced to indicate that at potentials below a thermodynamic potential, xanthate adsorbs on the surface, while at higher potentials chemical compounds such as X_2, MX and/or MX_2 are formed. Formation of the latter can be predicted from the thermodynamic data available for bulk reactions. However, the surface reactions are more difficult to predict due to the lack of appropriate thermodynamic data.

Spectroscopic studies showed that metal xanthates (MX_2) adsorb on the top of a monolayer of chemisorbed xanthate, forming multilayers. It has been shown that metal xanthates are hydrophobic[3-5]; therefore, they can be attracted to the hydrocarbon tails of the chemisorbed xanthate *via* hydrophobic interaction and form multi-layers. The multilayer formation effectively increases the chain length of xanthate and hence increases the hydrophobicity. It has been shown that the hydrophobicity of a metal xanthate varies depending on the electronegativity difference between sulfur and metal. Thus, the hydrophobic character of metal xanthates decreases in the order of $Hg_2X_2 > Cu_2X_2 > PbX_2 > ZnX_2$. According to this theory, dixanthogen should be more hydrophobic than metal xanthates, because the electronegativity difference between two sulfurs is zero. It may be of interest to note here that adding a metal xanthate precipitate to a flotation system often reduces mineral recovery[6].

In the present work, we have studied the mechanisms involved in the adsorption of potassium ethyl xanthate (KEX) on gold and silver at different potentials by monitoring the currents due to xanthate adsorption, water contact angles, and the hydrophobic forces acting between xanthate-coated surfaces. The hydrophobic forces measured using the atomic force microscope (AFM) may be useful for better understanding the mechanisms of xanthate adsorption particularly with regards to the role of the chemisorption mechanism in hydrophobizing gold and silver. Many investigators showed evidences for the chemisorption of xanthate on gold[7-9] and silver[10-12]. The results may also be useful for better understanding the origin of the long-range attractions observed between hydrophobic surfaces.

2.3 Experimental

2.3.1 Materials

For AFM surface force measurements, glass plates and spheres (Duke Scientific) were coated with gold and silver from vapor phase using the Electron Beam Physical Vapor Deposition (EBPVD) system (PVD-250). The coated plates were also used for electrochemical studies and contact angle measurements. Prior to the vapor deposition, the substrates were cleaned in Piranha solution (H_2O_2/H_2SO_4, 3:7 by volume) for 30 min at 120 °C, rinsed with pure water, and dried in an ultrapure N_2 gas stream. The cleaned glass substrates were coated first with a thin layer of chromium (~2 nm thickness) to enhance the adhesion between the substrate and the precious metals. The EBPDV unit allowed control of coating thicknesses to ~20 nm. The glass spheres were coated with gold (or silver) after the spheres had been glued onto AFM cantilevers with the Epon resin 1004F. The spring constants of the diving-board-shaped cantilevers (Nano world Innovative Technologies) were determined using the thermal tuning program provided with the multi-mode Nanoscope-V AFM.

Potassium ethyl xanthate (KEX, >90%, TCI America) was recrystallized twice from acetone (HPLC grade, Fisher Scientific, Inc.) using diethyl ether (>99.9%, Sigma-Aldrich, Inc.). Sodium tetraborate decahydrate (Sigma-Aldrich) was used as supporting electrolyte. All solutions were prepared freshly using the Millipore pure water with a conductivity of 18.2 MΩ·cm at 25°C.

2.3.2 Voltammetry

A three-electrode electrochemical cell was used for voltammetry experiment using gold- or silver-deposited glass plates as working electrode, a platinum mesh (10 × 20 mm) as counter electrode, and a calomel electrode as reference electrode. A potentiostat (Model 273A, EG&G Princeton Applied Research) was used to control electrode potentials. The potentials were reported versus standard hydrogen electrode. All of the measurements were conducted in a deoxygenated pH 9.2 buffer solution (0.05 M $Na_2B_4O_7$) under nitrogen atmosphere. The working electrode was cleaned electrochemically by ten rounds of potential sweeps between -600 and 1100 mV for gold and -500 mV and 600 mV for silver in borate solutions.

2.3.3 Contact Angle Measurement

Contact angle measurements were carried out at different potentials using the captive bubble technique. Electrode potentials were controlled using the three electrode system. In each measurement, a gold- or silver-coated glass plate was held initially at a reducing potential (-700 mV) for 2 min in a 0.05 M borate solution containing 10^{-3} M KEX and then stepped up to a desired potential. After 2 minutes of conditioning time, contact angles were measured using a goniometer. With a gold- or silver-coated electrode placed facedown, an N_2 bubble was brought to the surface from below. At a given potential, 3 to 4 measurements were conducted and averaged.

2.3.4 AFM Force Measurement

AFM force measurements were conducted in the same manner as described previously[13]. In each measurement, a pair of gold- or silver-coated glass sphere and plate was hydrophobized in a 10^{-3} M KEX borate solution at a given potential. The two macroscopic surfaces were treated under identical conditions, so that both have the same hydrophobicity (or contact angle). This was accomplished by gluing the cantilever with a sphere on the corner of a plate using a relatively weak glue (Norland Optical Adhesive 74, Norland Products, Inc.) and subjecting the sphere and plate assembly for gold (or silver) coating in the EBPVD system and for xanthate adsorption in the electrochemical cell. Since the cantilever with a sphere

was placed at a corner of the plate, the middle part of the plate was open for unhindered coatings of gold (or silver) and xanthate. After the xanthate adsorption, the sphere and plate assembly was removed from the electrochemical cell; and the sphere and plate were detached from each other by means of a clean pair of tweezers and used for AFM force measurement.

2.4 Result and Discussion

2.4.1 Gold

Figure 2.1 shows the voltammograms of the gold coated plate obtained in 0.05 M borate solutions (pH 9.2) with and without 10^{-3} M KEX. In the absence of KEX, gold was stable until potential was raised above ~600 mV, where oxide layers began to form. On the cathodic scan, three reduction peaks are shown, indicating more than one type of oxides were formed during the anodic scan. The contact angle measured after repeated potential sweeps[14] and cathodic polarization was 15°, which was close to the value reported (~10°)[15].

The voltammogram obtained in the presence of 10^{-3} M KEX was similar to those reported by others[5,16]. The anodic peak observed at 450 mV was due to the following reaction,

$$2EX^{-} \rightarrow (EX)_2 + 2e \qquad [2.3]$$

representing oxidation of ethyl xanthate to ethyl dixanthogen. The reversible potential (E_r) of Reaction [2.3] at 10^{-3} M KEX can be obtained using the Nernst equation,

$$E_r = E^o + \frac{RT}{nF}\ln\left[EX^{-}\right]^{-2} \qquad [2.4]$$

where E^o is the standard potential of Reaction [2.3]. From the value of E^o = -60mV[17], one obtains E_r = 117 mV at 10^{-3} M KEX and 298 K. The large cathodic peak observed at -450 mV is due to the reverse of Reaction [2.3][18]. Note that the reduction of dixanthogen involves a significant over potential. Although not shown in this communication, the FTIR spectra of the gold plate conditioned in 10^{-3} M KEX solutions showed characteristic absorption peaks for dixanthogen.

Figure 2.2 shows the AFM surface force measurements conducted using the gold-coated glass plate and sphere that had been hydrophobized in 10^{-3} M KEX solutions at different electrode potentials. As has already been noted, the two macroscopic surfaces were treated under identical conditions during gold coating, potential control, and xanthate adsorption. After the hydrophobization at a given potential, the sphere and plate were transferred quickly to the AFM liquid cell with minimal exposure to the atmosphere to minimize the possible loss of dixanthogen coating *via* evaporation. The measurements were conducted in pure water. It is unlikely that dixanthogen would desorb significantly in pure water, because its solubility is very low in water (1.14×10^{-5} M)[2]. It appears also that desorption of dixanthogen require a considerable over potential as shown in Figure 2.1.

As shown, the measured forces were substantially stronger and longer-ranged than the van der Waals force. The dashed line representing the van der Waals force was drawn using the value of the Hamaker constant ($A_{131} = 1.2\times10^{-20}$ J) for the interaction between gold in water (Wang and Yoon, 2008). Note also that the hydrophobic force increased with increasing potential and then decreased. The lowest potential at which an attractive force (hydrophobic force) considerably larger than the van der Waals force was 0 mV, which was substantially below the reversible potential (E_r = 117 mV) for dixanthogen formation (Eq. [2.3]). That gold-coated surface becomes hydrophobic at potentials below E_r indicates

under-potential deposition or *chemisorption* of ethyl xanthate. The hydrophobic force increased further until the potential was increased to 450 mV. At higher potentials (500 and 700 mV), the hydrophobic force decreased substantially. It appeared that at such high potentials the gold substrate was oxidized inhibiting further adsorption. In fact, the current *vs*. potential curves obtained in the absence and presence of xanthate was about the same at potentials above approximately 700 mV as shown in Figure 2.1. The solid lines of Figure 2.2 represent the experimental data fitted to the single exponential hydrophobic force law,

$$\frac{F}{R} = C \exp\left(-\frac{H}{D}\right) \qquad [2.5]$$

where F is the hydrophobic force, R the radius of the sphere, H the closest separation distance between the sphere and plate, and C and D are fitting parameters. The value of C represents the magnitude of the hydrophobic force at $H = 0$ and D shows how fast the force decays with H. Thus, D is the decay length of the hydrophobic force. The values of C and D obtained from the curve fitting exercise have been plotted *vs*. applied potentials in Figure 2.3. These results are similar to those reported previously[19] for the covellite-KEX system.

Also shown in Figure 2.3 are the contact angles (θ) measured in a 10^{-3} M KEX solution at different potentials. The changes in θ with potential agree well with those of C and D obtained from the AFM force measurements. The contact angle remained at 15^{o} and then increased sharply at 0 mV, reaching a maximum at 400 mV where the current density reached a maximum as shown in the voltammogram (Figure 2.1). As the potential was further increased, θ began to decrease most likely due to the oxidation of the gold substrate. The excellent agreement between the results obtained from the contact angle and surface force measurements provides strong evidence that the long-range attractions measured in the AFM force measurements are related to surface hydrophobicity.

Note here that the contact angles increased sharply at potentials close to 0 mV, which is below the reversible potential (E_r = 117 mV) for the oxidation of xanthate to dixanthogen. This finding can be attributed to chemisorption (or under potential deposition) of xanthate, which is known to occur at potentials below the thermodynamic potential. It has been shown that the chemisorption of ethyl xanthate begins to occur approximately 150 mV below the reversible potential[20], which has also been found to be the case in the present work. Thus, the dixanthogen formed by anodic oxidation (Eq. [2.3]) would adsorb on the top of the chemisorbed xanthate *via* hydrophobic interaction.

2.4.2 Silver

Figure 2.4 shows the voltammograms of a silver electrode immersed in 0.05 M borate solutions (pH 9.2) with and without 10^{-3} M KEX. In the absence of xanthate, anodic current began to flow at approximately 600 mV which is close to the potential range for silver oxide formation as shown by E_h-pH diagram[20]. In the presence of xanthate, a strong anodic current peak was observed beginning at about -100 mV due to xanthate adsorption. This potential is close to the potential for the formation of silver xanthate *via* the following reaction,

$$Ag^{0} + EX^{-} \rightarrow AgEX + e \qquad [2.6]$$

Using the Nernst equation, one can calculate the reversible potential (E_r) for this reaction to be -105 mV at 10^{-3} M KEX from the standard potential (E^{o} = -282mV) reported by Leppinen *et al.*[8]. Note also

that the voltammogram shows a small anodic peak which begins at -350 mV. It suggested that this peak represents the chemisorption of xanthate on silver[21].

Figure 2.5 shows the AFM force curves obtained for the interaction between the silver- coated glass sphere and plate. Both surfaces were hydrophobized simultaneously in a 0.05 M borate solution (pH 9.2) in the presence of 10^{-3} M KEX at different potentials. As was the case with the gold-coated surfaces, the forces measured in pure water were stronger than the van der Waals force. The dashed curve representing the van der Waals force was drawn using $A_{131} = 2\times10^{-20}$ J[22]. As shown, the hydrophobic force increased with increasing potentials, reaching a maximum at 50 mV, where the anodic current due to xanthate adsorption reached a maximum (see Figure 2.4). As the potential was increased further to 100 and 200 mV, the hydrophobic force decreased considerably. However, the hydrophobic force remained substantial at 200 mV.

The decrease in hydrophobic force above 50 mV may be attributed to the adsorption of silver ethyl xanthate (AgEX) in multi-layers. This interpretation is similar to what has been reported previously for the gold-xanthate system, in which multi-layer formation was shown to cause a decrease in hydrophobic force[23]. The silver xanthate adsorption in multi-layer would decrease the hydrophobicity due to the exposure of the polar head to the aqueous phase. This interpretation differs from the view that the metal xanthates in multi-layers effectively increase the chain lengths of short-chain xanthates and hence increase the hydrophobicity[3,23,24]

The surface force data obtained in the present work have been fitted to the single exponential force law (Eq. [2.5]), and the *C* and *D* parameters plotted in Figure 2.6. Also shown in the figure are the contact angles measured on the silver-coated glass plate hydrophobized in 10^{-3} M KEX solutions at different potentials. The contact angle and surface force data are in good agreement. As shown, both the contact angle and the surface forces increase at potentials above -400 mV, indicating that the anodic current observed beginning at -350 mV is due to xanthate adsorption. This finding is consistent with the observation reported by Woods *et al.*[12,20] that chemisorption of ethyl xanthate begins at -350 mV. However, the FTIR spectra obtained by Woods *et al.*[20] did not show the presence of chemisorbed xanthate at potentials below -150 mV. On the other hand, Leppinen *et al.*[8] observed absorption band at ~1200 cm^{-1} below -200 mV, indicating the presence chemisorbed xanthate on silver.

Note here that the *C* and *D vs.* potential curves given in Figure 2.6 show slope changes at potentials approximately -100 mV, which is close to the reversible potential (E_r = -105 mV) for AgEX formation. It is possible that at potentials below the reversible potential a monolayer of AgEX is formed possibly with a more or less flat orientation due to low surface coverage. At potentials above the E_r, more of the silver ions are liberated to form AgEX and form close-packed monolayers, resulting in high contact angles and stronger hydrophobic forces with large values of *C* and *D* as shown in Figure 2.6. Note also that the hydrophobic force observed at -300 mV was rather weak indicating possibly due to the low adsorption density and flat orientation. At potentials above 50 mV, a multi-layer of AgEX may be formed causing both the contact angle and hydrophobic force to decrease.

In Figure 2.7, the *C* and *D* parameters are plotted versus contact angles (θ). As sown, there are reasonable correlations between the two different parameters representing surface hydrophobicity. It appears that the force parameters may be uniquely defined by the contact angle regardless the process of xanthate films formed and the nature of the substrate. On the other hand, the xanthate films formed on gold tend to give a little stronger hydrophobic force than those formed on silver. The correlation between hydrophobic force and contact angle has also been shown previously[25-28].

It has been shown in the present work that ethyl xanthate chemisorbs on both gold and silver. On silver, the chemisorption occurs at a potential as low as -350 mv, which is 245 mV lower than the

reversible potential (E_r = -105 mV) for AgEX formation. On gold, the chemisorption occurs at a potential slightly below 0 mV, which is ~150 mV below the reversible potential (E_r = 117 mV) for dixanthogen ($(EX)_2$) formation. It is surprising that a short-chain xanthate such as ethyl xanthate chemisorbs at all on gold, which is one of the most inert materials known to humans. A significance of this finding is that chemisorbed xanthate may be the reason that dixanthogen – an oily substance – can stay on the surface. The oily substance formed *via* a simple electrochemical oxidation mechanism (Eq. [2.3]) adsorbs on the gold substrate *via* molecular-scale hydrophobic interaction and further increases the hydrophobicity and hydrophobic force.

2.5 Summary and Conclusion

An atomic force microscope (AFM) was used to measure the surface forces between gold-coated glass plate and sphere hydrophobized in 10^{-3} M KEX solutions at pH 9.2. The results showed that long-range attractions stronger than the van der Waals attraction are present in the thin liquid films between two hydrophobic surfaces. In general, the long-range attractions increased with increasing potential above the reversible potential (E_r = 117 mV) for dixanthogen formation. At potentials above 450 mV, the hydrophobic force decreased possibly due to the oxidation of gold substrate. In general, there was an excellent agreement between the contact angle and surface force data, indicating that the long-range attractions were hydrophobic forces. It was found also that the contact angles of gold began to increase sharply at potentials above approximately 0 mV, indicating chemisorption of xanthate.

The AFM force measurements were also between silver-coated surfaces hydrophobized in 10^{-3} M KEX solutions at pH 9.2. It was found that both hydrophobic forces and contact angles increased sharply at potentials above the reversible potential (E_r = -105 mV) for the formation of silver ethyl xanthate (AgEX). It was found, however, that significant hydrophobic forces and contact angles were also observed below the reversible potential, indicating chemisorption of xanthate. On the other hand, the hydrophobic forces were considerably weaker than those measured at potentials above the reversible potential, possibly due to the low surface coverage and/or flat orientation.

The results obtained in the present work showed clearly that the long-range attractions measured between xanthate-coated surfaces are closely related to the surface hydrophobicity. This finding suggests that the long-range attractions are due to hydrophobic interactions.

2.6 References

(1) Woods, R.; Basilio, C. I.; Kim, D. S.; Yoon, R. H. *Int. J. Miner. Process.* **1994**, *42*, 215.
(2) Woods, R.; Kim, D. S.; Basilio, C. I.; Yoon, R. H. *Colloid Surf., A* **1995**, *94*, 67.
(3) Leja, J. *Surface Chemistry of Froth Flotation*; Plenum: New York, 1982.
(4) Walker, G. W.; Walters, C. P.; Richardson, P. E. *Int. J. Miner. Process.* **1986**, *18*, 119.
(5) Woods, R. *J. Phys. Chem.* **1971**, *75*, 354.
(6) Leja, J. *Surface Chemistry of Froth Flotation*; Plenum: New York, 1982.
(7) Ihs, A.; Uvdal, K.; Liedberg, B. *Langmuir* **1993**, *9*, 733.
(8) Leppinen, J. O.; Yoon, R. H.; Mielczarski, J. A. *Colloids Surf.* **1991**, *61*, 189.
(9) Woods, R.; Hope, G. A.; Brown, G. M. *Colloid Surf., A* **1998**, *137*, 339.
(10) Buckley, A. N.; Woods, R. *Colloids Surf., A* **1995**, *104*, 295.
(11) Woods, R.; Hope, G. A.; Brown, G. M. *Colloid Surf., A* **1998**, *137*, 329.
(12) Woods, R.; Basilio, C. I.; Kim, D. S.; Yoon, R. H. *Colloids Surf., A* **1994**, *83*, 1.
(13) Wang, J. L.; Yoon, R. H. *Langmuir* **2008**, *24*, 7889.
(14) Fischer, L. M.; Tenje, M.; Heiskanen, A. R.; Masuda, N.; Castillo, J.; Bentien, A.; Emneus, J.; Jakobsen, M. H.; Boisen, A. *Microelectron. Eng.* **2009**, *86*, 1282.
(15) Gardner, J.; Woods, R. *Aust. J. Chem.* **1974**, *27*, 2139.

(16) Talonen, P.; Rastas, J.; Leppinen, J. *Surf. Interface Anal.* **1991**, *17*, 669.
(17) Pritzker, M. D.; Yoon, R. H. *Int. J. Miner. Process.* **1984**, *12*, 95.
(18) Talonen, P.; Sundholm, G.; Floate, S.; Nichols, R. J. *Phys. Chem. Chem. Phys.* **1999**, *1*, 3661.
(19) Yoon, R.; Pazhianur, R. *Colloid Surf., A* **1998**, *144*, 59.
(20) Woods, R.; Basilio, C. I.; Kim, D. S.; Yoon, R. H. *J. Electroanal. Chem.* **1992**, *328*, 179.
(21) Jeffrey, M.; Woods, R. *J. Electrochem. Soc.* **2001**, *148*, E79.
(22) Dagastine, R. R.; Grieser, F. *Langmuir* **2004**, *20*, 6742.
(23) Wang, J.; Yoon, R.-H. *ECS Trans.* **2010**, *28*, 3.
(24) Poling, G. W.; American Institute of Mining, Metallurgical, and Petroleum Engineers, Inc.: New York, 1976; Vol. 1, p 334.
(25) Rabinovich, Y. I.; Yoon, R. H. *Langmuir* **1994**, *10*, 1903.
(26) Yoon, R. H.; Ravishankar, S. A. *J. Colloid Interface Sci.* **1996**, *179*, 403.
(27) Yoon, R. H.; Flinn, D. H.; Rabinovich, Y. I. *J. Colloid Interface Sci.* **1997**, *185*, 363.
(28) Eriksson, J. C.; Yoon, R. H. In *Froth Flotation - A Century of Innovation*; Fuerstenau, M. C., Jameson, G., Yoon, R. H., Eds.; Society for Mining, Metallurgy, and Exploration, Inc.: Littleton, CO, 2007, p 133.

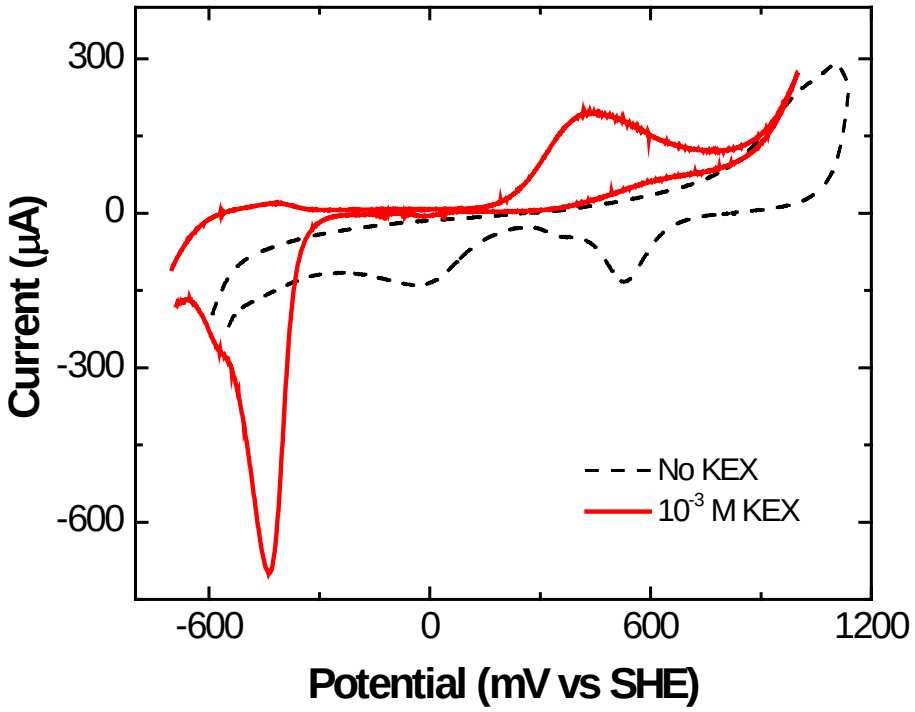

Figure 2.1 Voltammograms of gold in 0.05 M $Na_2B_4O_7$ (pH 9.2) solution with and without 10^{-3} M KEX. Sweep rate was 50 mVs^{-1}.

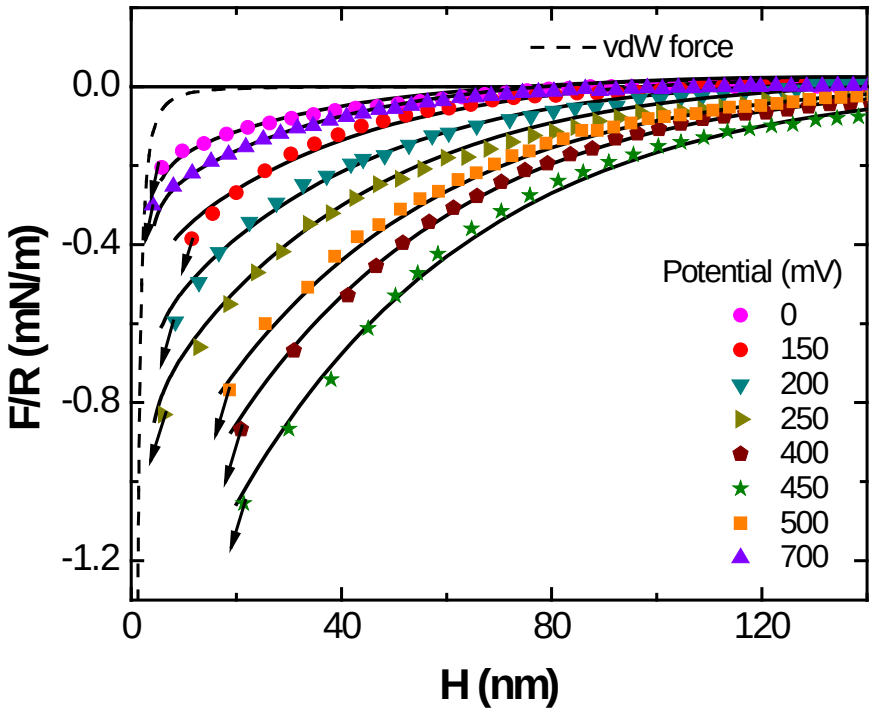

Figure 2.2 Force curves obtained in pure water between gold-coated glass surfaces treated in 10^{-3} M KEX solutions for 2 minutes at different potentials. The solid line represents the experimental data fitted to the single-exponential force law (Eq. [2.5]). The dashed line represents van der Waals force for the gold-water-gold system with Hamaker constant value of 1.2×10^{-20} J.

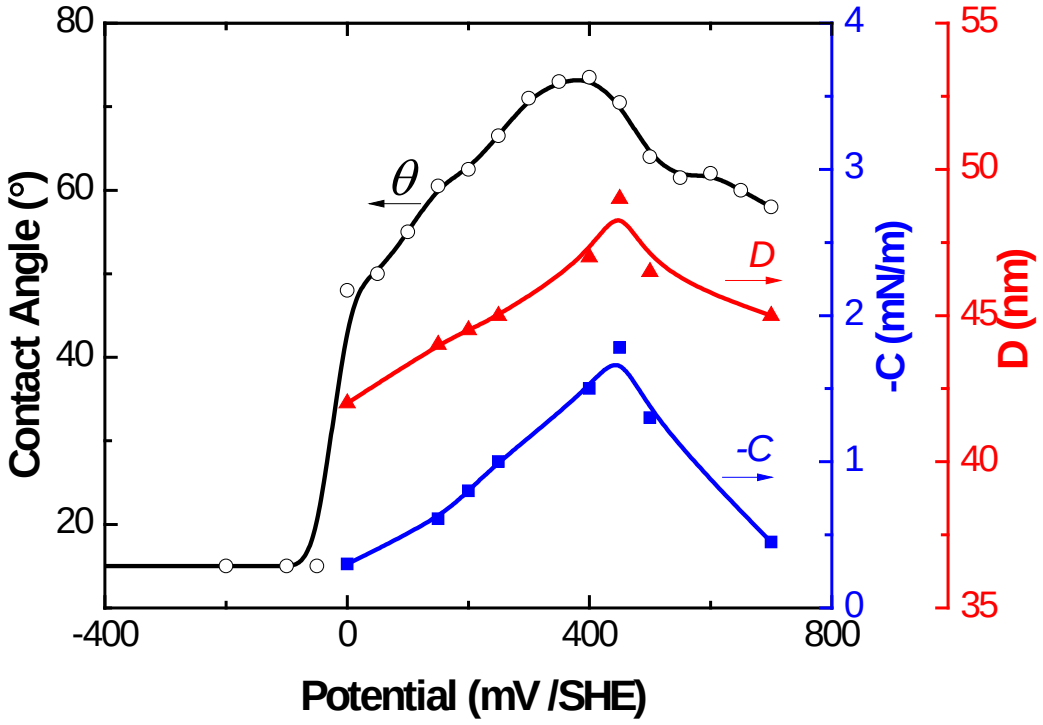

Figure 2.3 Effects of applied potentials on the contact angles and the *C* and *D* constants of the hydrophobic force law (Eq. [2.5]). The measurements were conducted with gold-coated surfaces treated in 10^{-3} M KEX solutions for 2 minutes.

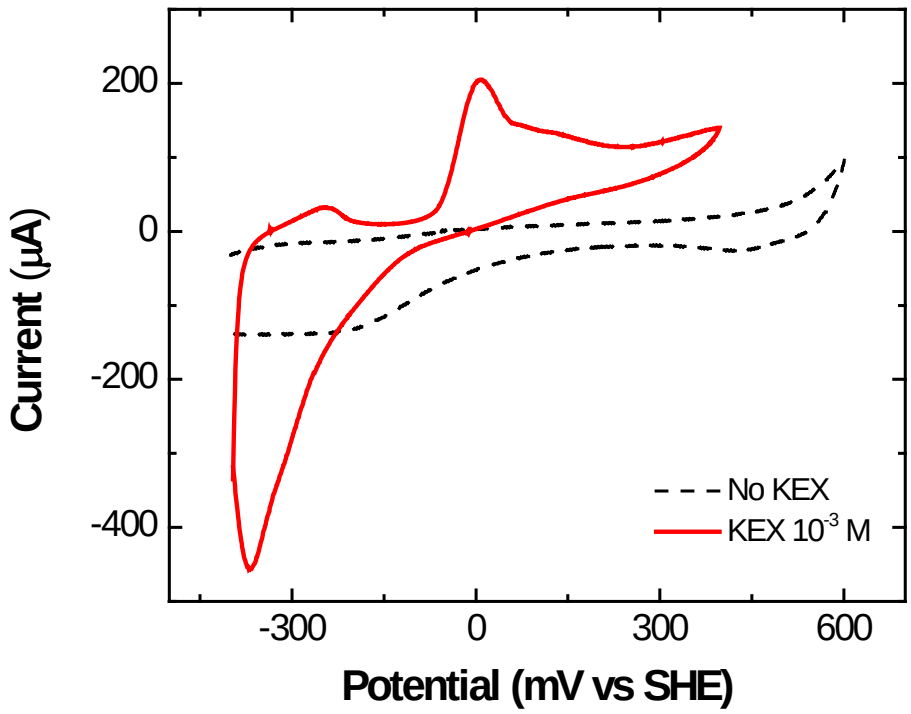

Figure 2.4 Voltammograms obtained with the silver-coated glass plate in the presence and absence of 10^{-3} M KEX at pH 9.2 at a sweep rate of 50 mV s^{-1}.

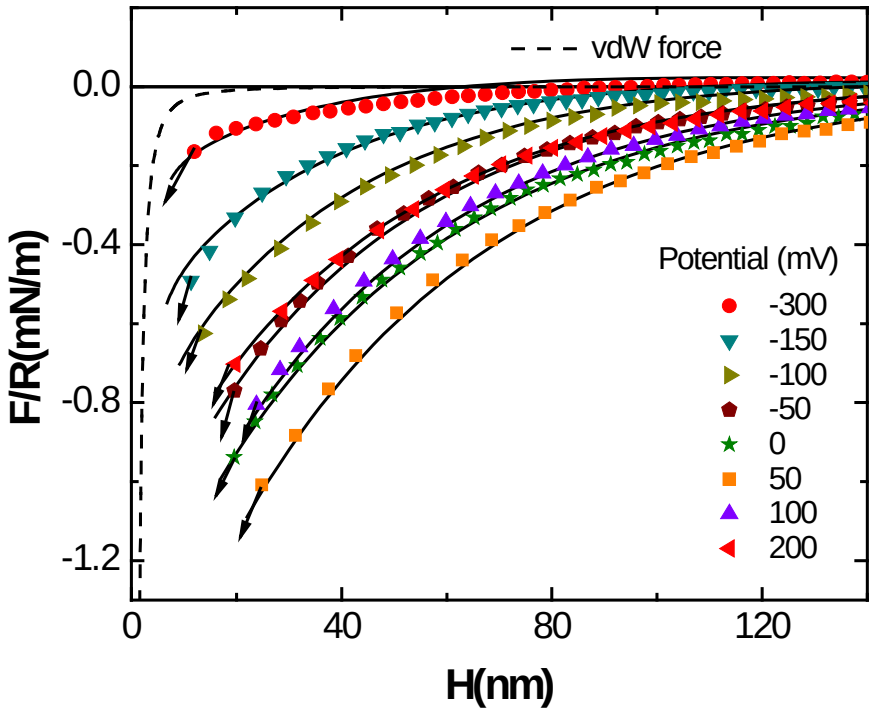

Figure 2.5 Forces curves obtained between silver-coated surfaces treated in 10^{-3} M KEX solutions at different potentials. The solid line represents the experimental data fitted to Eq. [2.5]. The dashed line represents van der Waals force for silver-water-silver system with Hamaker constant value of 2×10^{-20} J.

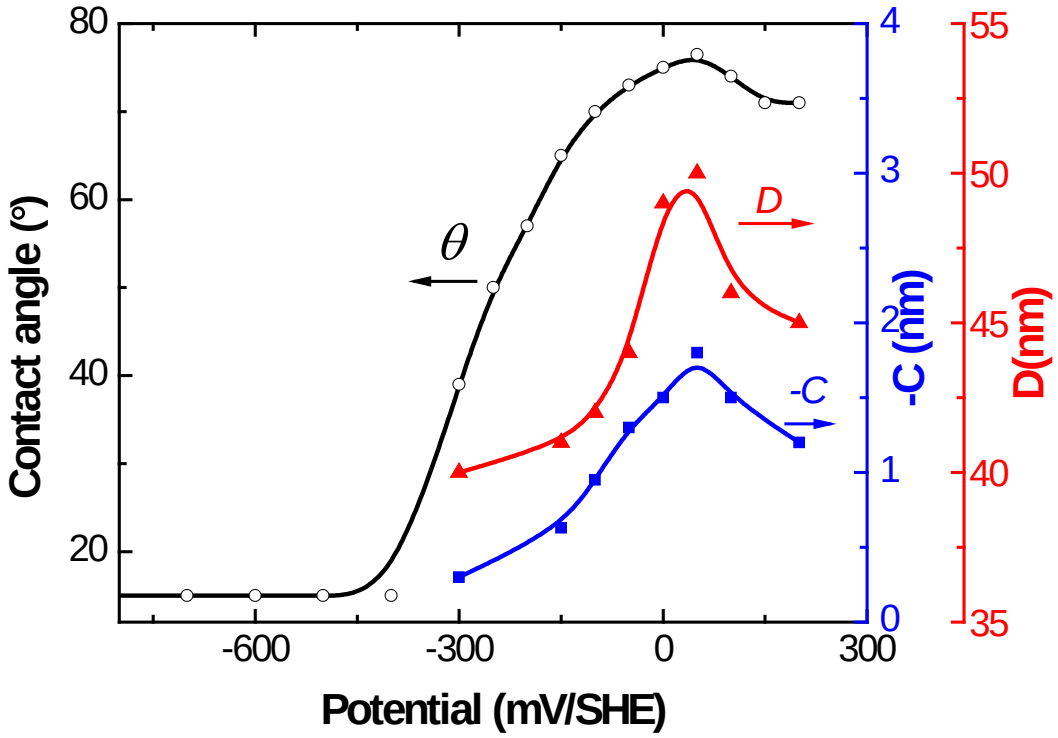

Figure 2.6 Effects of applied potentials on the contact angles (θ) and the hydrophobic force constants (C and D) measured with silver-coated surfaces treated in 10^{-3} M KEX solutions.

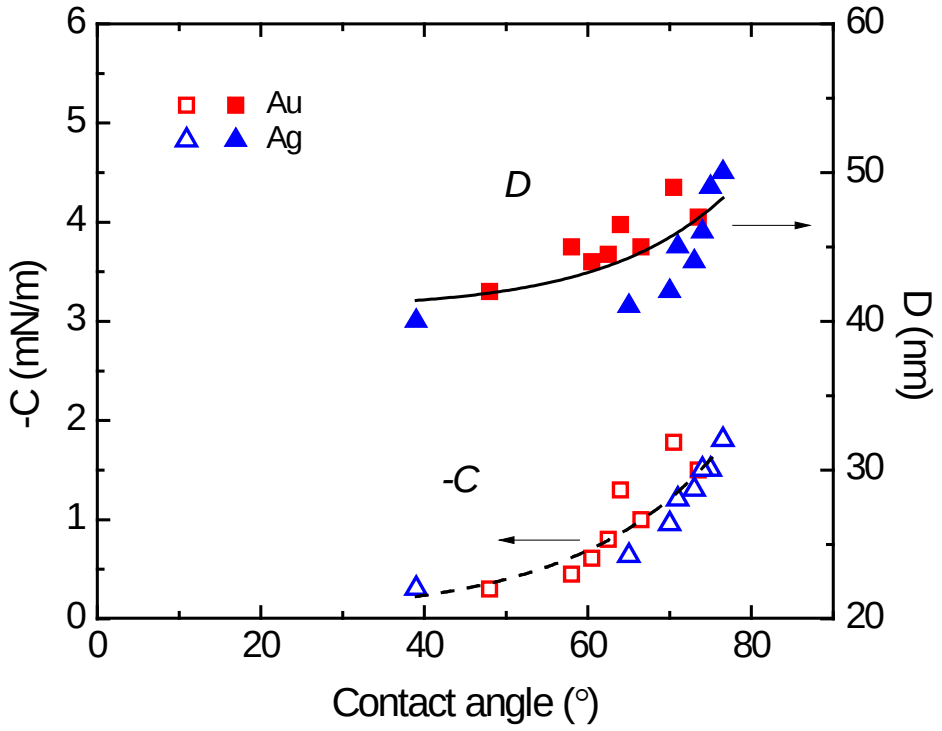

Figure 2.7 The force parameters (*C* and *D*) of Eq. [2.5] plotted *vs*. contact angle (θ) for the gold- and silver-coated glass surfaces in 10^{-3} M KEX solutions.

CHAPTER 3

AFM Surface Forces Measured between Xanthate Treated Gold Surfaces: *Effect of Salts*

3.1 Abstract

Although the stability of mineral particles in flotation has been described by classical DLVO theory quite well, in cases where hydrophobic minerals are involved, this theory fails to accurately describe stability unless an additional attractive interaction component—namely, hydrophobic force—is taken into consideration. In the present work, atomic force microscopy (AFM) using the colloidal probe technique was conducted to determine surface force measurements between gold surfaces treated with xanthate, a widely used collector for the flotation of sulfide minerals and precious metals. The measured long-range attractive forces are much stronger than the van der Waals force, and can be fitted by extended DLVO theory which incorporates a hydrophobic force component. Results showed that attractive forces increased with immersion time until reaching a maximum attractive force; at higher concentrations and with longer chain length xanthates, however, maximum attractive force was achieved under shorter immersion times. The increased efficiency of these surfactants on hydrophobic force was attributed to faster adsorption kinetics. In contrast, measured attractive force decreased when an electrolyte (NaCl) was added to pure water. The decay length (D) of the hydrophobic force was, however, not equal to half of the Debye length (κ^{-1}), which is inconsistent with the charged-patch model. The effect of the various anions was evaluated by comparing the impact of NaI, NaBr, NaCl as the electrolyte, while NaCl, $MgCl_2$, and $AlCl_3$ were used to evaluate the effect of different cations on measured force. Further discussion of the probable origins of hydrophobic force is based upon the force measurement results obtained in this study.

3.2 Introduction

Flotation, which is a widely-used solid-solid separation method in the mineral processing industry, is affected by the dosage of the collector and flotation time[1]. One commonly-used collector, alkylxanthate[2], adsorbs strongly on the surface of sulfide minerals and alters their wettability properties. As reported by Mermillod-Blondin *et al*., effective flotation results were obtained in the presence of a monolayer of xanthate on the surface of the minerals[3].

Surface force provides kinetic properties between air bubbles and mineral particles during the processes of adhesion and detachment, which occur during flotation. Laskowski and Kitchener first speculated that the hydrophobic influence, which is distinct from van der Waals force and electrostatic force, was responsible for flotation[4]. This influence is the so-called "hydrophobic force," which was first described by Blake and Kitchener in wetting films[5]. AFM has recently been used to measure the hydrophobic force between KEX-coated gold and silver surfaces, where the adsorption of a surfactant was controlled by electrochemical potential[6]. As the researchers showed, hydrophobic interaction, which was in good agreement with contact angle, provided more complete information for predicting flotation behavior than contact angle alone.

While the measurement of a hydrophobic interaction provides important information about the hydrophobicity of a given surface,[7] it also points to the underlying mechanism for the interaction[8,9]. The origins of hydrophobic force have been studied for years, and the most popular theories have attributed the measured attractive force between hydrophobic surfaces to the bridging of nanobubbles[10], electrostatic force[11,12], or the structuring of water films[13]—all of which are relevant to electrolytes in pure water. For those forces ascribed to bridging of nanobubbles or cavities, a negligible effect of NaCl was detected until the concentration exceeded 5 M[10], when an increase in liquid-vapor surface tension is assumed to be responsible for the 10% increase in attractive force. However, Craig *et al.*[14] reported that above a concentration of 0.1 M, NaCl begins to reduce the coalescence of air bubbles. Forces of electrostatic origin are sensitive to the presence of electrolytes, especially at a low concentration. According to Attard, the decay length should be equal to half of the Debye length[12]. The diminution effect also exists for hydrophobic forces that originate from water structuring, because the ordering of water is disturbed by the presence of non-adsorbing salt[13], thereby decreasing range while increasing the magnitude of the attractive force. By comparing the measured attractive force in pure water and an electrolyte solution, one can determine the origin of the hydrophobic force.

In the present work, we used AFM to measure the hydrophobic force between xanthate-coated gold spheres and plate surfaces. Two different chain length xanthates were used as surfactants: potassium ethyl xanthate (KEX) and potassium amyl xanthate (PAX). A long-range attractive force without discontinuities on the force curve was detected, with the strength of the force affected by both immersion time and the concentration and the xanthate chain length. It should also be noted that while the addition of salt decreased attractive force, the extent of that reduction was dependent on the salt concentration, with higher NaCl concentrations producing more significant decreases. The remainder of this discussion will further investigate the likely origins for these hydrophobic interactions.

3.3 Experimental

3.3.1 Materials

Two surfactants, potassium ethyl xanthate (KEX, >90%, TCI America) and potassium amyl xanthate, (PAX, >90%, TCI America) were recrystallized twice from acetone (HPLC grade, Fisher Scientific, Inc.) with diethyl ether (>=99.9%, Sigma-Aldrich, Inc.) before use. Sodium chloride (NaCl,

99.999%, Sigma-Aldrich) applied as an electrolyte was heated in an oven at 560°C for at least 4 hours to decompose organic impurities. Magnesium chloride ($MgCl_2$, 99.999%) and aluminum chloride ($AlCl_3$, 99.999%) were used as the electrolyte without further treatment. Sulfuric acid (H_2SO_4, 98%, VMR international) and hydrogen peroxide (H_2O_2, 29-32%, Alfa Aesar) were used to clean the gold-coated glass plates. Ultrapure water with a resistivity of 18.2 MΩ·cm at 25°C was produced from a Millipore Direct-Q 3 water purification system (Millipore, MA).

Gold spheres were created according to the method developed by Raiteri *et al.*[15] Gold wire with a diameter of 12.7 µm (>99.9%, Alfa Aesar) connected to a 120V power supply was heated by short circuit and gold spheres were produced in the spark. The diameters of the gold spheres measured with an Olympus BH-2 light microscope ranged from 6-40 µm. Spheres with diameters of 15-20 µm were selected and adhered to the tip of cantilevers, which then underwent UV-irradiation for 30 minutes to remove any possible organic contamination.

Gold-coated glass plates were bought directly from Evaporated Metal Films. A pre-deposited chromium layer of 5 nm guaranteed a robust adhesion between the upper gold layer of 100 nm and the glass plate. The received gold plates were cut into 0.5×0.5 inch square plates and cleaned in a H_2SO_4/H_2O_2 solution with a volume proportion of 2:1 (piranha solution) at 85°C for 30 minutes. The gold plates were then rinsed with ultrapure water in an ultrasonic bath for 10 minutes and blow-dried using a nitrogen stream before the atomic force measurement.

3.3.2 Surface Force Measurement

A Digital Instrument- Nanoscope V atomic force microscope (AFM) was used for the surface force measurements between the gold-coated glass plates and xanthate-treated gold spheres. The measurements were conducted at room temperature according to a manner described as the colloidal probe technique[16,17]. Silicon nitride AFM probes from Nano World with a spring constant of ~ 0.48N/m were used, and the cantilevers were calibrated by thermally tuning prior to the force measurement. For each experiment, a probe with a gold sphere attached was mounted on a standard AFM liquid cell. The gold-coated glass plate was placed on the top of the scanner E. An o-ring ensured a watertight space between the plate and the liquid cell to accommodate the injected surfactant solution. Hydrophobization of both the sphere and plate was initiated as soon as the xanthate solution was injected. Hydrophobicity was adjusted by moderating the concentration of surfactant and the immersion time. The force measurement was taken after the surfactant solution was replaced by pure water, electrolyte solutions or other liquids in the cell. Measured forces (F) normalized by the radius (R) of the gold sphere were plotted *vs*. the separation distance (h) between the sphere and plate.

3.4 Results and Discussion

3.4.1 Xanthate Adsorption Kinetics

Figure 3.1 shows AFM force measurements obtained after the gold-coated glass plate and gold sphere were immersed in 10^{-5} M KEX-in-water solution for different periods of minutes. Starting at 10 minutes, the detected attractive interaction was observed to be active over a greater distance and stronger than the van der Waals force calculated with a Hamaker constant of 1.2×10^{-20} J[18]. This finding suggests the appearance of an additional attractive force, using extended classical DLVO theory. The attractive force increased with immersion time up to 210 minutes, after which it started to decrease. A similar force-related trend with immersion time was observed when higher concentrations of 10^{-4} M KEX (Figure 3.2) and 10^{-3} M KEX (Figure 3.3) were used. As research has shown, adsorbed xanthate on gold surface facilitates its flotation because xanthate increases its hydrophobicity[19]. Additionally, studies indicate that

adsorption increases with time, accompanied by transition from the disordered phase to the ordered structure of a complete monolayer, with each molecule coordinating to the gold surface through two sulfur atoms[20]. The gold surface becomes more hydrophobic once a complete monolayer is formed, and additional KEX adsorbed onto the chemisorbed layer may decrease the hydrophobicity of the surfaces. As noted in flotation studies, a monolayer of xanthate is sufficient to obtain effective results[3]. This observation is further supported by the fact that force change with immersion time. Maximum attractive forces were obtained within 40 minutes when immersed in 10^{-4} M, and within 10 minutes when immersed in 10^{-3} M KEX, indicating a much faster adsorption rate with KEX than the initial reaction with 10^{-5} M KEX. The dependence of attractive force on xanthate concentration and reaction time is identical to that of the contact angle of xanthate-coated gold substrates as reported by Wang *et al.*[21], who stated that contact angle increases with reaction time prior to a maximum value, followed by a minor decrease. In addition, a higher concentration of KEX increases the contact angle more rapidly. Recently, Li and Yoon reported good agreement between the attractive force between KEX-coated gold surfaces and its contact angle, which was adjusted by controlling electrochemical potentials[6]. The long-range attractive force detected in the present work was determined by surface hydrophobicity.

Figure 3.4 presents the forces measured between gold surfaces treated by a longer chain xanthate-PAX as a function of immersion time. It took 10 minutes of immersion to obtain maximum attractive force with the 10^{-4} M PAX, whereas a period of 40 minutes was required to obtain maximum force for the KEX of the same concentration, as discussed above (Figure 3.2). Figure 3.5 illustrates maximum force results after the gold surfaces were exposed to PAX for 40 minutes, whereas the concentration (5×10^{-6} M) used here was only 5% of the KEX solution used in Figure 3.2 (10^{-4} M).

The more rapid kinetics of adsorption for longer chain xanthates is consistent with other reports in the literature. For example, as revealed by means of infrared reflection absorption spectroscopy (IRAS) and Auger electron spectroscopy (AES)[22], adsorption on metallic copper and silver surfaces was noted to be faster for octyl xanthate in comparison to ethyl xanthate. The faster adsorption for longer chain xanthate may be due to the nature of xanthate adsorption on minerals or metals from aqueous solutions as a reverse process of metal xanthate dissolution. Except for very long chain xanthates with poor solubility, the effect of xanthate as a flotation collector increases with hydrocarbon chain length. In addition, the longer chain length is believed to give rise to higher hydrophobicity. Therefore, we can say that measured force is a hydrophobicity related (or induced) force.

3.4.2 Salt Effect

AFM force measurements of gold plates and spheres in pure water and in the presence of NaCl are presented in Figure 3.6. The gold plates and spheres were treated by being immersed in 10^{-3} M KEX solution for 10 minutes. The first measurement was conducted after the KEX solution was replaced with pure water; subsequent measurements were obtained in NaCl solution at three different concentrations ranging from 10^{-5} M to 10^{-3} M. Finally, the salt solution was again replaced by pure water for the final measurement. As shown, attractive forces that were longer-ranged and stronger than the van der Waals force were detected in all the aqueous solutions. It should be noted, however, that the forces decreased with increasing concentrations of NaCl.

For those forces attributed to the bridging of nanobubbles or cavities[10], the effect of NaCl was negligible until the salt concentration was increased to 5 M, at which point it appears that an increase of liquid-vapor surface tension caused the 10% increase in attractive force. In a differing report, Craig *et al.*[14] reported that NaCl begins to reduce the coalescence of air bubbles after exceeding a 0.1 M concentration of NaCl. In general, the liquid-vapor interfaces are relatively stable in the presence of salt at low concentrations (< 0.1 M). The negative effect of salt (10^{-5} M-10^{-3} M) on the attractive forces

measured in the present work was not believed to be due to the change in surface tension. Therefore, the bridging of nanobubbles is not responsible for the long-range attraction observed here.

As noted by Podgornik, the NaCl plays a role in reducing the attractive force of electrostatic nature[23]. Later, Miklavic[24] proposed a charged-patch model for the forces between heterogeneous charged surfaces. The referred force decays exponentially with decay length (D), which is related closely to the Debye screening length (κ^{-1}). More precisely, the value of D for the force between charged patches should equal half the value of κ^{-1} which is decreased with the presence of salt[24,25]. To check the relation between D and κ^{-1}, the measured forces were fitted with extended DLVO theory, with a single exponential force law representing the hydrophobic force as follows:

$$\frac{F}{R} = -C\exp(-\frac{h}{D}) \qquad [3.1]$$

where C represents the magnitude of the hydrophobic force and D indicates decay length. The fitting parameters C and D for the forces in Figure 3.6 are presented *vs*. the concentration of NaCl in Table 3.1, with the values of κ^{-1} for comparison. The value in the last row represents the case when 1 mM NaCl solution was replaced by pure water. While both C and D decreased with increasing concentrations of salt, it was not possible to generalize a singular relation between κ^{-1} and D. As shown, D was smaller than $\frac{1}{2}\kappa^{-1}$ when NaCl concentration was equal to or less than 10^{-5} M, above which D approached to or exceeded κ^{-1}. This finding contradicts predictions for attractive force of electrostatic origin[12], which suggests that D should equal half of κ^{-1}.

Actually, electrostatic origin has been rejected as an explanation for the long-range attractive force between chemisorbed surfaces *i.e.*, silanated glass surfaces[26], since the force decays exponentially over the separation distance with D (5.6 nm) much greater than the value of κ^{-1} (3nm). Even for some physical-adsorption surfaces, exponentially-decaying attraction can extend as far as 40 nm in a cetylpyridinium chloride (CPC) solution[27] containing 0.1 M NaCl. The remaining attraction in such a high concentration of salt contradicts electrostatic mechanisms. Also, the Charged-patch model proposed by Miklavic[24] has been denied for the alkylammonium physically adsorbed-surfaces[28]. As reported by Zhang *et al.*[28], the lattice patch size, which was back calculated from the measured force, was much larger than those estimated from the aggregation numbers[29], with the latter one close to the value obtained by means of the scanning tunneling microscopic (STM) imaging. In other words, to obtain the strong attractive force as detected in the force measurements, the charged patch model ask for patches of significantly greater size than those actually observed with self-assembled monolayers. In addition, xanthate chemisorbed on gold surfaces lacks horizontal mobility, which is a prerequisite for electrostatic forces to be attractive. As stated by Christenson[30], the generation of long-range attraction requires either a shift of adsorption/desorption equilibrium or a lateral diffusion of surface patches.

In a contradictory study, the diminution effect of salt on long-range hydrophobic attraction has been shown to be related to the metastability of liquid films confined by hydrophobic surfaces[27]. As stated by Eriksson *et al.*[13], non-adsorbing ions or other solutes may disturb the water structure, causing a shorter decay length of the hydrophobic force. In the early 1970s, the solvation force interaction was predicted to have an exponential relationship to the separation distance. The measured forces in the present work agree well with the solvation force on the exponentially decaying property.

Note also that the long-range attractive force became comparable to the first measured force in pure water after the 10^{-3} M NaCl solution was replaced with pure water (Figure 3.6), as was indicated by the quite comparable fitting parameters for the hydrophobic forces measured in those two cases (Table 3.1). Actually, the recovery of hydrophobic force was observed as soon as the medium was replaced. This

finding indicates the following: 1) the chemisorption of KEX on gold is sufficiently stable to withstand the disturbances of salt, and 2) the effects of salt on hydrophobic force are reversible. Moreover, the recovery of attractive force suggests that NaCl is a non-adsorbing salt and therefore only affects the properties of the medium between the two hydrophobic surfaces. NaCl has been found to be an *H*-bonding network breaker[28] and the hydration of Na^+ or Cl^- has been shown to result in structural changes to water, as research has suggested[31,32]. Ions that increase the fluidity of water may also break the structure of water[33]. The reduction of force with increasing salt strength agrees with Eriksson *et al.*[13] who proposed that the attraction between two hydrophobic surfaces in water is due to *H*-bond-propagated ordering effects of thin water films confined between two hydrophobic surfaces—and that this force should have a shorter range when a nonadsorbing electrolyte is added.

Figure 3.7 shows AFM forces measured between KEX-coated gold surfaces in pure water and in 10^{-5} M sodium electrolytes with different anions (NaCl, NaBr, NaI). The attractive force obtained in pure water was shown to be stronger in comparison to results obtained with salt. Although not significant, the differences in the force curves obtained in the aqueous solutions were still observable, with NaI showing the greatest decrease in force, followed by NaBr and NaCl. This diminution effect was related to the increase in the atomic weight of the anions. Forces measured in pure water in the presence of chloride salts of different valences (NaCl, $MgCl_2$ and $AlCl_3$) were also compared with those obtained in pure water, as shown in Figure 3.8. Although the same concentration of 10^{-5} M was used for all salts, $AlCl_3$ was found to produce the greatest decrease in attractive force. The different effect of anions or cations on the hydrophobic force is probably related with their structure breaking abilities.

Since the solubility of oxygen in water decreases when sodium chloride is added[34], the decrease in force may be related to the dissolved gas. Chapter 6 presents a study of the effect of degassing on hydrophobic force. The observation that force decreases after degassing also supports the influence of dissolved gas on the hydrophobic force, which is reinforced by similar observations in the literature[35,36]. A clathrate model[9] for the structured water films confined by two hydrophobic surfaces indicates that gas molecules enhance the stability of the structured clathrates. Therefore, the effect of dissolved salt on the measured forces in the present work may be caused by the change in gas solubility, suggesting the possibility of water structuring as the origin of hydrophobic interaction.

3.5 Conclusions

Long range hydrophobic forces have been observed and characterized between xanthate-treated gold surfaces. The attractive forces were found to increase with immersion time until a maximum force was detected, after which a slight decrease was observed. The maximum force was detected after shorter immersion times only if higher concentrations or longer chain length xanthates were used, suggesting faster adsorption kinetics. Although measured force decreased in aqueous solution in the presence of electrolytes (NaCl, NaI, NaCl, $MgCl_2$, $AlCl_3$), the effect differed depending on the type of salt. Additionally, the decay length of the forces measured in the NaCl solution was not equal to half of the Debye length, which contradicts what we know of measured forces of the measured force of electrostatic origin.

3.6 References

(1) Lee, K.; Archibald, D.; McLean, J.; Reuter, M. A. *Miner. Eng.* **2009**, *22*, 395.
(2) Wang, X.-H.; Eric Forssberg, K. S. *Int. J. Miner. Process.* **1991**, *33*, 275.
(3) Mermillod-Blondin, R.; Kongolo, M.; Donato, P. d.; Benzaazoua, M.; Barres, O.; Bussiere, B.; Aubertin, M. In *Centenary of Flotation Symposium* Brisbane, Australia, 2005.
(4) Laskowski, J.; Kitchener, J. A. *J. Colloid Interface Sci.* **1969**, *29*, 670.

(5) Blake, T. D.; Kitchener, J. A. *Journal of the Chemical Society, Faraday Transactions 1: Physical Chemistry in Condensed Phases* **1972**, *68*, 1435.
(6) Li, Z.; Yoon, R.-H. *Miner. Eng.* **2012**.
(7) Yoon, R. H.; Flinn, D. H.; Rabinovich, Y. I. *J. Colloid Interface Sci.* **1997**, *185*, 363.
(8) Nguyen, A. V.; Nalaskowski, J.; Miller, J. D.; Butt, H. J. *Int. J. Miner. Process.* **2003**, *72*, 215.
(9) Wang, J.; Yoon, R.-H.; Eriksson, J. C. *J. Colloid Interface Sci.* **2011**, *364*, 257.
(10) Parker, J. L.; Claesson, P. M.; Attard, P. *J. Phys. Chem.* **1994**, *98*, 8468.
(11) Tsao, Y. H.; Evans, D. F.; Wennerstrom, H. *Langmuir* **1993**, *9*, 779.
(12) Attard, P. *J. Phys. Chem.* **1989**, *93*, 6441.
(13) Eriksson, J. C.; Ljunggren, S.; Claesson, P. M. *J. Chem. Soc., Faraday Trans. II* **1989**, *85*, 163.
(14) Craig, V. S. J.; Ninham, B. W.; Pashley, R. M. *J. Phys. Chem.* **1993**, *97*, 10192.
(15) Raiteri, R.; Preuss, M.; Grattarola, M.; Butt, H.-J. *Colloids Surf., A* **1998**, *136*, 191.
(16) Ducker, W. A.; Senden, T. J.; Pashley, R. M. *Nature* **1991**, *353*, 239.
(17) Ducker, W. A.; Senden, T. J.; Pashley, R. M. *Langmuir* **1992**, *8*, 1831.
(18) Wang, J. L.; Yoon, R. H. *Langmuir* **2008**, *24*, 7889.
(19) Talonen, P.; Rastas, J.; Leppinen, J. *Surf. Interface Anal.* **1991**, *17*, 669.
(20) Ihs, A.; Uvdal, K.; Liedberg, B. *Langmuir* **1993**, *9*, 733.
(21) Wang, J., Virginia Polytecnic Institute and State University, 2008.
(22) Ihs, A.; Liedberg, B. *Langmuir* **1994**, *10*, 734.
(23) Podgornik, R. *J. Chem. Phys.* **1989**, *91*, 5840.
(24) Miklavic, S. J.; Chan, D. Y. C.; White, L. R.; Healy, T. W. *J. Phys. Chem.* **1994**, *98*, 9022.
(25) Spalla, O.; Belloni, L. *Phys. Rev. Lett.* **1995**, *74*, 2515.
(26) Parker, J. L.; Claesson, P. M. *Langmuir* **1994**, *10*, 635.
(27) Craig, V. S. J.; Ninham, B. W.; Pashley, R. M. *Langmuir* **1998**, *14*, 3326.
(28) Zhang, J. H.; Yoon, R. H.; Eriksson, J. C. *Colloid Surf., A* **2007**, *300*, 335.
(29) Fan, A.; Somasundaran, P.; Turro, N. J. *Langmuir* **1997**, *13*, 506.
(30) Christenson, H. K.; Yaminsky, V. V. *Colloid Surf., A* **1997**, *130*, 67.
(31) Weissenborn, P. K.; Pugh, R. J. *J. Colloid Interface Sci.* **1996**, *184*, 550.
(32) Craig, V. S. J.; Ninham, B. W.; Pashley, R. M. *Nature* **1993**, *364*, 317.
(33) Frank, H. S.; Evans, M. W. *J. Chem. Phys.* **1945**, 507.
(34) MacArthur, C. G. *J. Phys. Chem.* **1915**, *20*, 495.
(35) Craig, V. S. J.; Ninham, B. W.; Pashley, R. M. *Langmuir* **1999**, *15*, 1562.
(36) Meyer, E. E.; Lin, Q.; Israelachvili, J. N. *Langmuir* **2005**, *21*, 256.

Table 3.1: The fitting parameters of *C* and *D* for the hydrophobic forces presented in Figure 3.6 (a: The solution of 1 mM NaCl was replaced by pure water).

NaCl (mM)	κ^{-1} (nm)	C (mN/m)	D (nm)
0	134.2	-1.7	46
0.01	94.9	-1.1	40
0.1	30	-1.05	29
1	9.5	-1.75	11.4
0[a]	134.2	-1.59	43.5

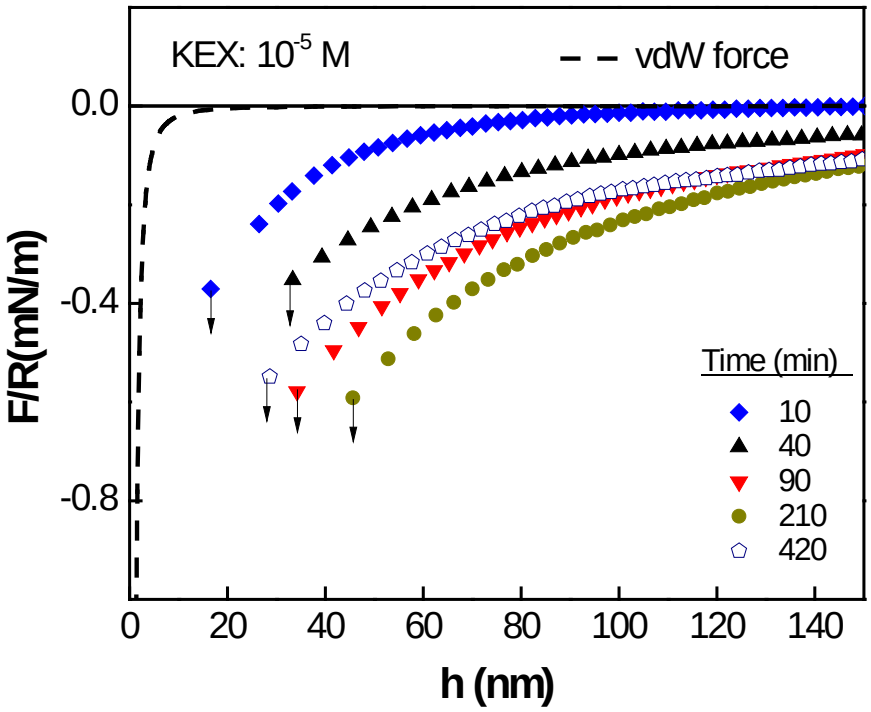

Figure 3.1 Surface forces measured in pure water between gold surfaces treated by 10^{-5} M KEX solution for different periods of time. The dashed line represents the van der Waals force calculated with a Hamaker constant of 1.2×10^{-20} J. The arrows indicate where the two surfaces make contact.

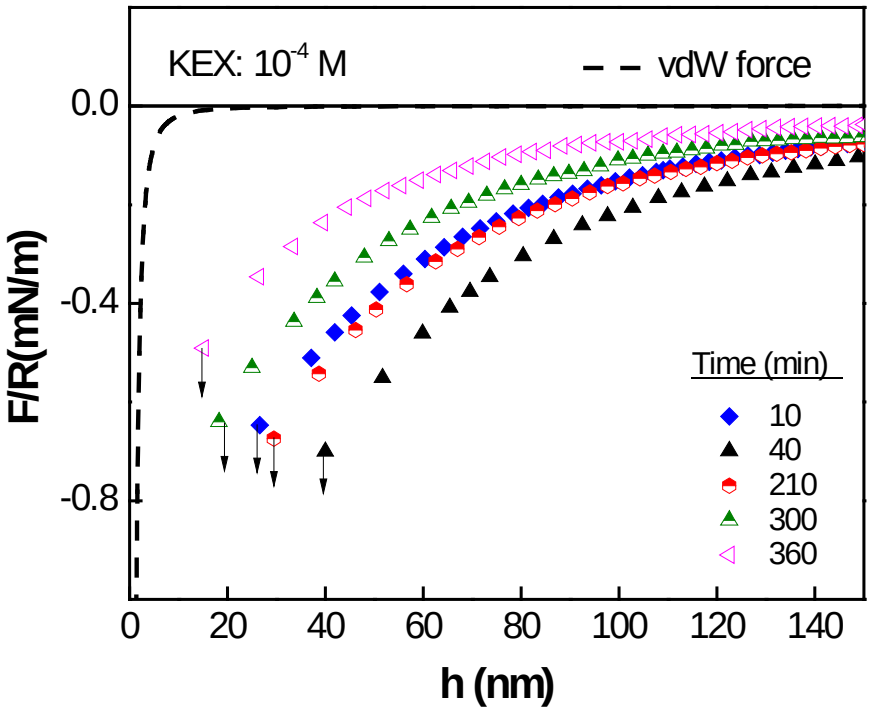

Figure 3.2 Surface forces measured in pure water between gold surfaces treated by 10^{-4} M KEX solution for different periods of time. The dashed line represents the van der Waals force. The arrows indicate where the two surfaces make contact.

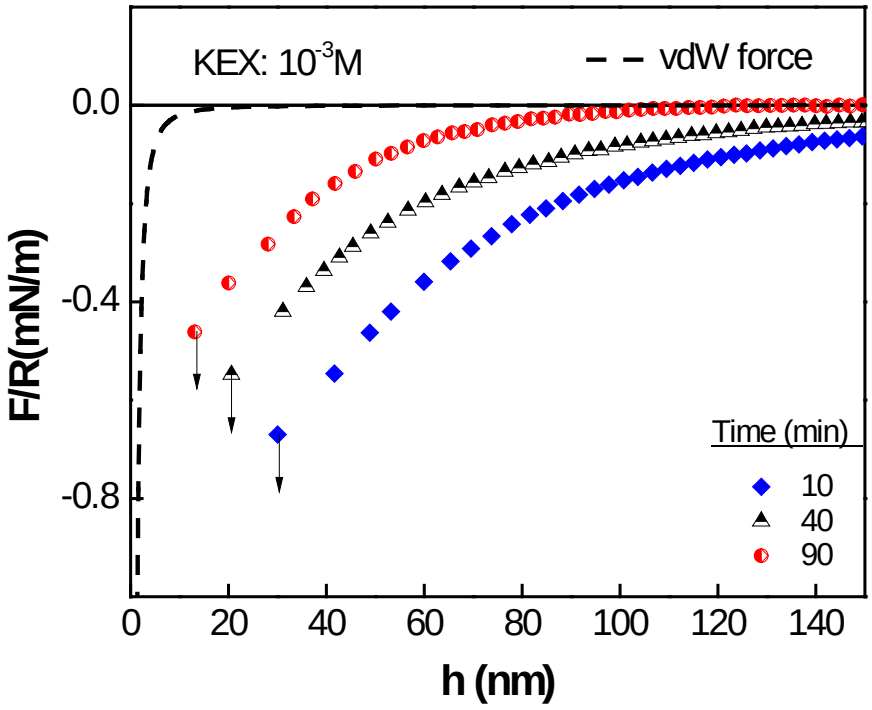

Figure 3.3 Surface forces measured in pure water between gold surfaces treated by 10^{-3} M KEX solution for different periods of time. The dashed line represents the van der Waals force. The arrows indicate where the two surfaces make contact.

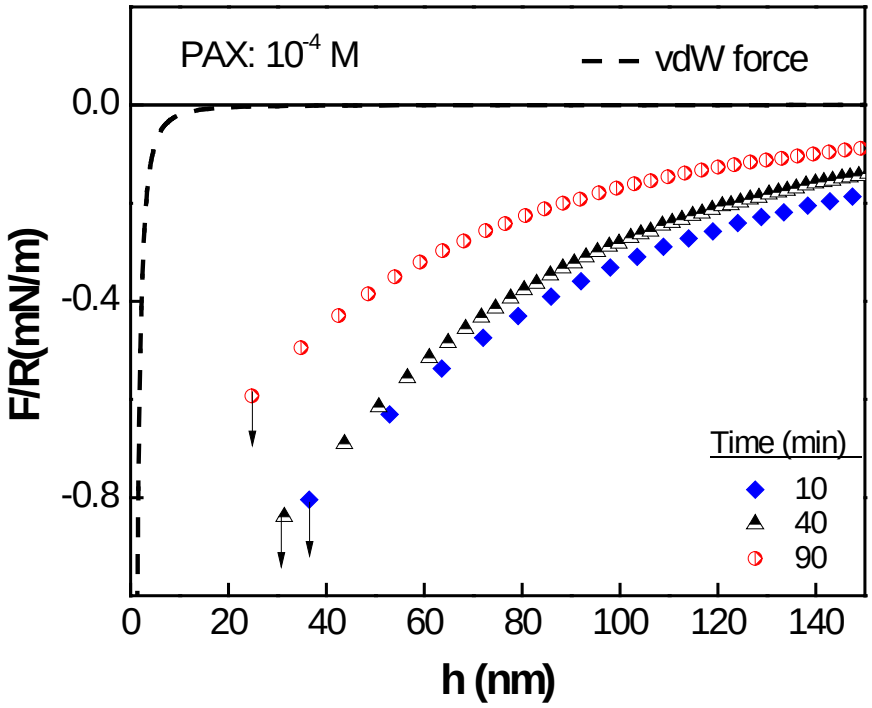

Figure 3.4 Surface forces measured in pure water between gold surfaces treated by 10^{-4} M PAX solution for different periods of time. The dashed line represents the van der Waals force. The arrows indicate where the two surfaces make contact.

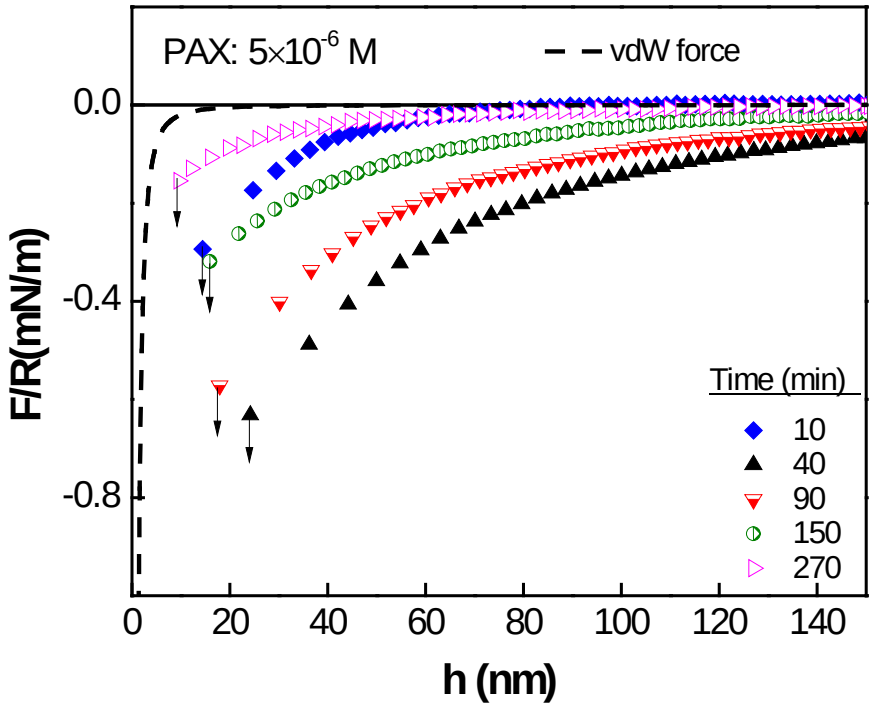

Figure 3.5 Surface forces measured in pure water between gold surfaces treated by 5×10^{-6} M PAX solution for different periods of time. The dashed line represents the van der Waals force. The arrows indicate where the two surfaces make contact.

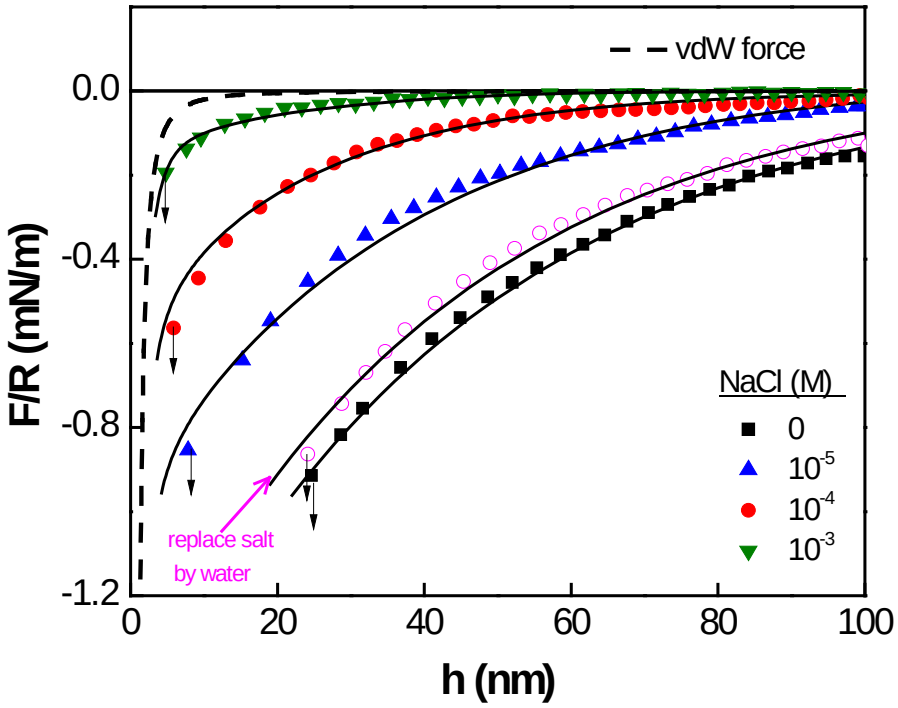

Figure 3.6 Surface forces between gold surfaces treated by 10^{-3} M KEX for 10 minutes conducted in NaCl solutions of various concentrations. The solid square symbol scatter represents the force curve measured between the hydrophobized gold surfaces in water, while the open round symbol is the one measured after the high concentration salt was replaced by pure water. The rest curves from bottom to top represent the forces measured in NaCl solution with a concentration from 10^{-5} M to 10^{-3} M.

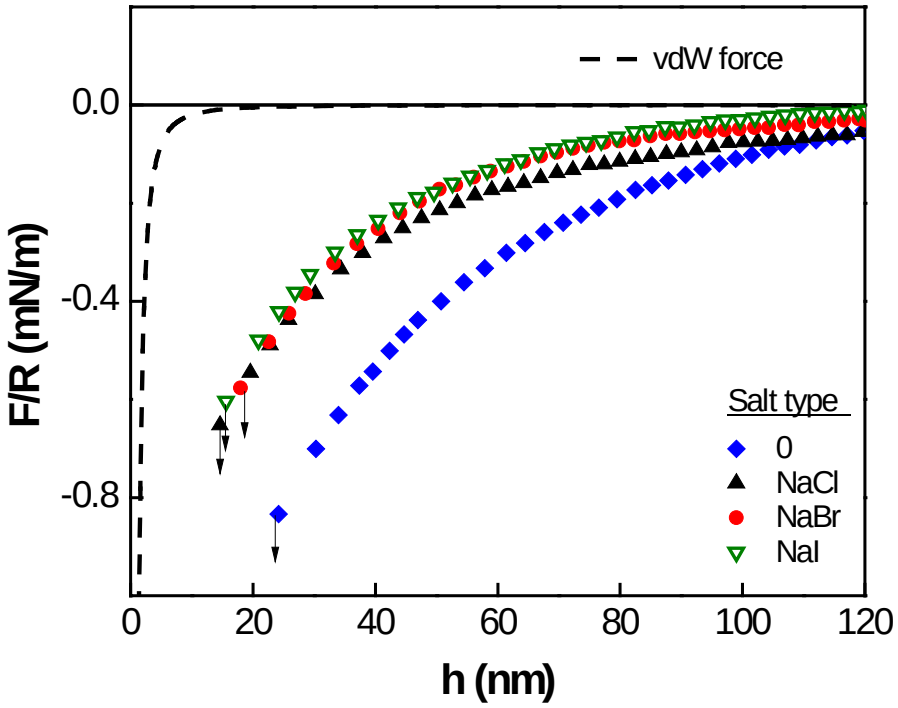

Figure 3.7 Surface forces between gold surfaces treated by 10^{-3} M KEX for 10 minutes. The measurements were conducted in pure water and 10^{-5} M sodium electrolytes-NaCl, NaBr and NaI- sequentially as presented from bottom to top.

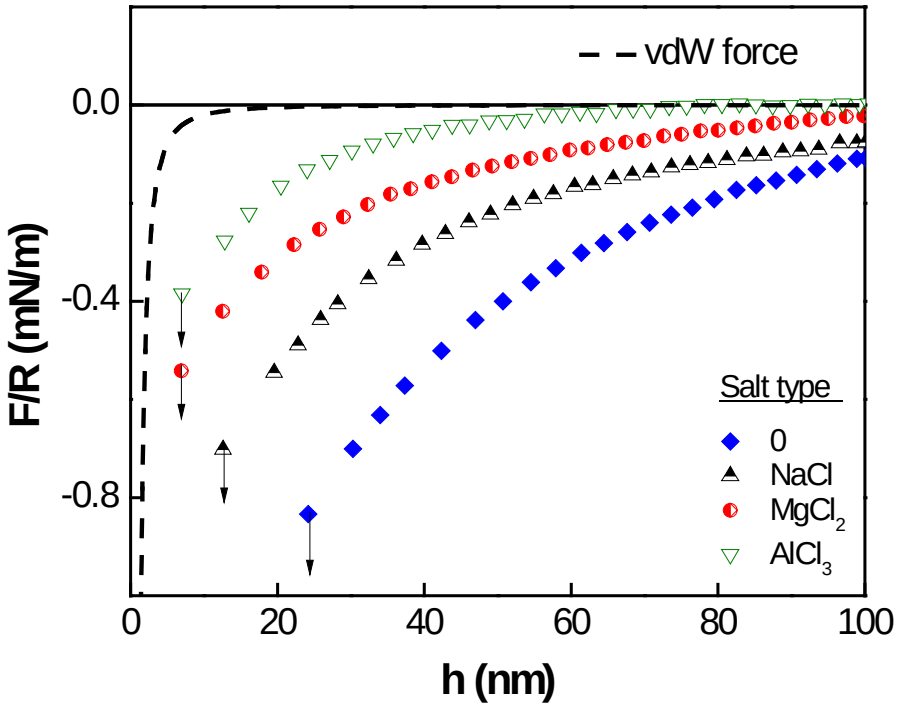

Figure 3.8 Surface forces between gold surfaces treated by 10^{-3} M KEX solution for 10 minutes. The measurements were conducted in pure water and 10^{-5} M chloride electrolytes-NaCl, $MgCl_2$, $AlCl_3$- sequentially as presented from bottom to top in the figure.

CHAPTER 4

Thermodynamics of Hydrophobic Interaction between Silica Surfaces Coated with Octadecyltrichlorosilane

4.1 Abstract

Surface force measurements conducted with thiolated gold surfaces showed previously that hydrophobic interaction entails a decrease in excess film entropy, suggesting that hydrophobic force originates from changes in the structure of the medium (water) confined between hydrophobic surfaces[1]. As a follow-up work, surface force measurements have been conducted in the present work using an atomic force microscope (AFM) with silica surfaces coated with octadecyltrichlorosilane (OTS) at temperatures in the range of 10 to 40°C. A thermodynamic analysis of the results show that both the excess film entropy (ΔS^f) and excess film enthalpy (ΔH^f) decrease with decreasing thickness of the water films between the hydrophobic surfaces. It has been found also that $|\Delta H^f| > |T\Delta S^f|$, which represents a necessary condition for the excess free energy change (ΔG^f) to be negative and hence the hydrophobic interaction be attractive. Thus, the results obtained with both the thiolated and silylated surfaces show that hydrophobic forces originate from the structural changes in the medium. It is believed that the water molecules in the thin liquid films (TLFs) of water form clusters as a means to reduce the free energy when they cannot form *H*-bonds to neighboring hydrophobic surfaces.

4.2 Introduction

Hydrophobic particles placed in water are attracted to each other much more readily than predicted by the DLVO theory due to the presence of the hydrophobic force[2,3], which is longer-ranged and stronger than the van der Waals force. Israelachvili and Pashley[4] reported the first direct measurement of hydrophobic force using the surface force apparatus (SFA). Many investigators[5-10] confirmed its existence and discussed possible origins, while others suggested that the hydrophobic force is an artifact due to bubbles or cavities[11-13]. Still others suggested that hydrophobic forces, particularly those of longer range, may originate from mechanisms that are unrelated to surface hydrophobicity[14,15].

In an effort to better understand the origin(s) of hydrophobic force, one of us determined the thermodynamic functions of the hydrophobic interactions by conducting surface force measurements at several different temperatures[1]. The results showed that macroscopic hydrophobic interactions entail decreases in both the excess entropy (S^f) and the excess enthalpy (H^f) of the thin liquid films (TLF) of water confined between hydrophobic surfaces. Here, the term "excess" refers to the thermodynamic indicator of the thin film in question relative to that of the infinitely thick film (or bulk water). It was found also that the changes in excess film enthalpy (ΔH^f) are slightly larger than the absolute temperature (T) times the changes in excess film entropy (ΔS^f). Based on these results, it was suggested that macroscopic hydrophobic interactions may involve building structures of water in the vicinity of hydrophobic surfaces. In effect, ΔH^f represents the energy gained in building the structures, while $T\Delta S^f$ represents the thermodynamic cost of building the structure. In this previous work, the surface force measurements were conducted using an atomic force microscope (AFM) with gold-coated silica surfaces hydrophobized with *n*-ethanethiol (C_2-SH) and *n*-hexadecane thiol (C_{16}-SH).

The thermodynamic studies described above suggested that hydrophobic force is a structural force, a term first used by Derjaguin and Kusakov[16] to describe the repulsive hydration force present in wetting films. In general, the term structural force refers to the non-DLVO force created when two boundary layers, whose structures are different from that of the bulk solution, overlap[17]. The non-DLVO forces observed between two hydrophilic surfaces are referred to as positive structural force, while those observed between hydrophobic surfaces are referred to as negative structural force[18]. Eriksson *et al.*[19] suggested that the long-range attractive forces observed between hydrophobic surfaces may be due to the surface-induced changes in water structure.

In the present work, we have conducted AFM force measurements using silica surfaces hydrophobized with octadecyltrichlorosilane (OTS) at temperatures in the range of 10 to 40°C. The results have been converted to the excess Gibbs free energies (ΔG^f) of the TLFs using the Derjaguin approximation[20], which were then used to determine ΔS^f and ΔH^f in the same manner as described previously[1].

Silylated silica may provide a more stable and robust hydrophobic surface than thiolated gold, as the latter is susceptible to oxidation. It has been shown that upon exposure to air under ambient conditions, self-assembled monolayers (SAMs) of alkane thiolates oxidize to alkane sulfonates[21,22]. In the presence of halide, the thiol groups oxidize to disulfide and subsequently to sulfonate, with the substrate (Au) being oxidized to Au^{3+} species[23].Stability of hydrophobic surfaces using thiolated gold may thus become an issue particularly when conducting force measurements at elevated temperatures. On the other hand, OTS-coated silica surfaces are stable at temperatures up to 175°C[24].

Surface force data obtained with silylated surfaces and reported in the literature are controversial. Some investigators showed strong hydrophobic forces[25,26], while others showed capillary forces related to bubbles or cavities[11,27,28]. The experimental data obtained in the present work showed the presence of

long-range hydrophobic forces with no evidences for bubbles or cavitation causing them. Thermodynamic analysis of the results led to the same conclusion as obtained previously using thiolated gold surfaces: hydrophobic forces originate from changes in the water structure[1].

4.3 Experimental

4.3.1 Materials

All experiments were conducted using ultrapure water obtained using a Direct-Q3 water purification system from Millipore. The water had a resistivity of 18.2 MΩ·cm and <10 ppb of total organic carbon. Silica spheres (Whitehouse Scientific) of ~10 μm radius and fused-quartz plates (Technical Glass Products Inc.) were used as macroscopic surfaces for surface force measurements. The spheres and plates were hydrophobized by immersion in octadecyltrichlorosilane (OTS, 95% purity, Alfa Aesar)-in-toluene (99.9% purity, Fisher Chemical, dried with a molecular sieve) solutions. The hydrophobized surfaces were rinsed with chloroform (99.9% purity, Fisher Chemical), acetone (99.9+% HPLC grade, Aldrich) and ultrapure water sequentially. Silicon wafers (Sumco, Oregon) were used for imaging the OTS-coated surfaces. Sulfuric acid (H_2SO_4, 98% purity, VMR international) and hydrogen peroxide (H_2O_2, 29.0-32.0% purity, Alfa Aesar) were used to clean the macroscopic surfaces before hydrophobization with OTS.

4.3.2 Sample Preparation

The macroscopic surfaces used in the present work were cleaned in piranha solutions (H_2O_2/H_2SO_4, 3:7 by volume) at ~80°C for 1 hour to remove organic contaminants. The plates were then rinsed thoroughly with ultrapure water in an ultrasonic bath for 10 minutes and blow-dried in a pure nitrogen stream.

The cleaned surfaces were hydrophobized by immersing them in freshly-prepared OTS-in-toluene solutions. Special care was taken to remove water from the solvent. The hydrophobicity of the silylated surfaces, as measured by water contact angles, was controlled by varying the immersion time in a 5×10^{-5} or 3×10^{-3} M OTS-in-toluene solutions contained in TFPE beakers. The excess OTS present on silylated surfaces was removed by subjecting the plates and spheres to ultrasonic vibration sequentially in chloroform, acetone, and pure water for a few minutes. The silylated surfaces free of excess OTS were then blow-dried with pure nitrogen gas and stored.

4.3.3 AFM Imaging

A Nanoscope V atomic force microscope (AFM), Veeco Instruments Inc., was used to capture the images of the silylated surfaces under contact mode in air. A silicon nitride AFM cantilever (Nano world Innovative Technologies) with a spring constant of ~0.48 N/m was used.

4.3.4 Surface Force Measurement

The Nanoscope V AFM was also used to measure the surface forces acting between silylated silica sphere and silica plate in ultrapure water. The AFM was equipped with a temperature control system, which allowed the measurement of surface forces at different temperatures. The measurement was conducted in the range of 10 to 40°C in the same manner as described previously[1]. For a given series of measurements, a silylated silica sphere was glued onto the tip of a cantilever (AI silicon probe, Budget Sensors) with a spring constant (k) of ~7.4 N/m using a polymer resin (EPON-1004F, Shell Chemical Co.). The resonant frequency technique[29] was used to accurately determine the spring constant for each cantilever.

4.3.5 Contact Angle Measurement

Droplets of ultrapure water were placed on the silylated fused-silica and silicon wafer surfaces to determine the contact angles using the sessile drop technique. A Ramé-Hart goniometer was used for the measurements. Advancing and receding angles were measured by changing the volume of the ultrapure water drops by means of a Microliter syringe. For a given surface, five different measurements were conducted and averaged.

4.4 Results and Discussion

4.4.1 OTS Monolayer on Silica

The AFM images of the fused-silica plates used in the present work showed grains of ~100 nm in dimension, and the distinct boundaries between them made it difficult to see the surfactant molecules adsorbed on the surface[30]. Further, some of the images showed lines representing scratches created during polishing. Therefore, we used silicon wafers for imaging OTS-coated surfaces. Silicon wafers readily oxidize to form silicon dioxide[31]; therefore, the information derived using the wafer may be relevant to the surface force data obtained using the silylated silica surfaces.

Figure 4.1 shows the water contact angles of ultrapure water placed on the surfaces of silicon wafers treated with OTS-in-toluene solutions at 5×10^{-5} and 3×10^{-3} M. Table 4.1 shows the data obtained at the lower concentration. As anticipated, both the advancing (θ_a) and receding angles (θ_r) increased with contact time, and the kinetics of adsorption was much faster at the higher concentration. Also shown is the contact angle hysteresis at the two different concentrations. In both cases, the hysteresis decreased with increasing contact time, indicating that as the adsorption density of OTS increased, the adsorption layers became smoother.

Figure 4.2 shows the AFM images of the silicon wafers contacted with 5×10^{-5} M OTS-in-toluene solutions for different time periods to obtain equilibrium contact angles (θ_e) of 30°, 80°, 93° and 101°. Untreated surface exhibited an equilibrium contact angle of 4°. The images were captured in air with a scan area of 1×1 μm and a vertical color scale of 3 nm. The vertical profiles shown under the images represent the changes in height along the horizontal lines drawn in the images. The bare silicon surface with $\theta_e = 4°$ showed RMS roughness of 0.11 nm, demonstrating that the silicon wafer surface was smooth (Figure 4.2a).

After a short contact time of 20 min, θ_e became 30° (Figure 4.2b) and small spots of ~20 μm diameter appeared. These spots indicated that OTS adsorbs in clusters due to lateral interactions. As θ_e increased to 80° (Figure 4.2c), the clusters became more abundant, larger (40-100 nm), and taller as shown in the vertical profiles. It appears that as θ_e increased to 93° (Figure 4.2d) and then to 101° (Figure 4.2e) with increasing contact time, the clusters coalesced and became larger, eventually creating a smooth monolayer.

The series of AFM images presented in Figure 4.2 shows that the monolayer coating has a thickness of approximately 2.5 nm, as was also reported by other investigators[32,33]. This value is close to the length of 18 carbon alkane chain, indicating that the OTS coatings obtained in the present work were monomolecular layers. It is believed that the key to forming a smooth monolayer was to ensure that the solvent (toluene) was completely dehydrated before use. The adsorption layers formed in the presence of water produced much thicker (~200 nm) layers[34], possibly indicating the formation of polymeric silanes.

4.4.2 Surface Forces and Contact Angle

In Figure 4.3, surface forces (F) measured between silylated silica plates and spheres normalized by the radii (R) of the spheres are plotted *vs*. thickness (h) of the TLF of water formed between the two macroscopic surfaces. In each experiment, a pair of silica plate and sphere was hydrophobized in an OTS solution (5×10^{-5} M in toluene) simultaneously, so that the two surfaces have identical contact angles. Figure 4.3 shows the results obtained with silica surfaces of θ_e = 50.0, 78 and 92.5°. The contact angles were varied by controlling the immersion time in the OTS solution. As shown, all of the force curves exhibited net attractive forces stronger than the van der Waals force with a Hamaker constant (A_{131}) of 0.8×10^{-20} J[35]. Note here that the force curve obtained at θ_e = 92.5° were smooth, showing no evidence for bubbles or vapor cavities affecting the measurement. Cavitation is thermodynamically possible at contact angles above 90°. If bubbles and/or cavities were the causes for the non-DLVO attractive forces[11], the forces measured at θ_e < 90° should be equal to the van der Waals force. The experimental results were contrary as shown in Figure 4.3. Further, the attractive forces increased with increasing contact angle, indicating that the non-DLVO forces shown in Figure 4.3 are related to the hydrophobicity of the surfaces used in the measurements.

The arrow on each curve represents the distance at which a sphere jumps into contact with a plate due to the presence of the attractive hydrophobic force in the TLF confined between the macroscopic hydrophobic surfaces. The solid lines in Figure 4.3 represent the surface forces calculated using the extended DLVO theory, which includes contributions from the van der Waals force, electrical double-layer force, and the hydrophobic force. The hydrophobic force is represented by the single-exponential form,

$$\frac{F}{R} = -C\,exp\left(-\frac{h}{D}\right) \qquad [4.1]$$

where C and D are fitting parameters. The double-layer force was calculated using the surface potential of -40 mV for the OTS-coated silica surfaces, which was assumed to be the same as the ζ-potential measured in the present work using the Zetasizer Nano-ZS, Malvern. We found that the ζ-potentials did not change significantly with the OTS concentrations used in the present work for hydrophobization. It was found that contributions from van der Waals and double-layer forces were minimal as compared to those from hydrophobic forces.

4.4.3 Effect of Temperature on Hydrophobic Force

Figures 4.4-4.5 show the surface forces measured with OTS-coated silica surfaces in ultrapure water at temperatures in the range of 10 to 40°C. The objective of these measurements was to determine the thermodynamic functions of the macroscopic hydrophobic interactions, which may help better understand the origin(s) of the hydrophobic force. It has been shown previously that hydrophobic interactions entail decrease in the excess entropy of the TLFs, which lead to a conclusion that the water structure becomes more ordered in thin films than in thick films.

Parker *et al.*[11] reported the measurement of attractive forces between silica surfaces hydrophobized with (tridecafluoro,1,1,2,2,-tetrahydroxyoctyl)dimethylchorosilane at 41°C and room temperature (22°C). They found that the forces became stronger at the higher temperature, which was contrary to what was observed in the present work. The fluorinated surfaces exhibited advancing and receding contact angles of 110° and 90°, respectively, and the surfaces showed no crystallinity. The force curve obtained at the room temperature showed significant steps, which became stronger at the higher

temperature. Therefore, the authors attributed the increase in attractive force with temperature to the growth of bubble size, which should promote the bridging mechanism.

In the present work, two sets of force measurements were conducted, one with OTS-coated silica surfaces of θ_e = 92.5° and θ_e = 78.0°. If the bridging mechanism played a role, the result obtained at the higher contact angle would have been similar to what has been reported by Parker *et al.*[11]. The results were diametrically opposite. *First*, the force curves obtained at θ_e = 92.5° were smooth, as shown in Figure 4.4, providing no evidence for bridging nano-bubbles affecting the force measurement. *Second*, the measured forces decreased with increasing temperature. Further, the hydrophobic forces increased with increasing surface hydrophobicity. It appears, therefore, that the long-range attractions observed in the present work were due to hydrophobic interactions rather than to bridging bubbles.

The results obtained with surfaces with θ_e = 78.0° are presented in Figure 4.5. Again, the force curves were smooth without visible steps, and yet the forces were substantially stronger than the van der Waals force with a Hamaker constant of 0.8×10^{-20} J. It may be of interest to note here that the surface force measurements began at 10°C, and then stepped up to 20°C, 30°C, and 40°C. After the last set of measurements, the temperature was brought down to 20°C and the measurements were repeated. The results were reproducible indicating that the OTS-coated surface was stable in the range of temperatures where the measurements were conducted. It has actually been reported that OTS-coated surfaces are stable up to 175°C as measured by water contact angle[24].

Note that Figure 4.4 shows the data obtain at temperatures at 10, 20 and 30°C only. At 40°C, we saw some bubbles nucleating on the OTS-coated silica plate with θ_e = 92.5°, and the results were not very reproducible. Nevertheless, the force curves were smooth and showed no discontinuities or steps. In view of the difficulties with reproducibility, we decided not to include the results obtained at 40°C in the data set presented in Figure 4.4. We did not have this problem with the OTS-coated silica surfaces with θ_e = 78.0° as shown in Figure 4.5. Obviously, bubbles can more readily nucleate on the more hydrophobic surface, and the surface force measurements become irreproducible in the presence of bubbles.

The solid lines of Figures 4.4-4.5 represent the extended DLVO theory, with the hydrophobic forces represented by Eq. [4.1]. The *C* and *D* parameters used to fit the experimental data are plotted in Figure 4.6. As shown, both of these parameters decrease linearly with increasing temperatures (*T*), indicating that hydrophobic forces decrease with increasing temperature. The slopes of the *C vs. T* plots obtained at θ_e = 92.5° and 78.0° are about the same. The slopes of the *D vs. T* plots are also about the same, although the slope obtained at θ_e = 92.5° tends to be slightly steeper than that obtained at θ_e = 78.0°. The results presented in Figure 4.6 are similar to those reported by Wang *et al.*[1] with gold surfaces thiolated with C_2SH and $C_{16}SH$. These results are consistent with those reported by other investigators. Israelachvili and Pashley[36] showed that the hydrophobic forces measured between mica surfaces coated with CTAB by self-assembly decreased as the temperature was increased from 21 to 50°C. Tsao *et al.*[37] also showed that the attractive forces measured between mica surfaces hydrophobized by L-B deposited double-chain cationic surfactants decreased as the temperature was raised from 25 to 50°C.

Using the Derjaguin approximation[20], one can relate the surface force (*F/R*) measured at a separation distance *h* to the Gibbs free energy change per unit area (ΔG^f) as follows,

$$\frac{F}{R} = 2\pi\Delta G^{f} \qquad [4.2]$$

where

$$\Delta G^{\mathrm{f}} = -\int_{\infty}^{h} \Pi(h)dh \qquad [4.3]$$

as shown in Eq. [4.3], the free energy change is the same in magnitude as the work done in thinning an infinitely-thick plane-parallel film to a finite thickness h against the disjoining pressure $\Pi(h)$, which in turn is a function of film thickness. For a water film confined between two hydrophobic surfaces, the disjoining pressure should include contributions from the hydrophobic force as discussed above.

The partial differential of ΔG^{f} with respect to T at a constant pressure and film thickness allows us to calculate the change in the excess film entropy for moving a plane-parallel film from an infinite thickness to an h as follows,

$$\left(\frac{\partial \Delta G^{\mathrm{f}}}{\partial T}\right)_{\mathrm{p,h}} = \left(\frac{\partial\left(F/2\pi R\right)}{\partial T}\right)_{\mathrm{p,h}} = -\Delta S^{\mathrm{f}} \qquad [4.4]$$

in which ΔS^{f} is the change in excess entropy per unit area of the liquid film confined between two hydrophobic surfaces.

From Eqs. [4.1], [4.2] and [4.4], one obtains,

$$\Delta S^{\mathrm{f}} = -\frac{F}{2\pi R}\left(\frac{d\ln C}{dT} + \frac{h}{D}\frac{d\ln D}{dT}\right) \qquad [4.5]$$

which can be used to calculate the changes in excess film entropy (ΔS^{f}) at different film thicknesses using the surface force data, such as F/R, D, and the temperature coefficients for the C and D parameters given in Figure 4.6.

Figure 4.7 gives the values of ΔS^{f} in this manner from the surface force data obtained with OTS-coated silica surfaces with θ_{e} = 78.0° and 92.5°. The entropy change becomes increasingly negative with decreasing h, indicating that the entropy (S^{f}) of the TLF confined between two hydrophobic surfaces decrease with decreasing film thickness. As has been suggested previously[1], the low entropy may be due to structuring of the water molecules in the vicinity of hydrophobic surfaces. The vicinal water molecules must be of high free energy state as they cannot form *H*-bonds to the hydrophobic surface. This is akin to the case for the non-*H*-bonded water molecules at the air/water and hydrocarbon-water interfaces being responsible for high interfacial tensions[38]. One way to expend the excess free energy would be to form structures, in which the 'frustrated' vicinal water molecules form stronger *H*-bonds with neighbors by taking advantage of the cooperative bonding mechanism first recognized by Frank and Wen[39] and used to explain the mechanism of hydrophobic hydration. It has been shown that the O-O distance between water molecules decreases with increasing number of water molecules in a structure (or cluster)[40]. The structure can be coplanar or concave (or clathrate-like) depending upon the temperature, pressure, and dissolved species[41,42]. It may be reasonable to assume that the clusters become larger and more abundant when water is confined in a TLF formed between very hydrophobic surfaces. Recent spectroscopic studies conducted in bulk water showed that water molecules can form low-density liquid (LDL) species more readily than previously thought to be possible[43-46]. These clusters may be collectively referred to as 'partial clathrates.' Clathrates are found in supercooled water or at high pressures and lower temperatures particularly in the presence of dissolved hydrophobic solutes[41,42].

Figure 4.7 shows also that ΔS^f becomes more negative with increasing hydrophobicity and decreasing temperature. The former may be due to the likelihood that the number of non-*H*-bonded water molecules increases with increasing surface hydrophobicity, while the latter can be attributed to the low kinetic energies of the water molecules at a low temperature and hence increased propensity to form clusters.

One can readily obtain ΔG^f from the surface force data using the Derjaguin approximation (Eq. [4.2]). From the values of ΔG^f and ΔS^f, the excess film enthalpy per unit area (ΔH^f) can be determined as follows,

$$\Delta H^f = \Delta G^f + T\Delta S^f \qquad [4.6]$$

Figure 4.8 shows the changes in ΔH^f determined in this manner. As shown, the enthalpy change associated in forming *H*-bonded structures becomes more negative with decreasing *h* and *T*. This finding suggests that both the number and size of the clusters increase with decreasing film thickness. Further, the strength and life time of the clusters may also increase as film becomes thinner. Figure 4.8 shows also that the enthalpy change becomes more negative as the confining surfaces become more hydrophobic and the temperature is lowered. As has been the case with the entropy change, the former may be related to the increased number of non-*H*-bonded water molecules, while the latter to decreased kinetic energies of water molecules.

The values of ΔG^f, $T\Delta S^f$ and ΔH^f determined in the manner described above are presented in Figure 4.9. These values represent the changes in the thermodynamic functions involved in the macroscopic hydrophobic interactions between the OTS-coated silica surfaces with θ_e = 78.0° and 92.5°C at 20°C. Note that at both contact angles $|\Delta H^f| > |T\Delta S^f|$, which is a necessary condition for the hydrophobic force to be attractive when both enthalpy and entropy changes are negative. The enthalpy term represents the free energy gained in building the structures, while the entropy ($T\Delta S^f$) term representing the thermodynamic cost for building structures. As a result of the enthalpy-entropy tradeoff, the hydrophobic forces in general are weak and are difficult to be measured. As noted by Eriksson *et al.*[19], the excess free energy per molecule related to the long-range attractions is in the range of 10^{-5} to 10^{-3} kT, while the energy of a hydrogen bond is about 7 kT. Note also that ΔG^f is more negative at the higher contact angle, which can be attributed to more negative ΔH^f.

The condition that $|\Delta H^f|$ be larger than $|T\Delta S^f|$ for macroscopic hydrophobic interactions is opposite to what is generally known for molecular-scale hydrophobic interactions or hydrophobic effect. For the latter, it is necessary that $|\Delta H^f| < |T\Delta S^f|$ for two hydrophobic molecules to attract each other as in self-assembly. It is generally accepted that the inequality arises from the entropy increase associated with the release of the water molecules surrounding hydrophobic moieties of high curvatures. The basic difference between the macroscopic- and molecular-scale hydrophobic interactions is due to the differences in curvatures of the surfaces involved, as discussed by Chandler[42].

The authors of this communication showed recently that long-range attractions are also observed in short-chain alcohols such as methanol, enthanol, and butabol–all well-known *H*-bonding liquids[47]. It has been suggested that the origin of the long-range attractions observed in these short-chain alcohols is the same as the hydrophobic forces observed in water, *i.e.*, structure formation. It was found also that the long-range attractions become stronger as the confining surfaces become more hydrophobic. The same has been observed in the present work with water as *H*-bonding liquid. It may be suggested, therefore, that hydrophobic force is the consequence of an *H*-bonding liquid striving to minimize free energy when it cannot form *H*-bonds to confining surfaces. Conversely, a key to increasing hydrophobic force is to eliminate *H*-bond sites from the confining surfaces.

There have been long-standing controversies concerning the origin of the hydrophobic force since Israelachvili and Pashley[4] published a seminal paper in 1982. It is hoped that the results presented in this communication have provided a basis for the hydrophobic force be recognized as a thermodynamic force rather than an artifact due to bubbles or cavities.

4.5 References

(1) Wang, J.; Yoon, R.-H.; Eriksson, J. C. *J. Colloid Interface Sci.* **2011**, *364*, 257.
(2) Xu, Z.; Yoon, R.-H. *J. Colloid Interface Sci.* **1989**, *132*, 532.
(3) Xu, Z.; Yoon, R.-H. *J. Colloid Interface Sci.* **1990**, *134*, 427.
(4) Israelachvili, J.; Pashley, R. *Nature* **1982**, *300*, 341.
(5) Christenson, H. K.; Claesson, P. M. *Adv. Colloid Interface Sci.* **2001**, *91*, 391.
(6) Meyer, E. E.; Rosenberg, K. J.; Israelachvili, J. *Proc. Natl. Acad. Sci. U. S. A.* **2006**, *103*, 15739.
(7) Yoon, R. H.; Ravishankar, S. A. *J. Colloid Interface Sci.* **1994**, *166*, 215.
(8) Rabinovich, Y. I.; Guzonas, D. A.; Yoon, R. H. *J. Colloid Interface Sci.* **1993**, *155*, 221.
(9) Rabinovich, Y. I.; Guzonas, D. A.; Yoon, R. H. *Langmuir* **1993**, *9*, 1168.
(10) Yoon, R. H.; Ravishankar, S. A. *J. Colloid Interface Sci.* **1996**, *179*, 391.
(11) Parker, J. L.; Claesson, P. M.; Attard, P. *J. Phys. Chem.* **1994**, *98*, 8468.
(12) Tyrrell, J. W. G.; Attard, P. *Phys. Rev. Lett.* **2001**, *87*, 176104.
(13) Sakamoto, M.; Kanda, Y.; Miyahara, M.; Higashitani, K. *Langmuir* **2002**, *18*, 5713.
(14) Meyer, E. E.; Lin, Q.; Israelachvili, J. N. *Langmuir* **2005**, *21*, 256.
(15) Hammer, M. U.; Anderson, T. H.; Chaimovich, A.; Shell, M. S.; Israelachvili, J. *Faraday Discuss.* **2010**, *146*, 299.
(16) Derjaguin, B. V.; Kusakov, M. M. *Izv. Akad. Nauk SSSR, Ser. Khim.* **1936**, *5*, 741.
(17) Derjaguin, B. V.; Churaev, N. V. *Langmuir* **1987**, *3*, 607.
(18) Churaev, N. V.; Derjaguin, B. V. *J. Colloid Interface Sci.* **1985**, *103*, 542.
(19) Eriksson, J. C.; Ljunggren, S.; Claesson, P. M. *J. Chem. Soc., Faraday Trans. II* **1989**, *85*, 163.
(20) Derjaguin, B. V. *Kolloid. Zeits.* **1934**, *69*, 155.
(21) Li, Y.; Huang, J.; McIver, R. T.; Hemminger, J. C. *J. Am. Chem. Soc.* **1992**, *114*, 2428.
(22) Schoenfisch, M. H.; Pemberton, J. E. *J. Am. Chem. Soc.* **1998**, *120*, 4502.
(23) Dasog, M.; Scott, R. W. J. *Langmuir* **2007**, *23*, 3381.
(24) Ashurst, W. R.; Yau, C.; Carraro, C.; Maboudian, R.; Dugger, M. T. *J Microelectromech S* **2001**, *10*, 41.
(25) Rabinovich, Y. I.; Yoon, R. H. *Langmuir* **1994**, *10*, 1903.
(26) Yoon, R. H.; Flinn, D. H.; Rabinovich, Y. I. *J. Colloid Interface Sci.* **1997**, *185*, 363.
(27) Ishida, N.; Kinoshita, N.; Miyahara, M.; Higashitani, K. *J. Colloid Interface Sci.* **1999**, *216*, 387.
(28) Ishida, N.; Sakamoto, M.; Miyahara, M.; Higashitani, K. *Langmuir* **2000**, *16*, 5681.
(29) Cleveland, J. P.; Manne, S.; Bocek, D.; Hansma, P. K. *Rev. Sci. Instrum.* **1993**, *64*, 403.
(30) Flinn, D. H.; Guzonas, D. A.; Yoon, R. H. *Colloid Surf., A* **1994**, *87*, 163.
(31) Carim, A. H.; Dovek, M. M.; Quate, C. F.; Sinclair, R.; Vorst, C. *Science* **1987**, *237*, 630.
(32) Tillman, N.; Ulman, A.; Schildkraut, J. S.; Penner, T. L. *J. Am. Chem. Soc.* **1988**, *110*, 6136.
(33) Mao, M.; Zhang, J. H.; Yoon, R. H.; Ducker, W. A. *Langmuir* **2004**, *20*, 4310.
(34) Wang, M. J.; Liechti, K. M.; Wang, Q.; White, J. M. *Langmuir* **2005**, *21*, 1848.
(35) Zhang, J. H.; Yoon, R. H.; Eriksson, J. C. *Colloid Surf., A* **2007**, *300*, 335.
(36) Israelachvili, J. N.; Pashley, R. M. *J. Colloid Interface Sci.* **1984**, *98*, 500.
(37) Tsao, Y. H.; Yang, S. X.; Evans, D. F.; Wennerstrom, H. *Langmuir* **1991**, *7*, 3154.
(38) Du, Q.; Freysz, E.; Shen, Y. R. *Science* **1994**, *264*, 826.
(39) Frank, H. S.; Wen, W.-Y. *Discuss. Faraday Soc.* **1957**, *24*, 133.
(40) Liu, K.; Cruzan, J. D.; Saykally, R. J. *Science* **1996**, *271*, 929.
(41) Stillinger, F. H. *Science* **1980**, *209*, 451.

(42) Chandler, D. *Nature* **2005**, *437*, 640.
(43) Mallamace, F.; Branca, C.; Broccio, M.; Corsaro, C.; Mou, C. Y.; Chen, S. H. *Proc. Natl. Acad. Sci. U. S. A.* **2007**, *104*, 18387.
(44) Mallamace, F.; Corsaro, C.; Broccio, M.; Branca, C.; Gonzalez-Segredo, N.; Spooren, J.; Chen, S. H.; Stanley, H. E. *Proc. Natl. Acad. Sci. U. S. A.* **2008**, *105*, 12725.
(45) Mallamace, F. *Proc. Natl. Acad. Sci. U. S. A.* **2009**, *106*, 15097.
(46) Mishima, O.; Stanley, H. E. *Nature* **1998**, *396*, 329.
(47) Wang, J.; Li, Z.; Yoon, R.-H.; Eriksson, J. C. *J. Colloid Interface Sci.* **2012**.

Table 4.1 Water Contact Angles and Surface Roughness of the Silicon Wafer Surfaces Treated in a 5×10^{-5} M OTS Solution at Different Contact Times

Contact Time (min)	Contact Angle (°)			Contact Angle Hysteresis (°)	Surface Roughness (nm)
	θ_e	θ_a	θ_r		
20	30	35	25	10.0	0.18
200	80	85	67.5	17.5	0.46
380	93	98	88	10.0	0.22
720	101	104	95	9.0	0.11

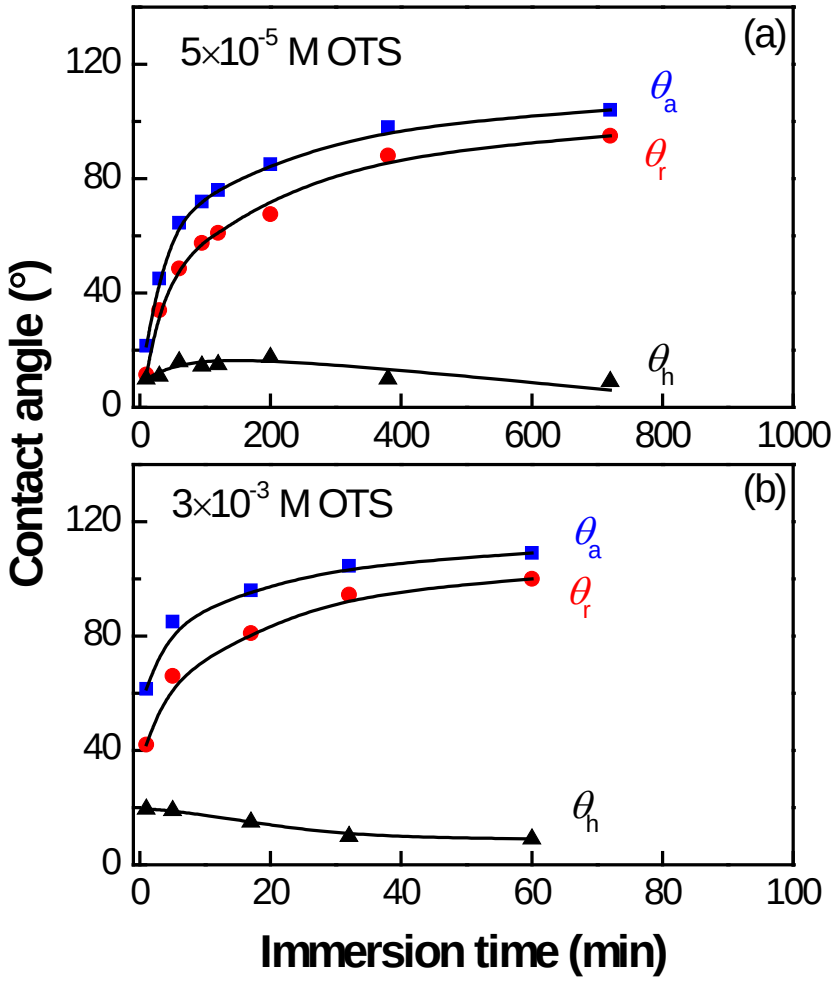

Figure 4.1 Effects of immersion time on the water contact angles of silicon wafer in a) 5×10^{-5} M and b) 3×10^{-3} M OTS-in-toluene solutions. θ_a and θ_r represent advancing and receding angles. The contact angle hysteresis (θ_h) decreases with time indicating formation of smoother OTS monolayers. OTS adsorbs much faster at the higher concentration.

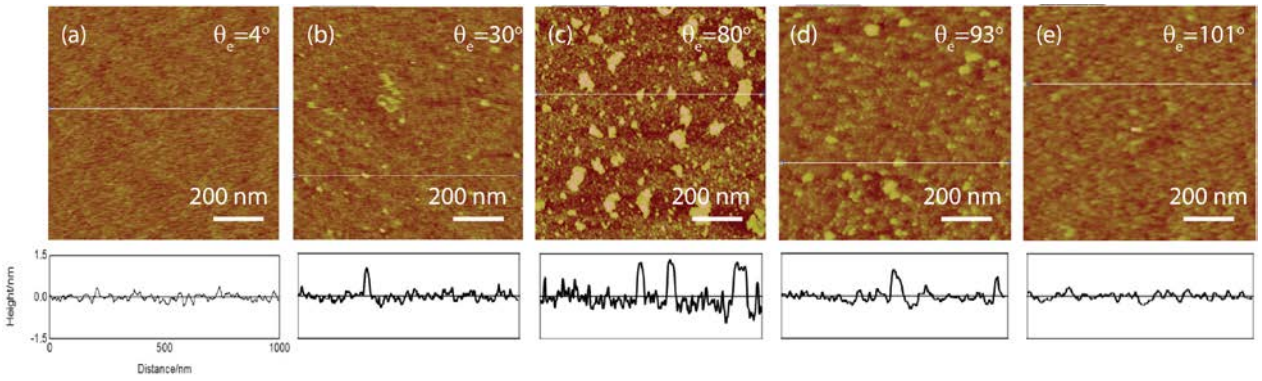

Figure 4.2 Contact mode 1×1 μm AFM images of the silicon wafers of different equilibrium contact angles. a) bare surface with θ_e = 4°, b-e) surfaces with different θ_e values as obtained by varying the immersion times in a 5×10^{-5} M OTS solution. Height profiles given below each image were obtained along the white line across the image. OTS adsorbs in patches, which coalesce to obtain a smooth monolayer.

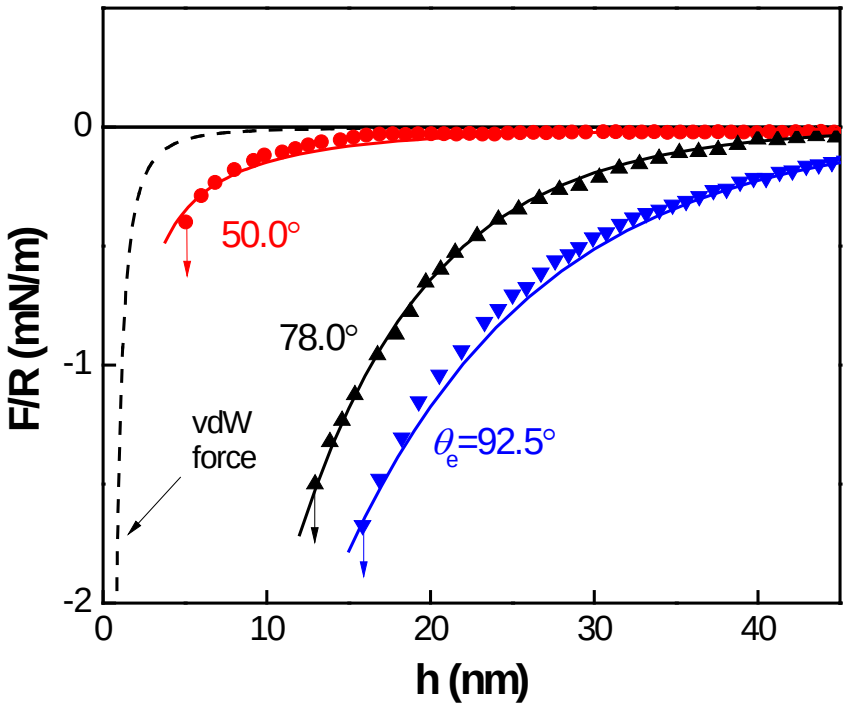

Figure 4.3 Surface forces (F) normalized by the radius (R) of spheres *vs*. the closest separation distance (h). The surfaces were treated in a 5×10^{-5} M OTS solution for different times to obtain different contact angles. Solid lines represent the extended DLVO plots with ψ_1 = -40 mV and $A_{131} = 0.8\times10^{-20}$ J. The double-layer and van der Waals forces are negligibly small particularly at longer separations. Thus, the measured forces practically represent the hydrophobic forces, which are shown to increase with θ_e. The arrows represent the separations at which two surfaces jumped into contact.

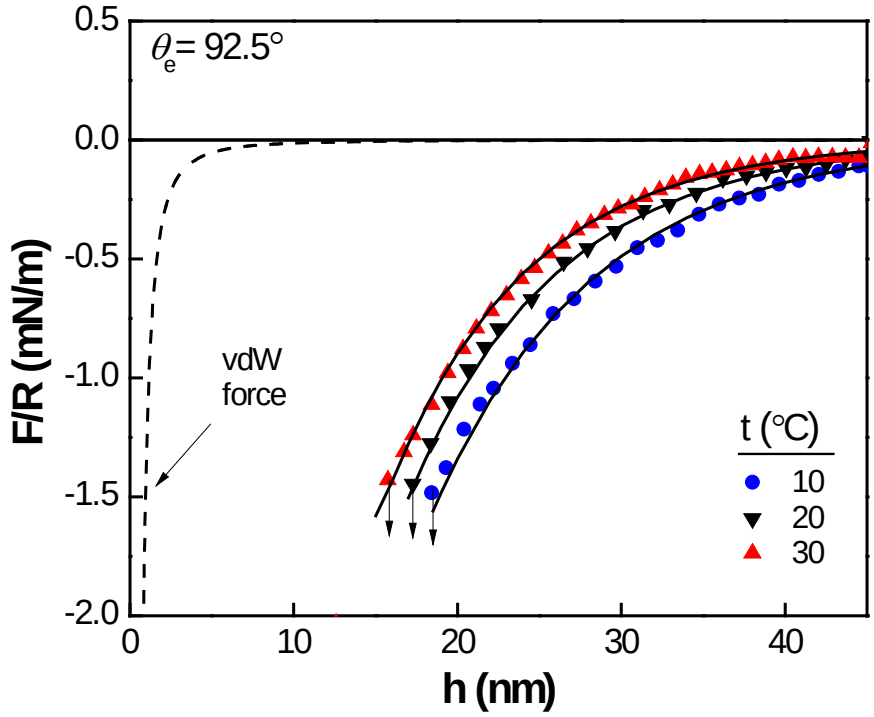

Figure 4.4 Surface forces (F) measured at different temperatures in the range of 10 to 30 °C and normalized by the radius of sphere (R) *vs*. separations (h). The silica surfaces were treated in a 5×10^{-5} M OTS solution to obtain θ_e = 92.5°. The measured forces became stronger and longer-ranged with decreasing temperature of the medium.

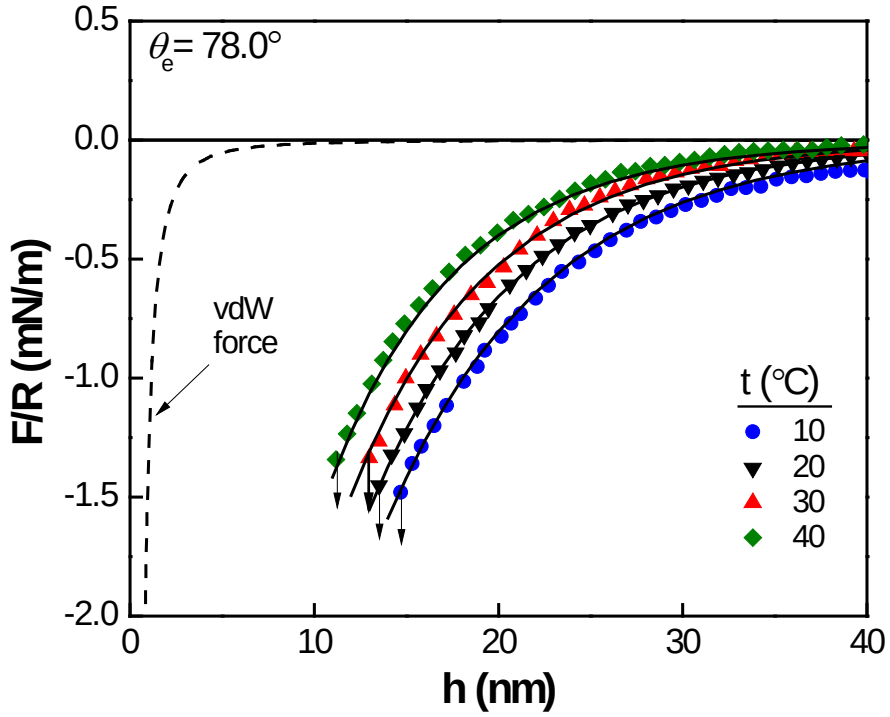

Figure 4.5 Surface forces (F) measured at different temperatures in the range of 10 to 40°C and normalized by the radius of sphere (R) *vs*. separations (h). The silica surfaces were treated in a 5×10^{-5} M OTS solution to obtain θ_e = 78°. The measured forces became stronger and longer-ranged with decreasing temperature of the medium.

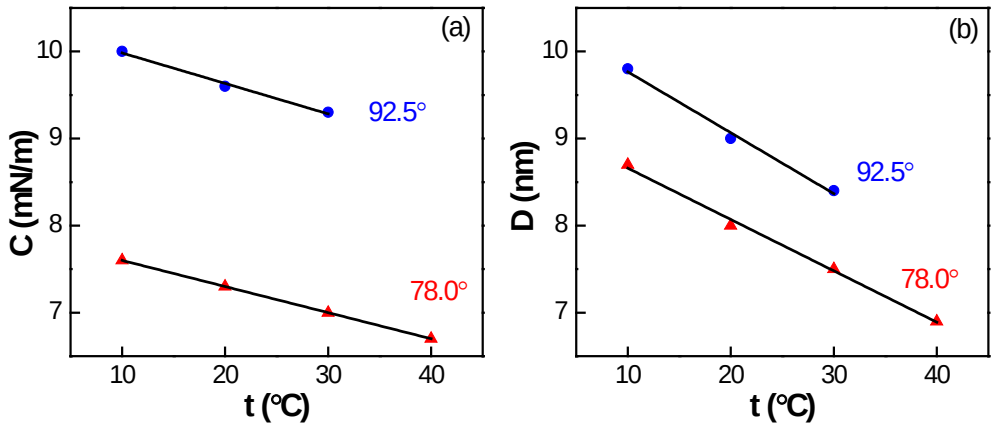

Figure 4.6 a) *C vs*. t and b) *D vs*, t plots. The C and D parameters of the hydrophobic force represented by Eq. [4.1] were obtained by fitting the experimental data presented in Figures 3. 4-3.5 to the extended DLVO theory with ψ_1 = -40 mV and $A_{131} = 0.8\times10^{-20}$ J.

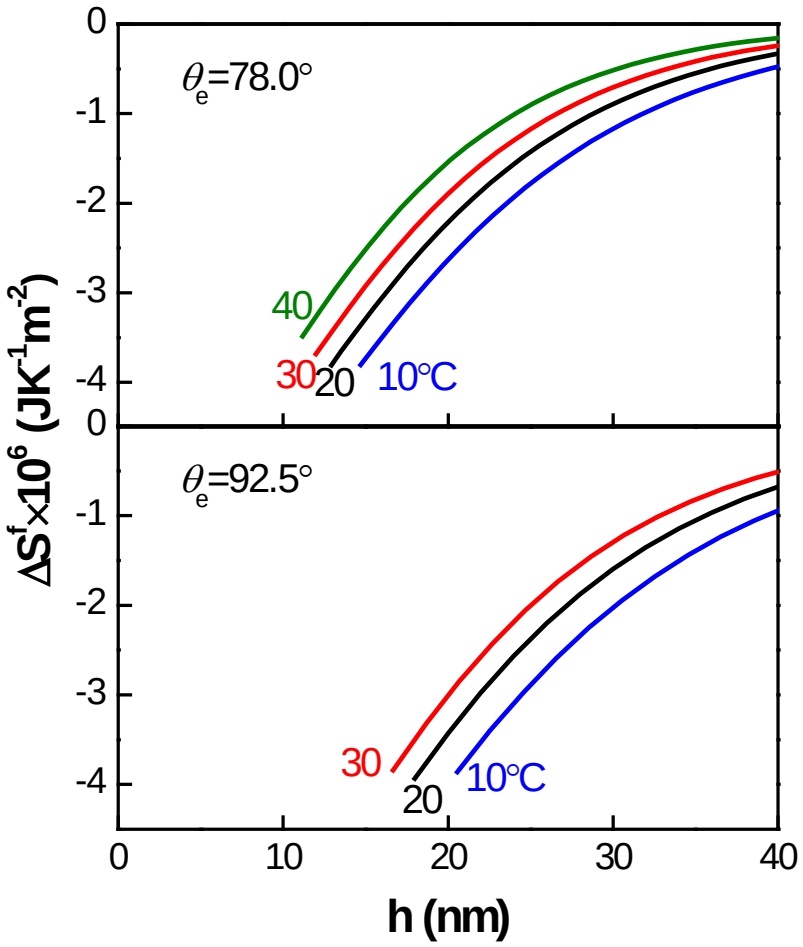

Figure 4.7 Changes in excess film entropy (ΔS^f) in the thin films of water between OTS-coated silica surfaces with contact angles of 78.0° and 92.5° at different medium temperatures.

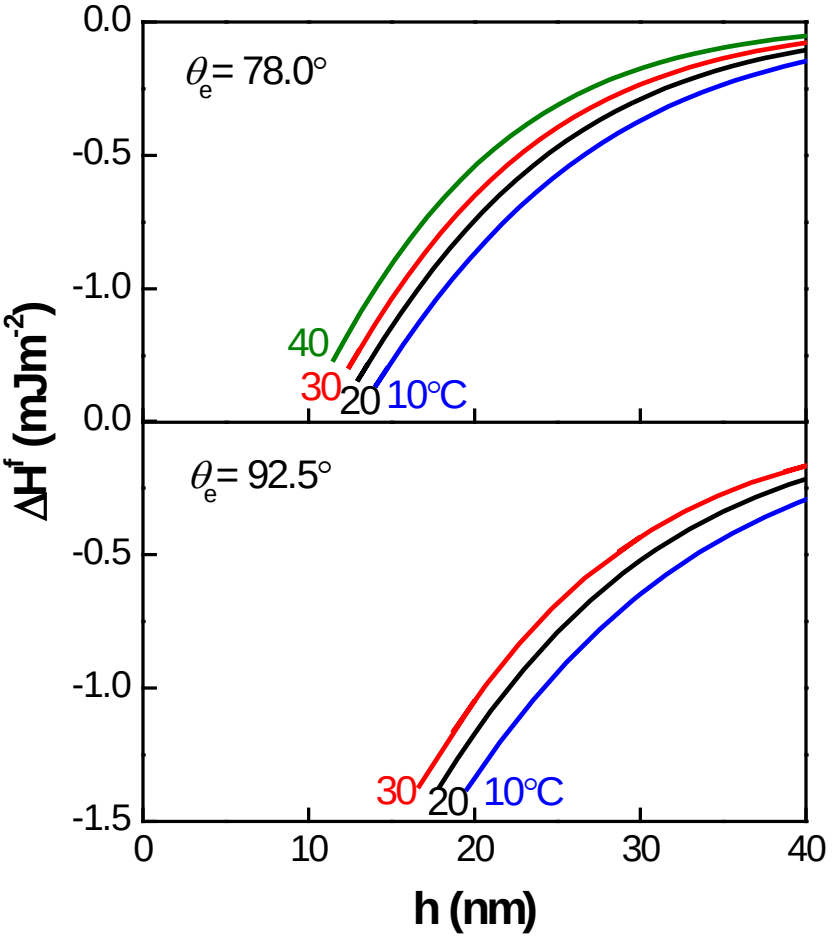

Figure 4.8 Changes in excess film enthalpy (ΔH^f) in the thin films of water between OTS-coated silica surfaces with contact angles of 78.0° and 92.5° at different medium temperatures.

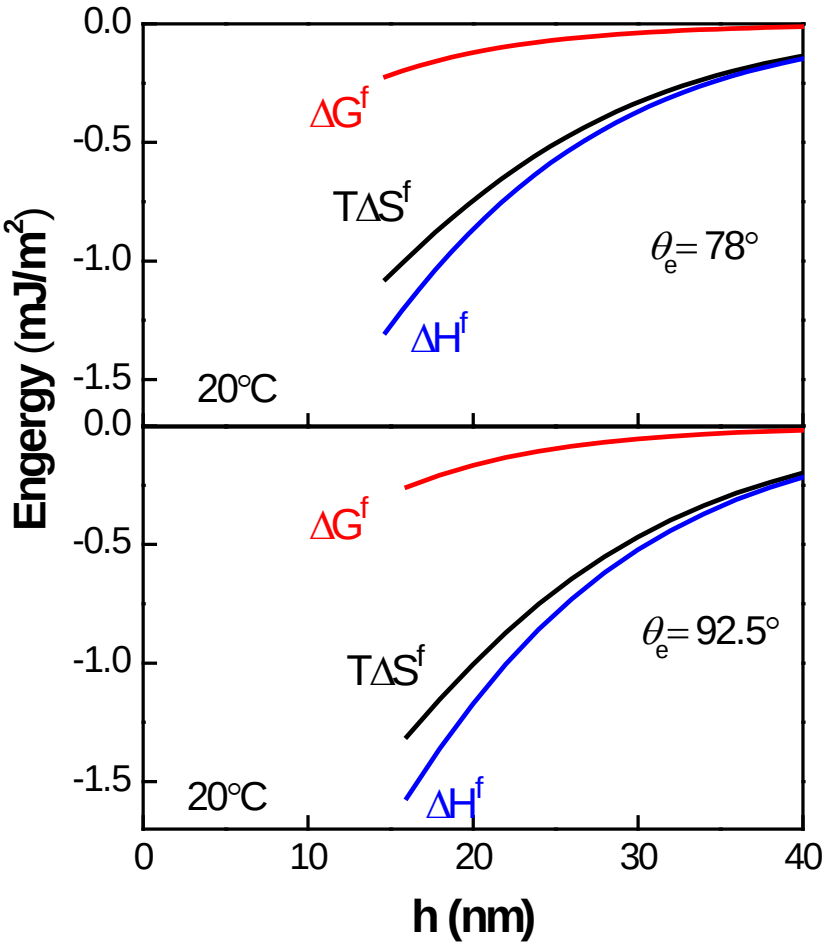

Figure 4.9 Changes in the excess thermodynamic properties for the thin liquid films between OTS-coated silica surfaces with θ_e = 78.0° and 92.5° at 20°C.

CHAPTER 5

Temperature Dependence of Surface Forces between Silica Surfaces in Octadecyltrimethylammonium Chloride Solution

5.1 Abstract

Hydrophobic forces between thiolated gold surfaces[1] and silylated silica surfaces[2] are believed to originate from the structuring of water confined by hydrophobic surfaces, as indicated by a decrease in hydrophobic forces at higher temperatures, accompanied by a less negative value for the change of excess entropy (ΔS^f). In the present work, AFM surface force measurements were carried out at temperatures in the range of 10 to 40°C between silica surfaces in solutions of octadecyltrimethylammonium chloride (C_{18}TACl). Long-range attractive forces were detected between these silica surfaces coated with physically adsorbed cationic surfactants. Furthermore, the measured forces were observed to decrease with increasing temperature, which is in agreement with the results found between chemisorbed surfaces[1]. Moreover, thermodynamic calculations confirmed that ΔS^f decreased when the two surfaces approach each other or when the temperature was decreased. Thermodynamic analysis of SFA force measurements[3] obtained at various temperatures revealed that ΔS^f was more negative at shorter ranges as compared to longer ranges. The results indicate that hydrophobic forces observed between surfaces coated with physically adsorbed surfactants may also be linked to changes in water structure, and this effect becomes more significant when the two hydrophobic surfaces are closer together.

5.2 Introduction

Two methods are typically used for preparing hydrophobic surfaces[4]: L-B films deposited on mica[5], or surfactant films adsorbed to mica from cyclohexane[3]. Both of these techniques give rise to strong attractive force with both short-range and long-range components as detected by SFA[3]. Additionally, the following methods enhance the stability of the hydrophobic surfaces: (1) via polymerized L-B deposited on mica[6], (2) by creating hydrophobic surfaces of silylated silica and mica[7], (3) via thiol self-assembling on gold[8]. The last one, on the other hand, may produce less stable hydrophobic surfaces by preparing surfaces through the in-situ adsorption of surfactants. As noted by Christenson[4], the particular preparation method can give rise to specialized surface features, as indicated by direct surface force measurements. Important to this study is the fact that researchers have not always agreed on whether the origin of hydrophobic forces can be attributed to the formation of cavities or the bridging of nanobubbles[9,10], to electrostatic origin[11], or to the structuring of water[12]. Thus, investigating the forces measured between different types of hydrophobic surfaces may be helpful in solving the controversy.

The influence of temperature on hydrophobic interactions has been carried out between thiolated gold surfaces[1] by means of atomic force microscope (AFM). Specifically, the hydrophobic interactions between these surfaces using chemisorbed surfactants were found to decrease with increasing temperature, which was accompanied by a less negative value for the excess film enthalpy (ΔS^f). Follow-up studies were conducted using more stable silylated silica surfaces due to the concern that the thiolated gold surfaces may oxidize to alkane sulfonates under ambient conditions upon exposure to air[13,14]; in contrast, OTS-coated silica surfaces have been shown to be stable at temperatures up to 175°C[15]. Force measurement results for the OTS-coated silica surfaces were comparable to those obtained for the thiolated surfaces. In summary, studies have indicated that long-range attractive forces may be attributed to the structuring of water induced by the hydrophobic surfaces.

Conversely, surfactant in situ adsorption surfaces are not typically as hydrophobic in comparison to electrically-neutral L-B deposition monolayer surfaces; additionally, the contact angle of the former (<90°) tends to be smaller than the latter (>90°)[16]. However, researchers have shown that a neutral monolayer is formed under optimal conditions—namely, when incomplete or additional adsorption can be avoided by using a specific concentration[17], which gives rise to highly hydrophobic surfaces[18]. The attractive force between neutral mica surfaces with double-chained alkylammonium acetate adsorbed[19] from water solution is much stronger than the van der Waals force and is extended to a separation distance of 10 nm. Moreover, the attractive force is very sensitive to hydrophobicity, which is attributed to the structure of water that results from surface hydrophobicity. In fact, macroscopic hydrophobic surface induced hydrogen bonding is believed to extend farther than the structuring of water in the vicinity of hydrophobic molecules[19].

The present work was designed to study the influence of temperature on measured force using a surface well known to be less stable—namely, a silica surface hydrophobized by in-situ adsorption of C_{18}TACl. Hydrophobic interactions between these surfaces were found to decrease in the same manner that the forces between thiolated[1] and silylated surfaces were observed to do. Thermodynamic analysis results confirmed that both the change of excess film entropy (ΔS^f) and of the excess film enthalpy (ΔH^f) is more negative with decreasing temperature, suggesting that a more structured phase of water had formed under the same conditions, even between the physical adsorption surfaces.

However, controversy persists regarding whether the hydrophobic forces in different ranges (*i.e.*: short-range and long-range) are due to different mechanisms. Some investigators, who observed intact short-range force and disappearance of long-range attraction upon removal of dissolved gas in water, proposed two distinct force regimes for the hydrophobic interaction forces. Most recently, Hammer *et al.*[20] tried to explain the hydrophobic force by a three-regime force-law: form 10-20 nm to 100 nm, the

force is due to electrostatic attractions and/or bridging vapor cavities; in the range of 1.5-15 nm, the "pure" attractive force is attributed to the enhanced Hamaker constant; while the attractions below 1.5 nm is ascribed to *H*-bond associated water structuring. Therefore, the hydrophobic forces in different ranges were supposed to be caused by different mechanisms. On the other hand, the disjoining pressure determined by thin film pressure balance (TFPB) technique indicated that while the short-range hydrophobic force is in charge of film rupture, the long-range hydrophobic force which speeds up the film thinning is also essential. Additionally, dependence of hydrophobic force on temperature was observed in both short-range and long-range, with the effect in the previous range much more significant compared to the latter one[3].

Through the use of surface forces apparatus (SFA), it is possible to obtain surface force composed of both short-range and long-rang components. L-B depositions of dimethyldioctadecyl-ammonium bromide (DDOA) monolayers on smooth mica[3] were confirmed to be tightly packed as revealed by X-ray photoelectron spectroscopy, with the thickness of the deposition constant (2 nm) in both air and water. The SFA surface force[3] measured between the prepared hydrophobic surfaces over a temperature range of 25-50°C was approximated using the double exponential function. Results revealed no detectable double-layer force due to the very small surface charge. The influence of temperature on resulting force measurements is not consistent with cavitation mechanisms or bridging nanobubbles[9], which suggested an increase of attractive force upon increasing temperatures. On the other hand, observed decreases in force with increasing temperature agrees well with predictions of water structuring[12]. Additionally, the greater effect of temperature on the short-range components in comparison with the long-range component was observed. Thermodynamic analysis of the hydrophobic interaction revealed the molecular orientational preferences of thin water film was more significant when the water film is thinner.

5.3 Experimental

5.3.1 Materials

Ultrapure water with a resistivity of 18.2 MΩ·cm at 25°C was produced using a Millipore Direct-Q3 water purification system (Millipore, MA). The surfactants octadecyltrimethylammonium chloride (C_{18}TACl) from TCI was recrystallized twice by acetone from ethanol before using. Silica spheres (Whitehouse Scientific) with radius of ~10 μm and fused-quartz plates (Technical Glass Products Inc.) were used for force measurements. H_2SO_4 (98% purity, VMR international) and H_2O_2 (29.0-32.0% purity, Alfa Aesar) were used to rinse the silica plates and spheres.

5.3.2 Cleaning of Quartz Plate and Silica Spheres

Quartz plates were boiled in a piranha solution (H_2O_2/H_2SO_4, 3:7 by volume) at ~120°C for 1 hour, rinsed with ultrapure water in an ultrasonic bath for 5 minutes, and then blown dry with nitrogen before using. The silica spheres were rinsed by the same method but collected with filter paper, then dried in a fume hood and placed in a sealed glass vial for further use.

5.3.3 Surface Force Measurements

A Nanoscope IV atomic force microscope (AFM) was utilized to obtain the surface force measurements between the quartz plate and silica sphere according to the colloid probe technique[21] at various temperatures. Silicon nitride AFM probes from Nano World with a spring constant of ~0.48 N/m were applied, which were calibrated using the resonant frequency technique[22]. A cleaned silica sphere was attached to the tip of the calibrated cantilever with a polymer resin (EPON-1004F, Shell Chemical Co.). The diameter of the sphere was measured using an Olympus BH-2 microscope. A probe with a

sphere was then fixed in the AFM liquid cell. The quartz plate was placed on the heater/cooler element that was attached on the top of scanner "J". A Digital Instrument Thermal Applications Controller (TAC) was utilized to set and control the temperature of the liquid in the AFM cell. Typically, a 10°C rise in temperature took about 10 minutes in the temperature range of 10°C to 40°C. 5×10^{-6} M C_{18}TACl was injected into the cell to initiate the hydrophobization of the silica plate and sphere at 10°C, then ramped up to higher temperatures. All force measurements were obtained after the temperature equilibrium was obtained. Measured force (F) normalized by the radius of sphere (R) was calculated versus the distance between sphere and plate.

5.4 Results and Discussion

5.4.1 Temperature Dependence of Long-range Attraction

The stability of the physisorption-surface was an issue for the detection of temperature effect on the hydrophobic force. Therefore, the steadiness of the measured surface force at the same temperature was assessed over a temperature range of 10-40°C. Representative results at 10°C and 20°C are presented in Figures 5.1-5.2. The hydrophobization of the silica plate and sphere was initiated at 10°C once a solution of 5×10^{-6} M C_{18}TACl was injected into the AFM liquid cell. As shown in Figure 5.1, long-range attractive force was initially detected at the 5-minute mark, after which it increased until 20-minute mark, at which point it remained very stable for up to 90 min. Then the temperature was stepped to 20°C, the adsorption equilibrium was achieved in only 5 minutes, and the force was stable for up to 40 min or even longer (Figure 5.2). Temperatures were further increased to 30, 35 and 40 °C sequentially to assess force stability, with similar outcomes. Thus, long range attraction was found to be stable at the same temperatures and for long immersion times. Additional adsorption is unlikely to occur after a complete monolayer or adsorption equilibrium is formed, even after an extended period of time.

Although either incomplete or additional adsorption associated with in-situ adsorption typically results in shorter-range attractive forces in comparison to L-B deposition techniques, in-situ adsorption can still give rise to comparably strong forces as long as optimum conditions are satisfied[17]. The strongest attractive forces have been identified between surfaces hydrophobized by in-situ adsorption of surfactants with a concentration around the p.c.n.[4,11,18,23]. The concentration of 5×10^{-6} M used the present work for the C_{18}TACl solution is also close to the p.c.n.[24], as proven by the strong long-range attractive force shown in Figures 5.1-5.2. The measured force is much stronger than the van der Waals force (dashed line), which was calculated with a Hamaker constant value of 0.8×10^{-20} J[24]. Continuous force curves, *i.e.*, without a step, do not support the possible bridging of nanobubbles[9]. In fact, refractive index values as detected by ellipsometry have revealed the absence of air bubbles on the C_{18}TA-adsorbed silica surfaces[24]. In addition, the contact angles of surfaces prepared with long-chained C_{18}TACl have been shown to be lower than 60°[24], which is much smaller than the lower limit for the thermodynamic formation of cavities. In fact, the survival of long-range attractive force in degassed C_{18}TACl solution[24] proved that the measured force did not originate from the bridging of nanobubbles. Instead, the long-range attractive forces between CnTACl (n=12-18) adsorbed surfaces were found to be associated with surface hydrophobicity measured by contact angles, which is related to chain length of the surfactant[25].

Depending on the stability of the long range attraction at the same temperature as measured between silica surfaces in a solution of 5×10^{-6} M C_{18}TACl, AFM studies were conducted to determine the influence of temperature on the attraction. As shown in Figure 5.3, attractive forces were strongly evident across the entire temperature range from 10-40°C without any discontinuities on the force curves. Although the measured forces decreased with increasing temperature, the weakest one, which was obtained at 40°C, was still much stronger than the van der Waals force. This finding corresponds to the reported results obtained in studies of silylated surfaces[2] and thiolated gold surfaces[1]. The measured

forces were then fitted to extended DLVO theory—with hydrophobic force described by a single exponential force law, as represented in the following equation:

$$\frac{F}{R} = -C\exp(-\frac{h}{D}) \qquad [5.1]$$

where the hydrophobic force (F) is normalized by the radius of the silica sphere (R), h is the closest separation distance between the silica sphere and silica plate, C represents the magnitude of the force, and D is the decay length. The fitting parameters of C and D are shown in Figure 5.4. The decrease of C and D along with temperature increments corresponds to the diminution of hydrophobic force as a function of temperature.

The force data (Figure 5.3) obtained at various temperatures was subsequently used for the thermodynamic analysis of hydrophobic interactions to clarify the relation between the measured force and the properties of the confined liquid, as described by Wang *et al.*[1]. The measured forces normalized by R at a separation distance of h are related to changes in the Gibbs free energy per unit area (ΔG^f), as well as changes in the surface tension ($\Delta\gamma^f$) of the thin liquid films according to the Derjaguin approximation[26] as follows:

$$\frac{F}{2\pi R} = \gamma^f - \gamma^{f,\infty} = \Delta\gamma^f = \Delta G^f \qquad [5.2]$$

where $\Delta\gamma^f$ equals γ^f (the film tension of the planar water film with thickness h) minus $\gamma^{f,\infty}$ (the film tension at infinite separation), $\Delta\gamma^f$ represents the change in excess film tension when two surfaces approach each other from infinite distance to a given distance of h. The partial differential of $\Delta\gamma^f$ with respect to temperature (T) at constant pressure (P) and distance (h) is related to changes in excess film entropy, as reflected in the following equation:

$$\left(\frac{\alpha\Delta\gamma^f}{\partial T}\right)_{P,h} = -\Delta S^f \qquad [5.3]$$

where ΔS^f is the change in excess film entropy per unit area. Thus, the following equation is obtained:

$$\Delta S^f = -\Delta\gamma^f(\frac{d\ln C}{dT} + \frac{h}{D}\frac{d\ln D}{dT}) \qquad [5.4]$$

which was then used to calculate ΔS^f based on the results from the force measurements obtained at various temperatures.

Figure 5.5 presents ΔS^f as a function of temperature, as calculated from the force data obtained earlier (Figure 5.3). As illustrated, ΔS^f results became increasingly negative as the distance between the two hydrophobic surfaces became smaller and the confined thin water film became thinner. As is well known, entropy represents a critical thermodynamic property for measuring the degree of structuring of a system in solution[27]; for example, low entropy is representative of more structured aqueous films[1]. Correspondingly, aqueous films become more structured when compressed by two hydrophobic surfaces. On the other hand, when less negative ΔS^f values are noted with increasing temperature, one can assume that the structuring of water has been adversely affected by high temperature. As suggested by Laskowski and Kitchener[28], hydrophobic influences associated with the rupture of the wetting films around methylated particles are likely related to the instability of the water structure in the vicinity of the

hydrophobic surface. Similarly, stronger hydrophobic forces at low temperature (Figure 5.3) are probably correlated with more structured water under the same experimental conditions.

Hydrophobicity is featured with the growth of free OH-bonds in the confined water film[29]. Just like nonpolar solutes which fail to form *H*-bond with the neighboring water molecules[30], the macroscopic hydrophobic surfaces cannot readily hydrogen bond to the water molecules in the vicinity neither. As a result, the water film confined by hydrophobic surfaces experiences an increase in free energy[29]. In order to return to a low free energy state, the "frustrated" water molecules bond to their neighboring water molecules and become more stable. Once a first *H*-bond is formed, the charge distribution involved in the monomers transforms to result in: previous *H* acceptor growing to be better *H* donor and former *H* donor obtaining increased capability to be an acceptor. This mutual reinforcement effect gives rise to the cooperative *H*-bonding in water film, with shorter mean bond length compared to the simple dimer[31]. The hydrophobicity induced *H*-bonding clusters can be called low-density liquid (LDL)[32] which is characterized by "ice-like" *H*-bond complex and favored at low temperatures.

The structure formation is, in effect, associated with the change of excess film enthalpy per unit area (ΔH^f), representing the free energy gained in building the structures, which is obtained by the sum of ΔG^f and $T\Delta S^f$,

$$\Delta H^f = \Delta G^f + T\Delta S^f \qquad [5.5]$$

where $T\Delta S^f$ represents the thermodynamic cost of building the structure. Negative value of ΔH^f is an indication that structured clusters is formed. The existing form of structured water or LDL is supposed to be partial clathrates[1] which become more pronounced at lower temperatures. Since *H*-bonded networks are cooperatively strengthened, namely, clusters with greater sizes are essentially more stable than that with smaller sizes[33]. When a more negative ΔH^f value is obtained with thinner films or under lower temperature conditions (or both), one can infer that the size and the number of clusters is increasing, as was the case in our results (Figure 5.6).

Figure 5.7 depicts ΔG^f, $T\Delta S^f$ and ΔH^f results that were determined in the manner described above. $\Delta G^f < 0$ is the condition for the hydrophobic force to be attractive, in other words, $|\Delta H^f| > |T\Delta S^f|$ represents an essential relationship when both $T\Delta S^f$ and ΔH^f are negative. As shown, the absolute value of ΔH^f is larger than that of $T\Delta S^f$, it supports the presence of long-range hydrophobic forces as found in Figures 5.1-5.3. Different from the entropic, hydrophobic interaction in molecular scale, which become stronger at higher temperatures[34], the hydrophobic force in macroscopic scale which decrease with increasing temperature is enthalpic. The difference for the hydrophobic interaction in macroscopic scale and molecular scale is attributed to the different dimension of the hydrophobic units involved[34].

5.4.2 Temperature Dependence Extended to Short-range Component

Although some investigators tried to explain the hydrophobic force in different ranges (*i.e.*, short-range and long-range) by different mechanisms[20,35], the disjoining pressure determined by thin film pressure balance (TFPB) technique indicates that both short-range and long-range hydrophobic forces are essential for the thinning of film. Additionally, the dependence of the hydrophobic force on temperature was observed at both short-range and long-range[3]. This result indicates a single origin accountable for the hydrophobic force of the whole detectable range. The above discussion revealed that the structuring of confined liquid is responsible for the long-range hydrophobic force. The following study illuminates the mechanism behind the short-range hydrophobic force.

Unlike the case of *in-situ* equilibrium adsorption from solution[19], additional or incomplete adsorption of surfactant is avoided by utilizing the L-B deposition technique in a surfactant-free media. Based on reported procedures, hydrophobic surfaces were prepared using a modified L-B technique[5,36] involving the adsorption of dioctadecyldimethylammonium acetate (DODAA) from an apolar cyclohexane solution[3] on mica. Subsequent AFM imaging revealed a uniform and continuous monolayer of surfactant on the prepared mica surfaces[3]. The adsorbed monolayer of DODA also exhibited high stability. The surface force measurements obtained at 25°C, 40°C and 50°C using surface force apparatus (SFA) provided force curves with both short-range and long-range components. The force plot presented in the form of d(F/R)/dh vs. h was then fitted to the double exponential force law as follows:

$$\frac{F}{R} = -C_1 \exp\left(-\frac{h}{D_1}\right) - C_2 \exp\left(-\frac{h}{D_2}\right) \qquad [5.6]$$

where C_1 and C_2 represent the magnitude of the short- and long-range components of the hydrophobic force, respectively, and where D_1 and D_2 represent the decay lengths. The four parameters: C_1, C_2, D_1 and D_2 at various temperatures are presented in Table 5.1. As shown, both range and magnitude decreased with increasing temperature for both the short- and long-range components of the force. The fitting of the hydrophobic force was then presented as a function of temperature in Figure 5.8. Obviously, the temperature dependence of attractive force is especially substantial at higher temperatures. This finding is in accordance with the apparent decrease of force and the corresponding fitting parameters from 30 to 40°C, as shown in Figures 5.3-5.4. Specifically, D_1 and D_2 decreased to approximately half of the respective values as the temperature was increased from 20 to 50°C. Note that the temperature-dependent change in C_1 was much more significant than the analogous finding for C_2, *i.e.*, increasing the temperature decreased the magnitude of the short-range component much more significantly. In general, the decrease of hydrophobic force at both long-range and short-range indicates that both components probably arise from the same mechanism.

By using the surface force data, thermodynamic analysis of the hydrophobic interactions was extended to include the short-range component in the present work. Depending on the choice of calculation described above (Eqs. [5.2-5.5]), we developed a modified way to assess the attractive force of short-range and long-range components. The long-range (F_{short}) and short-range hydrophobic force (F_{long}) is related to the changes in surface tension ($\Delta\gamma^{\text{f}}$), as well as changes in Gibbs free energy per unit area (ΔG^{f}) as follows:

$$\frac{F}{2\pi R} = \Delta\gamma^{f} = \Delta G^{f} = \frac{F_{short} + F_{long}}{2\pi R} = \Delta\gamma^{f}_{short} + \Delta\gamma^{f}_{long} \qquad [5.7]$$

where the film tension can be separated into two parts: $\Delta\gamma^{\text{f}}_{\text{short}}$ and $\Delta\gamma^{\text{f}}_{\text{long}}$ respectively. The partial differential of film tension with respect to temperature at constant pressure (P) and thickness (h) is then related to the changes in excess film entropy (ΔS^{f}):

$$\left(\frac{\partial\Delta\gamma^{f}}{\partial T}\right)_{p,h} = -\Delta S^{f} = \frac{1}{2\pi R}\left(\frac{\partial F_{short}}{\partial T}\right)_{p,h} + \frac{1}{2\pi R}\left(\frac{\partial F_{long}}{\partial T}\right)_{p,h} \qquad [5.8]$$

With the force data and the temperature coefficients of C_1, C_2, D_1 and D_2 parameters, one can make a calculation of ΔS^{f}, as follows:

$$\Delta S^{f} = \frac{F_{short}}{2\pi R}\left(\frac{dC_1}{C_1 dT} + \frac{H}{D_1^2}\frac{dD_1}{dT}\right) + \frac{F_{long}}{2\pi R}\left(\frac{dC_2}{C_2 dT} + \frac{H}{D_2^2}\frac{dD_2}{dT}\right) \quad [5.9]$$

the change in excess film enthalpy (ΔH^f) can then be obtained by adding $\Delta\gamma^f$ (or ΔG^f) to $T\Delta S^f$ as shown in Eq. [5.5]. In particular, the ΔS^f can be calculated using Eq. [5.9], which is also presented in Figure 5.9. As shown, ΔS^f tends to be more negative at lower temperatures and when the film thickness is smaller. This observation supports the results shown in Figure 5.5, which illustrates how more structured water is likely to be formed under the same conditions. It is interesting to note the especially negative value for the short-range component in comparison to the value for the long-range component. Moreover, the slope of ΔS^f vs. *h* plot was much larger for the short-range element, which corresponds to the fact that when a thin film is compressed to a certain thickness (lower than 20 nm), the structuring becomes easier to form. Also significant is the fact that the transition point was smaller at higher temperatures than at lower temperatures, further confirming that the structuring of water is favored at lower temperatures. Specifically, the entropy change in the detectable range (20nm) which is about 0.008% of the comparable figure for the water-to-ice phase transition[1] may be associated with a less structured phase for the hydrophobic surfaces confined water film compared to ice. However, as reported herein, the significantly larger change value for the short-range components corresponds to the much more ordered water film, which is related to the much stronger attractive force at the short-range than at the long-range. Therefore, the limit of molecular dynamic simulation to detect the water structuring, which is effective only for the thickness of a few layers of water molecules[37-40], may be attributed to the restricted accuracy of simulation for the unconspicuous structuring in the longer range. Furthermore, simulations have not always been reliable or straightforward. Some classic simulations[37] describing density changes in thin water film based on simplistic water potential could also be considered suspect, especially since structural rearrangements of water molecules are known to occur without any notable changes in volume[41]. In this regard, thermodynamic calculations of both short-range and long-range components, which reveals the structuring of water at both ranges, is essential for providing complete information on the ordering changes in thin water films associated with the presence of hydrophobic surfaces.

Figure 5.10 shows the change of excess film enthalpy (ΔH^f) as a function of temperature. The negative value of ΔH^f is associated with the formation of *H*-bonded clusters which may be in the form of partial clathrates[1], resembling the clathrate cages[42] formed in the water phase with the presence of nonpolar solute molecules. Obviously, the structured clusters are favored at lower temperatures as shown by the more negative value of ΔH^f at the same conditions, because of the stability of formed clusters at lower temperature and also the increased likelihood for formation of clusters when the water molecules bear decreased kinetic energies at low temperatures. Since clusters of greater sizes are essentially more stable than that with smaller sizes[33] owing to the cooperative effect, a more negative ΔH^f value obtained with thinner films or under lower temperature conditions (or both) is a sign for the increasing of size and even larger number of clusters. The much more negative values of ΔH^f at the short-range than at the long-range indicate that the increasing speed for the formation of bigger structured clusters along with *h* get through a promotion at the transition point from F_{short} to F_{long}.

Since both of ΔH^f and ΔS^f are negative, the condition for the hydrophobic force to be attractive is that the absolute value of ΔH^f is larger than that of $T\Delta S^f$. Figure 5.11 presents the value of $|\Delta H^f| - |\Delta S^f|$ *vs.* thickness of the thin water film confined by the hydrophobic mica surfaces (*h*). The positive value over the whole range (0-60 nm) demonstrates that $|\Delta H^f|$ is larger than $|T\Delta S^f|$, which satisfied the condition for the presence of attractive hydrophobic force. For the same *h*, the value of $|\Delta H^f| - |\Delta S^f|$ is larger at low temperature, therefore, hydrophobic force is favored at low temperature. Besides, a transition of the slope of $|\Delta H^f| - |\Delta S^f|$ *vs. h* plot is observed at a point which separates the long-range

and short-range hydrophobic forces. As a result, after the water film is compressed to thinner than this specific point, the hydrophobic force become more possible.

5.5 Conclusions

AFM force measurement studies conducted between silica surfaces in a C_{18}TACl solution revealed long-range hydrophobic attractive forces without any visible steps present on the force curves. The stability of the measured force at a given temperature confirmed that the decrease of hydrophobic force with increasing temperature is caused by only temperature rather than other factors. Subsequent thermodynamic analysis of hydrophobic interactions showed more negative ΔS^f at lower temperatures or as the film is thinner confined by hydrophobic surfaces, which is in good agreement with the stronger forces measured under the same experimental conditions. The results indicate that the forces between hydrophobic surfaces typically associated with the physical adsorption of surfactants may also be linked to a change in the degree of structuring of the water. This investigation also used published force data[3] to look at the influence of short-range component of the hydrophobic forces. Our findings revealed that thin water films are much more structured, principally because the two surfaces are confined by hydrophobic surfaces to thinner than 20 nm.

5.6 References

(1) Wang, J.; Yoon, R.-H.; Eriksson, J. C. *J. Colloid Interface Sci.* **2011**, *364*, 257.
(2) Li, Z.; Yoon, R.-H. *J. Colloid Interface Sci.* **2012**.
(3) Tsao, Y. H.; Yang, S. X.; Evans, D. F.; Wennerstrom, H. *Langmuir* **1991**, *7*, 3154.
(4) Christenson, H. K.; Claesson, P. M. *Adv. Colloid Interface Sci.* **2001**, *91*, 391.
(5) Claesson, P. M.; Blom, C. E.; Herder, P. C.; Ninham, B. W. *J. Colloid Interface Sci.* **1986**, *114*, 234.
(6) Wood, J.; Sharma, R. *Langmuir* **1994**, *10*, 2307.
(7) Rabinovich, Y. I.; Derjaguin, B. V. *Colloids Surf.* **1988**, *30*, 243.
(8) Kokkoli, E.; Zukoski, C. F. *Langmuir* **1998**, *14*, 1189.
(9) Parker, J. L.; Claesson, P. M.; Attard, P. *J. Phys. Chem.* **1994**, *98*, 8468.
(10) Ishida, N.; Kinoshita, N.; Miyahara, M.; Higashitani, K. *J. Colloid Interface Sci.* **1999**, *216*, 387.
(11) Kékicheff, P.; Spalla, O. *Phys. Rev. Lett.* **1995**, *75*, 1851.
(12) Eriksson, J. C.; Ljunggren, S.; Claesson, P. M. *J. Chem. Soc., Faraday Trans. II* **1989**, *85*, 163.
(13) Li, Y.; Huang, J.; McIver, R. T.; Hemminger, J. C. *J. Am. Chem. Soc.* **1992**, *114*, 2428.
(14) Schoenfisch, M. H.; Pemberton, J. E. *J. Am. Chem. Soc.* **1998**, *120*, 4502.
(15) Ashurst, W. R.; Yau, C.; Carraro, C.; Maboudian, R.; Dugger, M. T. *J Microelectromech S* **2001**, *10*, 41.
(16) Israelachvili, J.; Pashley, R. *Nature* **1982**, *300*, 341.
(17) Christenson, H. K.; Claesson, P. M.; Berg, J.; Herder, P. C. *J. Phys. Chem.* **1989**, *93*, 1472.
(18) Parker, J. L.; Yaminsky, V. V.; Claesson, P. M. *J. Phys. Chem.* **1993**, *97*, 7706.
(19) Pashley, R. M.; Mcguiggan, P. M.; Ninham, B. W.; Evans, D. F. *Science* **1985**, *229*, 1088.
(20) Hammer, M. U.; Anderson, T. H.; Chaimovich, A.; Shell, M. S.; Israelachvili, J. *Faraday Discuss.* **2010**, *146*, 299.
(21) Ducker, W. A.; Senden, T. J.; Pashley, R. M. *Nature* **1991**, *353*, 239.
(22) Cleveland, J. P.; Manne, S.; Bocek, D.; Hansma, P. K. *Rev. Sci. Instrum.* **1993**, *64*, 403.
(23) Rutland, M. W.; Parker, J. L. *Langmuir* **1994**, *10*, 1110.
(24) Zhang, J. H.; Yoon, R. H.; Mao, M.; Ducker, W. A. *Langmuir* **2005**, *21*, 5831.
(25) Zhang, J. H.; Yoon, R. H.; Eriksson, J. C. *Colloid Surf., A* **2007**, *300*, 335.
(26) Derjaguin, B. V. *Colloid Polym. Sci.* **1934**, *69*, 155.
(27) Stillinger, F. H. *J. Solution Chem.* **1973**, *2*, 141.

(28) Laskowski, J.; Kitchener, J. A. *J. Colloid Interface Sci.* **1969**, *29*, 670.
(29) Du, Q.; Freysz, E.; Shen, Y. R. *Science* **1994**, *264*, 826.
(30) Stillinger, F. H. *Science* **1980**, *209*, 451.
(31) Frank, H. S.; Wen, W.-Y. *Discuss. Faraday Soc.* **1957**, *24*, 133.
(32) Mallamace, F. *Proc. Natl. Acad. Sci. U. S. A.* **2009**, *106*, 15097.
(33) Eriksson, J. C.; Henriksson, U. *Langmuir* **2007**, *23*, 10026.
(34) Chandler, D. *Nature* **2005**, *437*, 640.
(35) Meyer, E. E.; Lin, Q.; Israelachvili, J. N. *Langmuir* **2005**, *21*, 256.
(36) Claesson, P. M.; Christenson, H. K. *J. Phys. Chem.* **1988**, *92*, 1650.
(37) Lee, C. Y.; Mccammon, J. A.; Rossky, P. J. *J. Chem. Phys.* **1984**, *80*, 4448.
(38) Sakurai, M.; Tamagawa, H.; Ariga, K.; Kunitake, T.; Inoue, Y. *Chem. Phys. Lett.* **1998**, *289*, 567.
(39) Fa, K. Q.; Nguyen, A. V.; Miller, J. D. *J. Phys. Chem. B* **2005**, *109*, 13112.
(40) Layfield, J. P.; Troya, D. *J. Phys. Chem. B* **2011**, *115*, 4662.
(41) Eriksson, J. C.; Yoon, R.-H. In *Colloid Stability: The Role of Surface Forces*; Tadros, T. F., Ed.; WILEY-VCH Verlag GmbH & Co. KGaA: Weinheim, Germany, 2007; Vol. 1, p 99.
(42) Guillot, B.; Guissani, Y. *J. Chem. Phys.* **1993**, *99*, 8075.

Table 5.1 Fitting parameters C_1, D_1, C_2, D_2 for the hydrophobic forces measured at various temperatures between DODA monolayer adsorbed mica surfaces at various temperatures.

Temperature (°C)	C_1 (mN/m)	D_1 (nm)	C_2 (mN/m)	D_2 (nm)
25	331	2.07	1.25	25
40	175	1.75	0.75	15
50	4.2	1.4	0.25	10

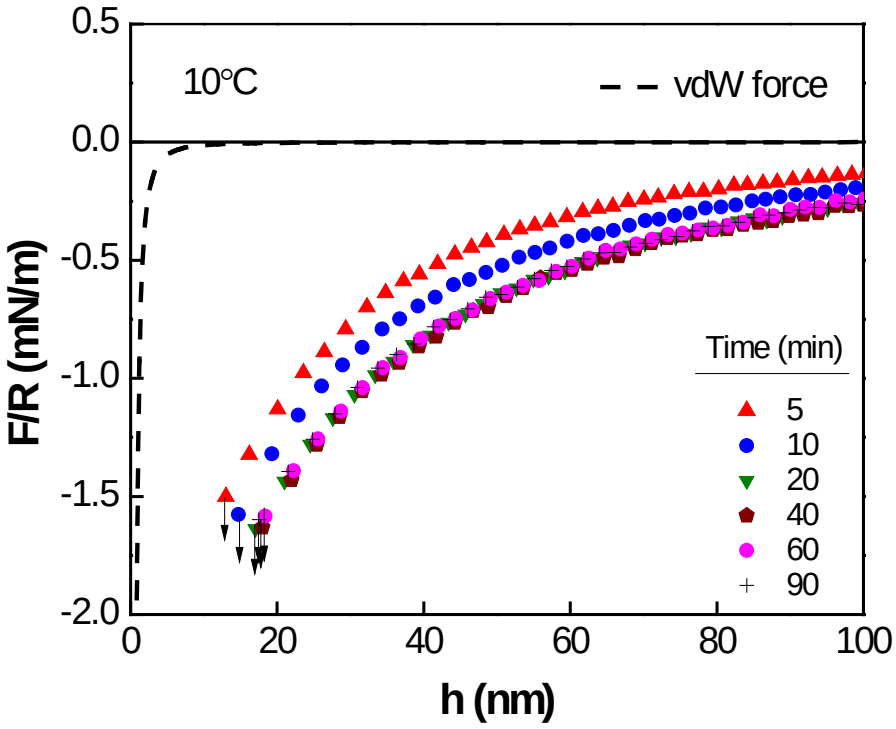

Figure 5.1 AFM surface force measurement conducted at 10°C between silica surfaces in 5×10^{-6} M C_{18}TACl solution after the surfaces has been exposed to the surfactant for different periods of times. The arrows indicate where the two surfaces jump into contact. The dashed line represents the van der Waals force.

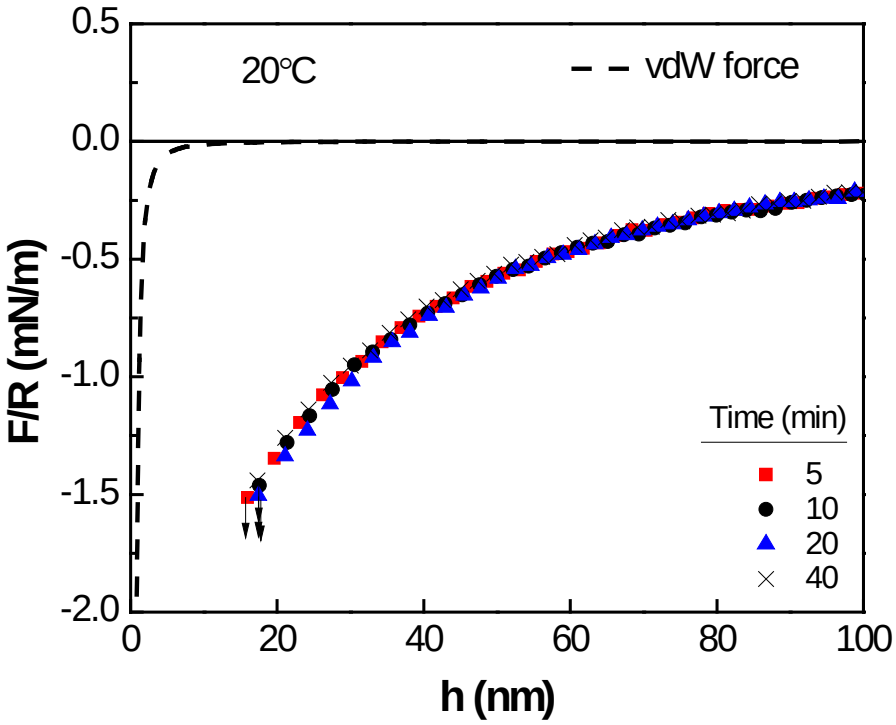

Figure 5.2 AFM surface force measurement conducted at 20°C between silica surfaces in 5×10^{-6} M C_{18}TACl solution after the surfaces has been exposed to the surfactant for different periods of times. The arrows indicate where the two surfaces jump into contact. The dashed line represents the van der Waals force.

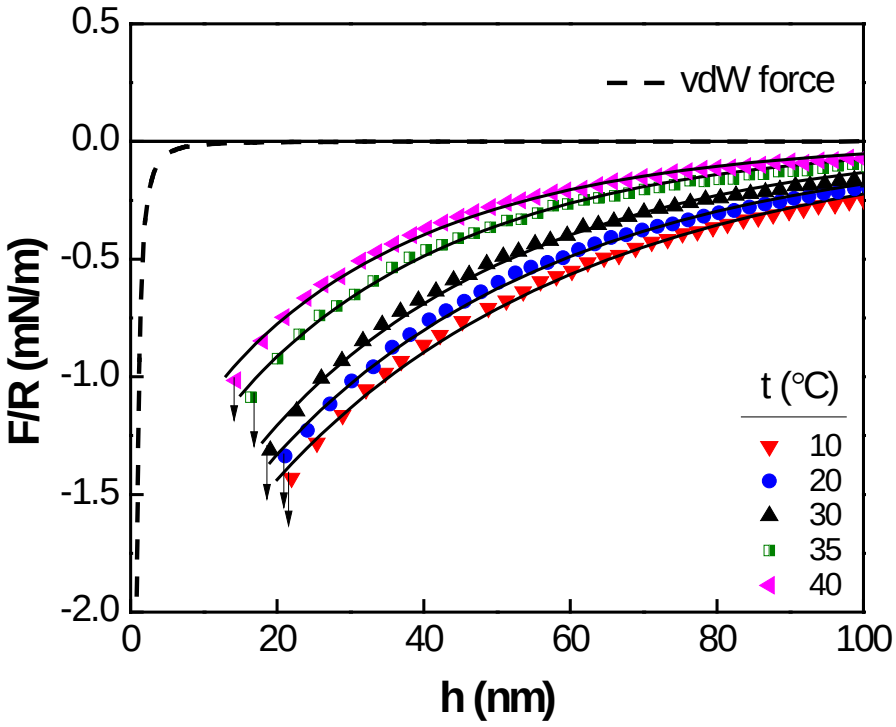

Figure 5.3 AFM surface force measurement conducted between silica surfaces in 5×10^{-6} M C_{18}TACl solution at various temperatures. The arrows indicate where the two surfaces jump into contact. The dashed line represents the van der Waals force, while the solid lines are the fitting of the experimental data by extended DLVO theory.

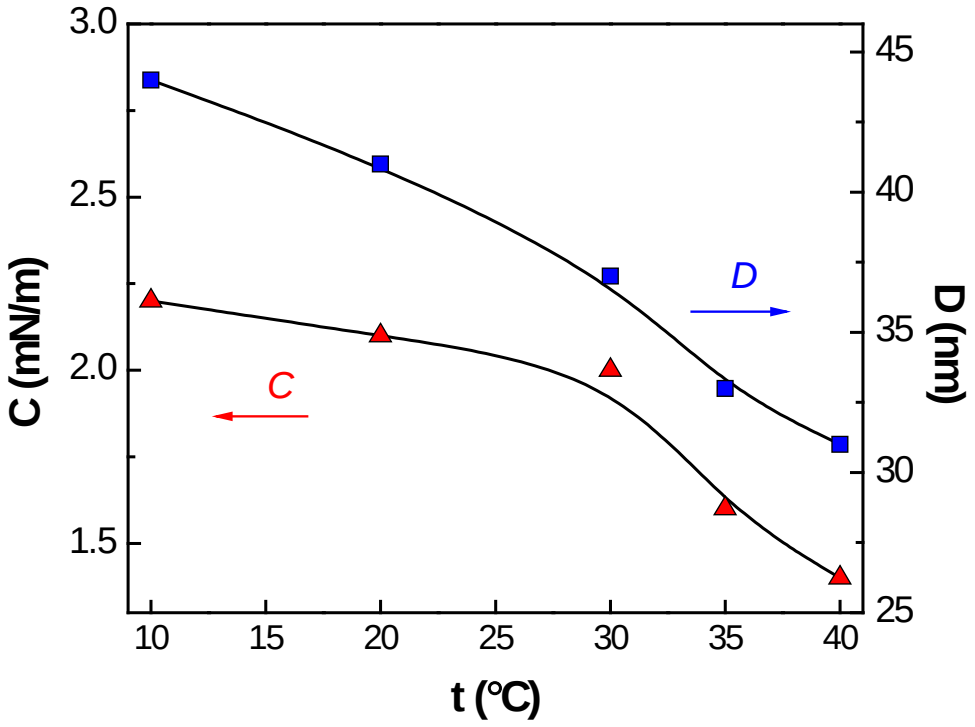

Figure 5.4 Fitting parameters of *C* and *D* as a function of temperatures for the hydrophobic forces presented in Figure 5.3.

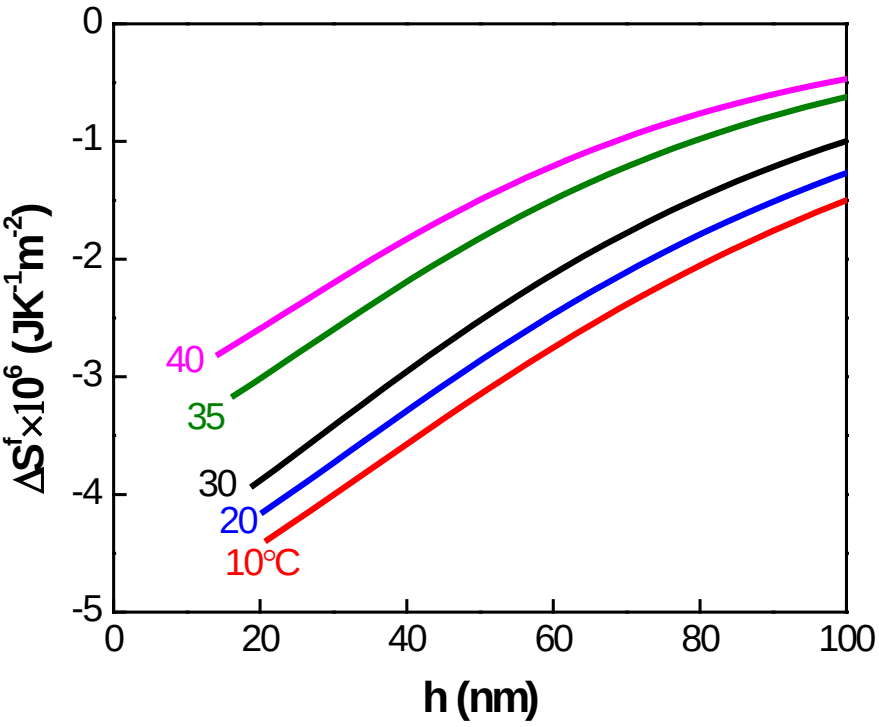

Figure 5.5 The change of excess film entropy (ΔS^f) per m^2 in the thin aqueous film with the presence of 5×10^{-6} M C_{18}TACl at various temperatures.

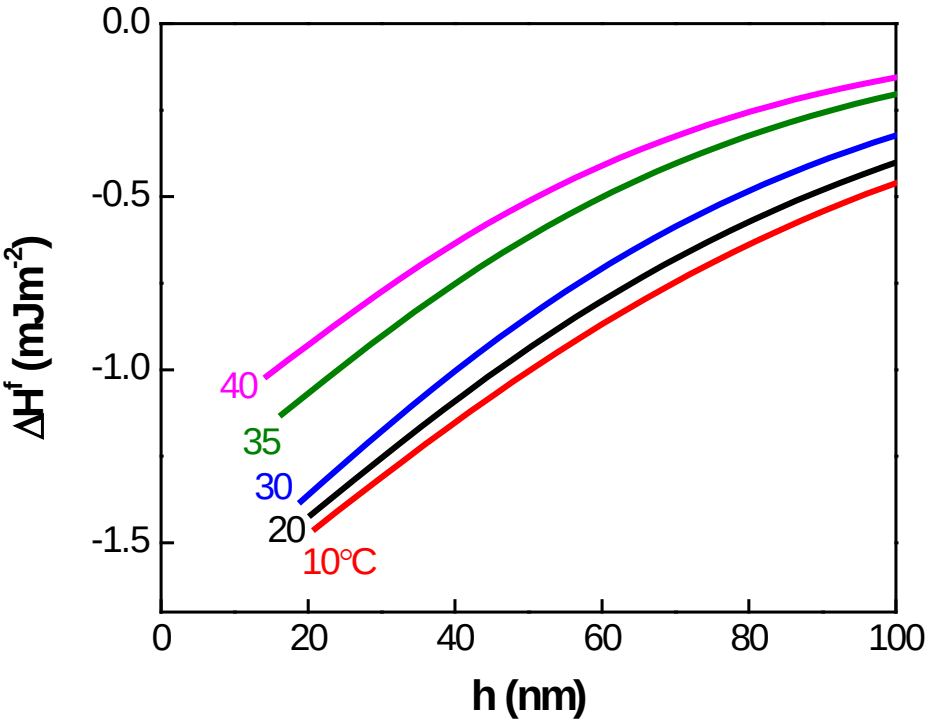

Figure 5.6 The change of excess film enthalpy (ΔH^f) per m^2 in the thin aqueous film with the presence of 5×10^{-6} M C_{18}TACl at various temperatures.

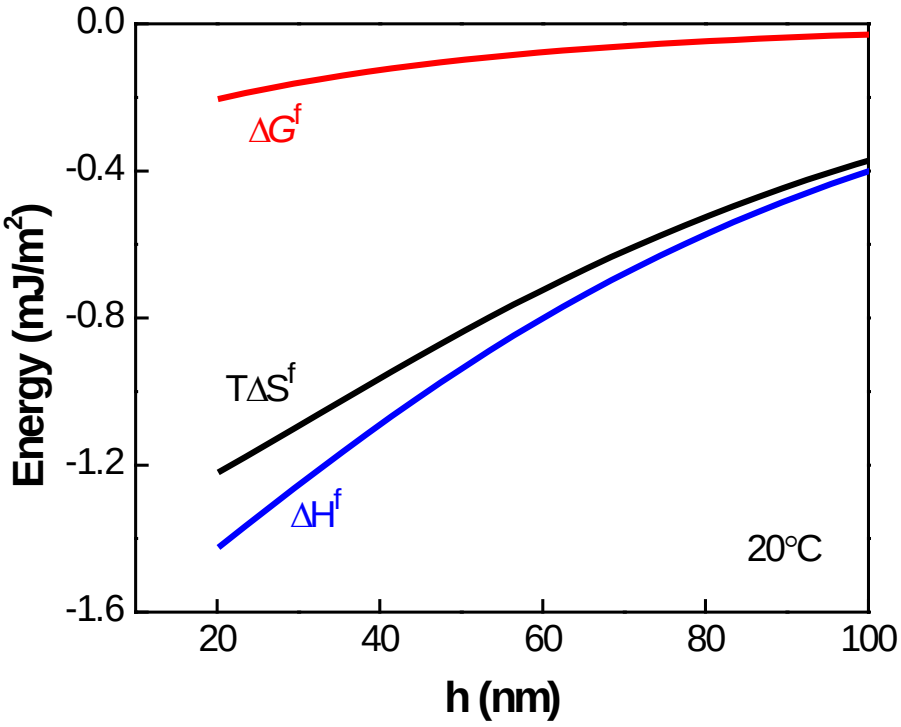

Figure 5.7 Changes in the excess thermodynamic functions for the hydrophobic interaction between hydrophobic silica surfaces in 5×10^{-6} M C_{18}TACl at 20°C.

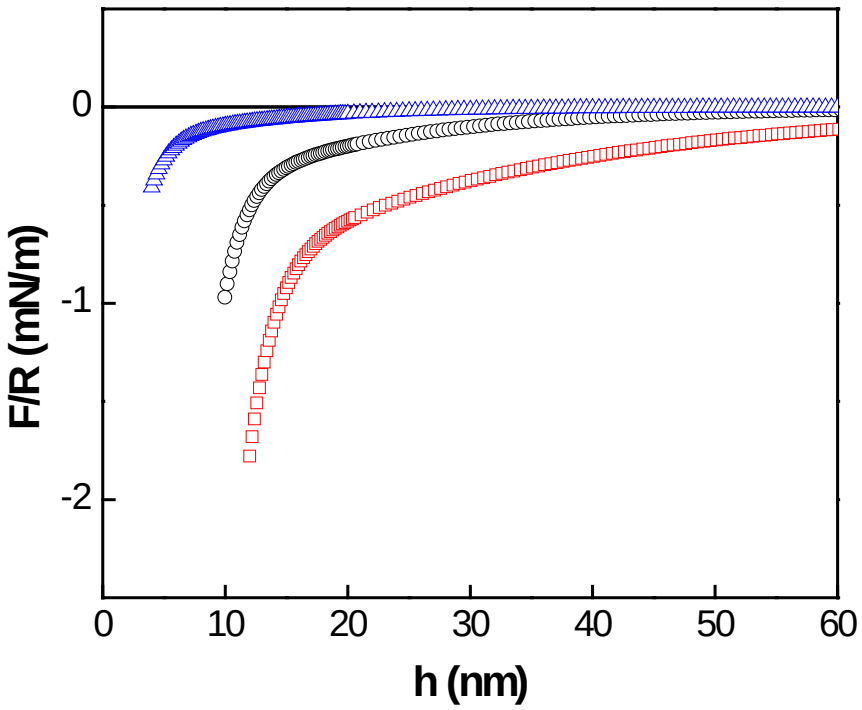

Figure 5.8 The calculated hydrophobic force from the fitting parameters (Table 4.1) as measured between two hydrophobized mica surfaces by the monolayer deposition of dioctadecyldimethylammonium (DODA).

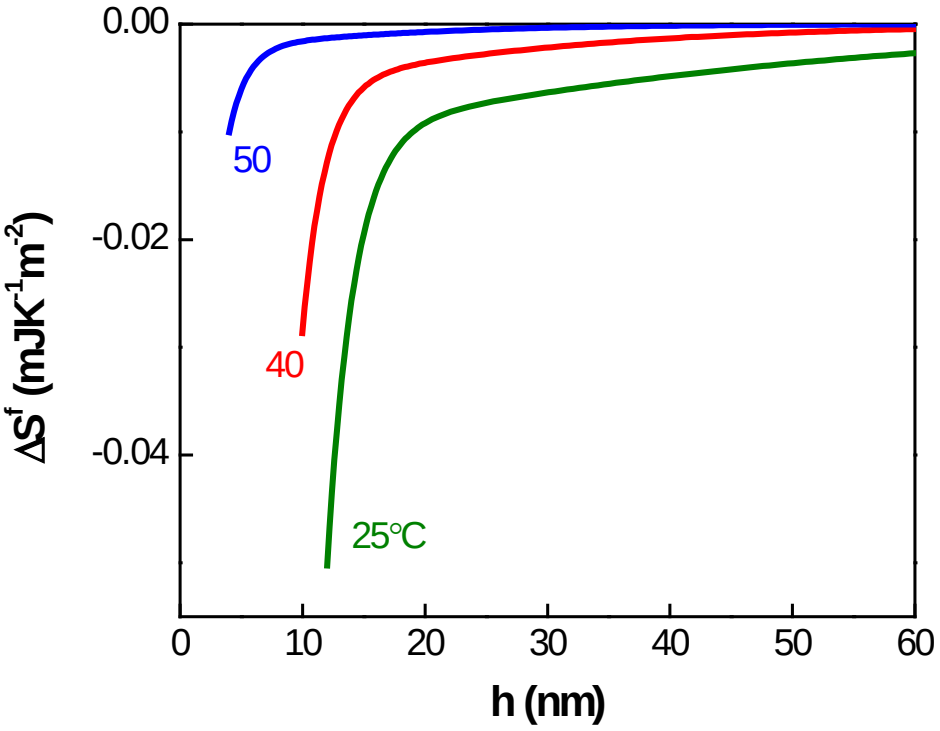

Figure 5.9 The change of excess film entropy (ΔS^f) per m^2 at various temperatures in the thin water film confined between two hydrophobized mica surfaces by the monolayer deposition of dioctadecyldimethylammonium (DODA).

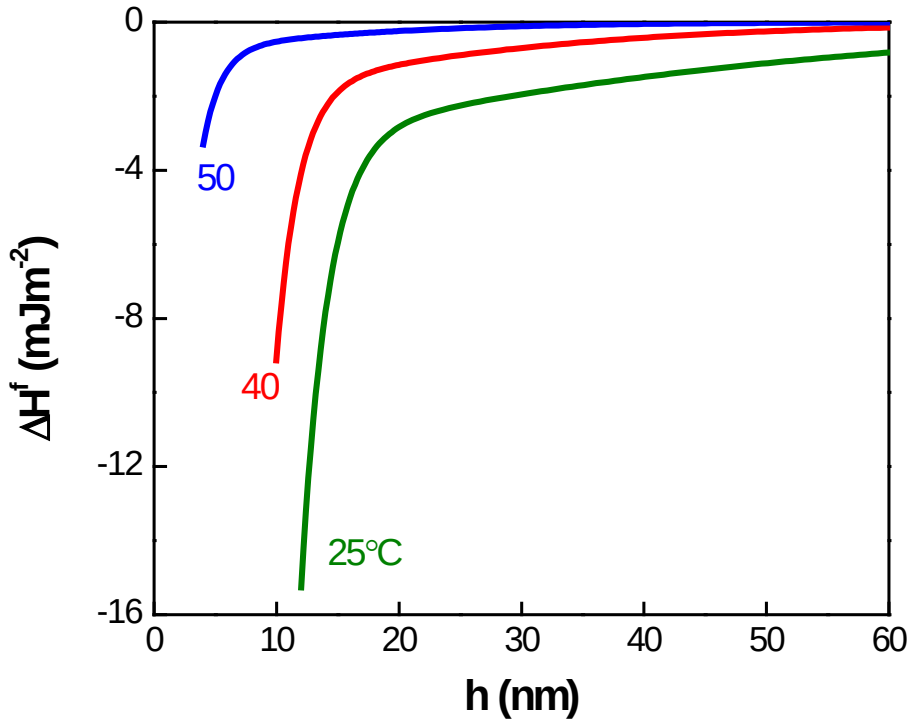

Figure 5.10 The change of excess film enthalpy (ΔH^f) per m^2 at various temperatures in the thin water film confined between two hydrophobized mica surfaces by monolayer deposition of dioctadecyldimethylammonium (DODA).

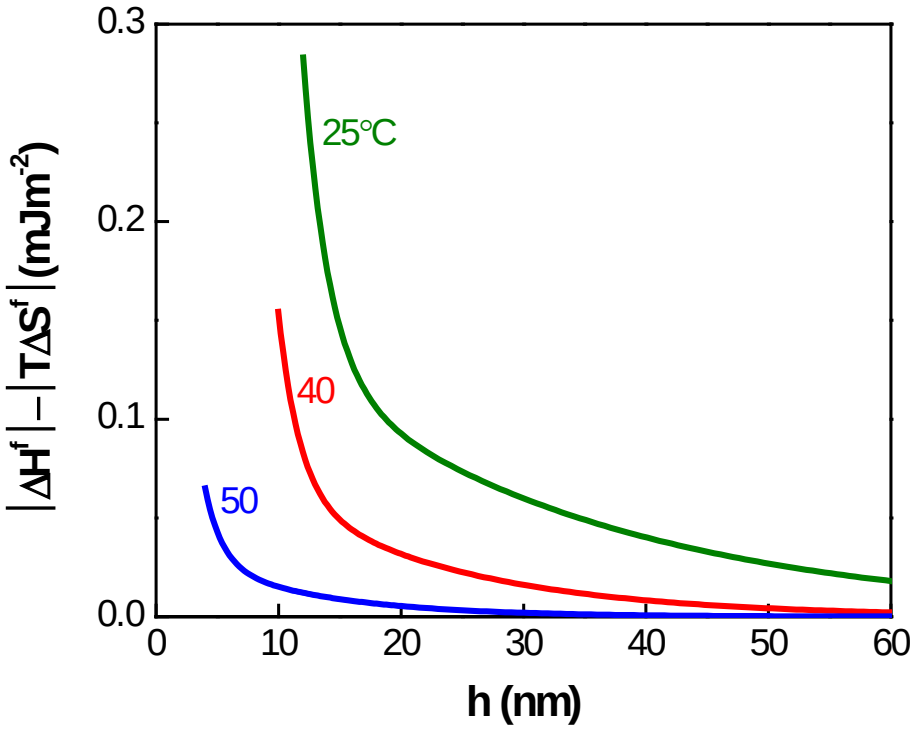

Figure 5.11 The difference between $|\Delta H^f|$ and $|T\Delta S^f|$ vs. the thickness of the water film confined between hydrophobic DODA deposited mica surfaces at different temperatures.

CHAPTER 6

Effect of Dissolved Gases on Long-Range Hydrophobic Force and Structuring of Water

6.1 Abstract

Surface force measurements conducted between thiolated gold surfaces exhibited a decrease in hydrophobic interactions at higher temperatures, accompanied by a less negative value for the change in excess entropy (ΔS^f), indicating that the hydrophobic force originates from the structuring of water induced by hydrophobic surfaces[1]. In the present work, the effect of dissolved air on the hydrophobic force was studied. Although the attractive force decreased in degassed water in comparison to results obtained in equilibrated water, it was still much stronger than the van der Waals force. As a result, air is not a prerequisite for the appearance of a hydrophobic force. Furthermore, force measurements were also conducted in gas (helium, nitrogen, argon or carbon dioxide) equilibrated water. The results showed that the dependence of hydrophobic force on these gases was related not only with their solubility, but also their type.

The absence of discontinuities or steps on the force curves precluded the possibility of nanobubbles causing the long-range attractions. On the other hand, the long-range attractions increased in the presence of certain type of dissolved gases, which may be attributed to enhancement of partial clathrate structures in the presence of gases[1].

6.2 Introduction

The stability of oil in a water emulsion was found to increase after degassing[2]. This phenomena indicates that hydrophobic interactions, which tend to destabilize oil droplets, was reduced by removing the dissolved gas[3]. Direct force measurements confirmed the decrease of long-range attractive forces upon degassing[3-5]. As reported by Meagher and Craig[3], the range of the hydrophobic interaction between polypropylene surfaces is shorter in a degassed dilute NaCl solution than in an untreated NaCl solution. In Mahnke *et al.*'s study on the symmetric interaction forces between methylated surfaces or dehydroxylated surfaces, the large jump-in distance (> 25 nm) representing an extra attraction decreased significantly after the electrolyte solution was degassed[5]. In addition, it has been reported that the diminution effect of degassing water on the attractive force was confined to only the long-rang component[6,7], leaving the short-range component intact[4]. In other words, the elimination of dissolved gas in water was accompanied by the absence of long-range attraction. Researchers have also assessed attractive force between polyethylene surfaces in water in the presence of various types of dissolved gases[8]. The presence of more soluble gases such as argon and butane results in more step-like irregularities on obtained force curves. These findings suggested that the measured long-range attractive force originated from the bridging of nanobubbles[9,10].

The study on the effect of degassing and dissolved gases on the attractive force, actually, made two important observations which support the "nanobubbles theory": 1) the presence of discontinuities (or "steps") on force curves, 2) the disappearance of long-range attractive forces once the medium has been degassed. However, more recent reports have indicated the presence of long-range attraction even in degassed aqueous solutions[11,12]. Additionally, Wang and Yoon showed that previously-observed steps on force curves could be eliminated by adjusting experimental conditions and procedures[13].

While AFM tapping mode imaging technique showed the formation of nanobubbles on the hydrophobic surfaces when the surfaces are brought into aqueous solutions[10,14,15], the imaged hydrophobic samples are usually treated by an alcohol-water exchange procedure which consists of flushing the AFM liquid cell by water, ethanol and water sequentially[10,15]. On the other hand, it is not necessary to treat the force measurement samples by the same procedure[13,16] to obtain the long-range attractive force. Most importantly, the force curve did not show the featured "steps" on the force curves. In this regard, the relation between the presence of nanobubbles and the measured long-range hydrophobic force is questionable.

On the other hand, hydrophobic force may be related with the structuring of water. The smooth attractive force between thiolated gold surfaces was found to be stronger at lower temperatures than at higher temperatures. Thermodynamic analysis (excess entropy, excess enthalpy, and excess energy) involved in the hydrophobic interactions between thiolated gold surfaces confirmed that the structuring of water is weakened under higher temperatures[1]. As a result, hydrophobic force is related with the structuring of water film. Researchers have also proposed a model for the structured water in the form of clathrate induced by hydrophobic surfaces and hydrophobicity[1]. Specifically, they suggested that the dissolved gas strengthens the stability of the clathrate cages by the van der Waals force between the gas molecules and the surrounding the water molecules, thereby increasing hydrophobic interactions—although it should be noted that dissolved gas is not necessary for the formation of clathrate cages and the appearance of the hydrophobic force.

Therefore, the aim of present work is to find out the role of dissolved air or gases on the hydrophobic force, so as to reveal the origin of hydrophobic force. We have conducted AFM force measurements between alkanethiols-coated gold surfaces in degassed water. Strong Attractive forces in the absence of dissolved gas are unlikely to be due to the bridging of nanobubbles. Furthermore, the force is related with the hydrophobicity of the surfaces. As will be discussed, although the degassing of water

decreased attractive force, long-range attractive forces were still observed even in completely degassed water. The results suggested that dissolved air is not a prerequisite for the appearance of long-range attractive force. This observation reputes the prediction of nanobubble theory which predicts the disappearance of long-range attractive force in degassed liquid, but corresponds to reported models for structured water molecules in the form of clathrates[1]. To find out how the dissolved gas molecules promote the hydrophobic force, force measurements were also conducted in gas (helium, nitrogen, argon or carbon dioxide) equilibrated water. The results showed that the dependence of hydrophobic force on these gases was related not only with their solubility, but also their type. The absence of discontinuities or steps on the force curves indicated that dissolved gas molecules do not exist in the forms of nanobubbles.

6.3 Experimental

6.3.1 Materials

Gold plate and sphere: Gold-coated silicon plates were obtained by physical vapor deposition of pure gold onto silicon surfaces with a thickness of 50 nm. A thin layer of chromium (5 nm) was deposited under the gold to achieve stronger bonding between the gold and silicon. The deposition was accomplished by means of an Electron Beam Physical Vapor Deposition system (EBPVD), Model -250. Gold spheres were produced in accordance with procedures established by Raiteri *et al.*[17]. Gold wire (radius: 0.0127 mm, 99.9%, Alfa Aesar) was connected to a 120V power supply, after which the wire was heated by the short circuited current and gold spheres were produced in the spark. The spheres with various redii were collected over a petri dish; the diameter of the sphere was measured by taking advantage of a simple optical microscopy. The ones with a radius of around 10 μm were chosen and attached to the tip of a cantilever by means of resin (EPON, 1004F) which is insoluble in ethanol. The cantilever with spring constant of ~ 0.48 N/m was calibrated via the thermal tune function and the calibration process was monitored by the AFM Nanoscope V 7.3 software.

Boiling piranha solution−a mixture of sulfuric acid (H_2SO_4, 98%, VMR International) and hydrogen peroxide (H_2O_2, 29.0-32.0%, Alfa Aesar)− was used to clean the gold-coated silicon plates for 20 minutes. After that, the plates were taken out by a pair of forceps and washed in a beaker containing ultrapure water and subjected to an ultrasonic bath for 5 minutes. The treated plates were then rinsed repeatedly by ultrapure water and dried by nitrogen stream before using.

The gold sphere attached to cantilever was not rinsed cleaned by boiling piranha solution because the solution can dissolve the 1004F resin. Instead, the sphere-cantilever assembly was irradiated under an ultraviolet lamp with the wave length of 254 nm turned on for 1 hr to remove possible organic contaminants.

A Millipore water purification system provided deionized ultrapure water with a resistivity of 18.2 MΩ·cm at 25°C. The hydrophobizing agents: Ethanethiol (C_2SH, 98%, TCI America), 1-butanethiol (C_4SH, 97%, TCI America), 1-dodecanethiol ($C_{12}SH$, 98%, TCI America) and 1-hexadecanethiol ($C_{16}SH$, 97%, TCI America) were dissolved in ethanol (200-proof, >99.5% pure, Decon labs, Inc.) just before using. Potassium ethyl xanthate (KEX, >90.0%, TCI America) was recrystallized by diethyl ether (>99%, Alfa Aesar) from acetone (99.8%, Fisher Scientific) at least twice to remove any impurities.

6.3.2 Hydrophobization of Gold Surfaces

After being flushed in ethanol, a pair of cleaned gold-coated silicon plate and gold sphere cantilever assembly was immersed in a freshly prepared thiol-in-ethanol solution immediately for hydrophobization. The hydrophobicity of the surfaces was controlled by the immersion times and the chain lengths of thiols, while same condition for each set of plate and sphere guarantee same

hydrophoibicity of them. Four sets of gold-coated silicon plate and gold sphere were then treated in the following solutions: 10^{-5} M C_2SH (55 mins), 10^{-5} M C_4SH (17 mins), 10^{-5} M $C_{12}SH$ (23 mins), and 10^{-5} M $C_{16}SH$ (45 mins). After hydrophobization, the plates and spheres were rinsed with ethanol to remove any residual alkanethiol on the surface. The hydrophobization of the gold-coated silicon plates and gold spheres with KEX was accomplished by *in- situ* adsorption in an AFM liquid cell.

6.3.3 Preparation of Degassed Water and Gas-Equilibrated Water

Ultrapure water was degassed via a minimum of three freeze-pump-thaw cycles, as reported in the literature[18], as follows: ultrapure water was placed in a Schlenk flask, vacuumed for 30 mins, frozen completely in a liquid nitrogen bath (freeze), and then pumped off atmosphere for 1 hour (pump). The sealed flask was then placed in a tepid water bath to thaw the water (thaw). The freeze-pump-thaw cycles were repeated until no gas evolution was observed during thawing[19]. The degassed water was used within several minutes following de-gassing.

To obtain the gas-equilibrated water, the ultrapure water was maintained in a flask with the desired gas while bubbling for 6 to 8 hours to afford helium (He), nitrogen (N_2), argon (Ar) and carbon dioxide (CO_2) equilibrated water respectively.

6.3.4 AFM Force Measurement

A Nanoscope V Atomic Force Microscope (AFM) was utilized to conduct the force measurement according to the colloidal probe technique described previously[13]. For measurement between thiolated gold surfaces conducted in degassed water, the AFM was placed in an airtight hood connected to a vacuum pump before conducting force measurements. The flask containing degassed water was connected to an AFM liquid cell via a tube, whose outlet was joined to another sealed flask. Just prior to measurement, a vacuum was applied to the flask joined with the outlet to pull the water through the cell. After the cell was filled with degassed water, the inlet and outlet of the cell was sealed and the force measurements initiated. After force measurements in degassed water were obtained, air equilibrated water was injected into the AFM liquid cell to determine those force measurements.

In order to compare the difference between the surface forces measured in air-equilibrated water and the other gas (He, N_2, Ar or CO_2)-equilibrated water solutions, after gold surfaces had reacted with KEX for specific period of time to obtain the reaction equilibrium, the KEX solution was replaced first by air-equilibrated ultrapure water and then by one gas-equilibrated ultrapure water. Force measurement was conducted as soon as the air or gas-equilibrated water was injected into the cell. Four sets of tests were carried out by using gases: He, N_2, Ar and CO_2 respectively.

All the measured forces (F) normalized by the radius of sphere (R) was plotted *vs.* the distance (h) between the sphere and plate.

6.4 Results and Discussion

6.4.1 Effect of Degassing on Hydrophobic Force

Figure 6.1 illustrates the results of AFM surface force measurements conducted in air-equilibrated water and degassed water between gold plates and spheres hydrophobized by C_2SH, C_4SH, $C_{12}SH$ and $C_{16}SH$, respectively. The hydrophobization was conducted in a low concentration thiol in ethanol solution (10^{-5} M) and the immersion time was controlled in less than 1 hour. Note that the result of the force measurement is independent on the position of the surfaces where the measurement was conducted. The van der Waals force between gold surfaces in water represented by the dashed line was

calculated with a Hamaker constant of 1.2×10^{-20} J[20]. As shown in the figure, the attractive force measured in degassed water (open symbols) is clearly weaker compared with the corresponding result in air-equilibrated water (solid symbols). This finding was not unexpected since a number of studies have reported the diminution effect of degassing of the liquid medium on the measured attractive forces between hydrophobic surfaces[3,21]. In cases where an additional attractive force between polypropylene surfaces existed in air-equilibrated NaCl solution (as indicated by a larger jump distance than van der Waals force), the oscillating jump distances typically became smaller in a degassed NaCl solution[3]. The range of the long-range attractive interaction was also found to decrease after the dissolved gas was removed[3,21], which is related to the fact that air dissolved in water generally enhances long-range attractive forces.

However, there was no observation of discontinuities or "steps" (or the intervention of nanobubbles) on the force curve between thiolated gold surfaces which was hydrophobized in 10^{-5} M solution. Conversely, when the gold surfaces were hydrophobized in a higher concentration of $C_{16}SH$ (10^{-3} M) for longer than 15 hours, steps appeared on the corresponding attractive force curves[22]. This finding indicates that "steps" are avoidable by adjusting the experimental conditions[13]. Most importantly, although the force in degassed water was smaller than the analogous result obtained in air-equilibrated water, it was still much stronger than the van der Waals force. In fact, under the condition when there were no nanobubbles on the hydrophobic surfaces, some studies have already detected an additional attractive force[10,23,24], with the range of a few tens of nanometers. The weakest attractions measured in dearated water were four times stronger than van der Waals forces between Teflon surfaces[18] in the absence of surface nanobubbles. The range of the force measured in degassed water in the present work is actually comparable to the attractive force, which (extended to 50 nm) detected between a carbon sphere and an ordered pyrolytic graphite (HOPG) surfaces without presence of nanobubbles on them[24]. These findings confirm, therefore, that although the dissolved air in water increases the magnitude of long-range attractive forces measured between hydrophobic surfaces in air-equilibrated water, presence of air is not a prerequisite for the appearance of long-range attractive force. So far at least, our observation reputes the prediction of nanobubble theory on the disappearance of long-range attractive force in degassed liquid and on the presence of steps on the long-range attractive force.

It has been reported that the diminution effect of degassed water on attractive force is confined to the long-rang component[6,7], leaving the short-range component intact[4]. Therefore, they tried to explain hydrophobic force in different ranges by different mechanisms[4]. Due to the small spring constant used (~0.48 N/m) in the present work, the two hydrophobic surfaces jumped into contact at a distance of approximately 10 to 20 nm, while no detailed information on the shorter-range component was observed. However, as revealed in Figure 6.1, once the water was degassed the force continuously decreased over the entire force curve range. In other words, it was not interrupted by the limits associated with short-range and long-range force (~ 20-25 nm). Moreover, the decrease in force magnitude becomes even stronger when the distance between the two surfaces was smaller. We speculated that this degassing effect probably extended to even shorter-range part of the force. In this regard, the force in the whole range should be caused by the same mechanism rather than by different ones in different ranges.

6.4.2 Relation between Hydrophobic Force and Surface Hydrophobicity

The equilibrium water contact angles (θ_e) of the gold surfaces treated by C_2SH, C_4SH, $C_{12}SH$ and $C_{16}SH$ were 80°, 92°, 102° and 107°, respectively, as listed on Table 6.1. Also presented are the advancing (θ_a) and receding contact angles (θ_r). As shown, the surface hydrophobicity measured by contact angle is related to the chain length of the alkanethiols. As has been proposed, contact angle as a common measure of hydrophobicity is in good correspondence with the hydrophobicity results associated with variations in chain length of the analog surfactant used[25]. As shown in Figure 6.1, the attractive force measured in air-equilibrated water becomes longer ranged and of greater magnitude in accordance with

increasing chain length and contact angles. The force measured between C_2SH surfaces is particularly informative due to the low contact angle (80°) of the surfaces, which is less than the 90° threshold for cavity formation. Depending on the theory of capillary force, the force between surfaces lower than 90° is the same as the van der Waals force[26,27]. This is obviously different from the long-range attractive force found in the present work.

The measured force can be fitted by extended DLVO theory, which combines the effects of the van der Waals attraction, electrostatic force, as well as an additional hydrophobic force. The hydrophobic force is represented by a single exponential force law, as follows:

$$\frac{F}{R} = -C\exp(-\frac{h}{D}) \qquad [6.1]$$

where F is the measured hydrophobic force, R the radius of the gold sphere, h the closest separation distance between the sphere and plate, and C and D are fitting parameters representing the magnitude and the decay length of the hydrophobic force, respectively. The values of C and D (solid symbols), which best fit the force curves (Figure 6.1), were plotted *vs*. contact angle of the surfaces (θ) in Figure 6.2. As shown, both C and D (solid symbols) which represents the force observed in air-equilibrated water increased with θ. It quantified the relation between hydrophobic force and surface hydrophobicity. Obviously, the smooth transition of the fitting parameters through the point of 90° does not support cavity or bridging nanobubbles.

Even though, some researcher hesitated to classify bridging force as "true" hydrophobic attraction, because the force is not only related to the hydrophobic nature of the substrates but also to the intervention of the bubbles or gas content in the medium. As a result, the hydrophobic force measured in the degassed water is of great interest. The forces measured in degassed water could not be linked to the formation of nanobubbles whose formation is highly unlikely under degassing condition[28]. Furthermore, the measured force lacks measurement-position dependence as mentioned above, while the attractive force attributed to nanobubbles varied with the position where the force was detected[23]. As shown in Figure 6.2 by the empty symbols, C and D representing the long-range attractive force measured in degassed water increased with the surface contact angle and the surface hydrophobicity. This change is especially significant for C. After precluding the involvement of the bubbles attached onto hydrophobic surfaces, the hydrophobicity dependence of the force is an indication that the measured force is "true" hydrophobic force.

Actually, the hydrophobicity dependence has been predicted as the most important characteristics of short-range hydrophobic force which is assumed to be "true" hydrophobic force[29,30]. Although the range of the usually mentioned short-range hydrophobic force is less than 20 nm or even 10 nm, as obtained between silylated mica[31] or glass[32] surfaces, plasma-polymerized films on mica[33] surfaces and bulk polymer surfaces[3], more recently study confirmed longer-ranged attractive forces without presence of nanobubbles[29]. Present work detected long-range attractive force, which is closely related with the surfaces hydrophobicity, has the nature of the true hydrophobic force as well. Therefore, we believe that although dissolved air promotes hydrophobic force, the air is not a prerequisite for the presence of long-range hydrophobic force. Air dissolved in water increase hydrophobic attractions between hydrophobic surfaces in a way other than nanobubbles.

6.4.3 Structuring of Water

Surface force measurements conducted between thiolated gold surfaces exhibited a decrease in hydrophobic forces under higher temperatures, accompanied by a less negative value for the change in

excess entropy (ΔS^f), indicating that hydrophobic force originates from the structuring of water induced by hydrophobic surfaces[1]. In the present work, forces measured in degassed water were found to have similar features as those in air equilibrated water—only smaller and shorter ranged. As already noted, even though dissolved air in water tends to promote hydrophobic force, it is not a prerequisite for it. Therefore, dissolved gas does promote hydrophobic force in ways other than via cavity formation or the bridging of nanobubbles. Rather, in keeping with the clathrate model[1], which suggests that the structuring of water confined between two hydrophobic surfaces may be in the form of partial clathrate cages, and the formation of clathrate is boosted by dissolved gas molecules. As indicated by that model, the presence of gas molecules is not a necessary requirement for structure formation; rather, they facilitate and strengthen the formation of clathrates[1].

Akin to the case for the non-*H*-bonded water molecules at the air/water and hydrogen/water interfaces being responsible for high interfacial tensions[34], the vicinal water molecules must be of high free energy state as they cannot form *H*-bonds to the hydrophobic surfaces. One way to reduce the free energy is forming *H*-bonded networks with neighboring water molecules, while the formation of "clathrate-like" structures, which embrace both convex cages and pentagonal rings, cost minimum entropy for building the structures[1]. As a result, partial clathrates may form at ambient conditions in the water film confined by two hydrophobic surfaces, as indicated by the negative entropy change with the film thinning[1]. The dissolved air molecules, which are encompassed in the clathrates, further decrease the free energy because of the van der Waals force between the air molecules and the surrounding water molecules. As a result, dissolved air make the clathrates structure more stable and even increase the density of formed clathrates when the film is confined to the same thickness (*h*). Correspondingly, the attractive force is stronger at the same *h* in air-equilibrated water than in degassed water. Furthermore, the formation of clathrates can extend to longer *h* in air-equilibrated water, which explains the longer range of the hydrophobic force under the same experimental conditions.

Since the likelihood that the number of non-*H*-bonded water molecules increases with increasing surface hydrophobicity[35], the water film is supposed to be more structured when confined by more hydrophobic surfaces. The increase of both *C* and *D* with the increase of water contact angle of surfaces is, actually observed in the air-equilibrated water and degassed water, which means hydrophobicity is an important determinant for the structuring of water and for the corresponding hydrophobic force no matter air is present or not. In other words, dissolved air is not the origin for the hydrophobic force but only a promoter.

6.4.4 Effect of Dissolved Gas on Hydrophobic Force

An additional component of this research involved comparing AFM forces measured in air-equilibrated water and other types of gas-equilibrated water—and results are presented in Figures 6.3-6.4. The hydrophobic surfaces utilized were KEX-coated gold surfaces. Figure 6.3a, Figure 6.3b, Figure 6.4a and Figure 6.4b are captured between four different sets of gold surfaces which were treated by the same method. For each set of gold surfaces, the force measurement was conducted first in air equilibrated water, then in one other type of gas-equilibrated water. As shown (Figures 6.3-6.4), the long-range attractive force was smooth without any visible steps or discontinuities on the force curve. No sign of bridging of nanobubbles are found here. Research has reported that attractive forces between KEX-coated gold surfaces correspond to the contact angle of the surfaces and the surface hydrophobicity[36]. It is the same as for the hydrophobic force between thiolated gold surfaces as talked above. As shown in Figure 6.3, there was no difference between the forces measured in air-equilibrated water and in N_2-equilibrated water (Figure 6.3a) or air-equilibrated water and He-equilibrated water. A significant increase of the attractive force was found in Ar-equilibrated water in comparison with that in air-equilibrated water (Figure 6.4b). Note that the solubility of Ar (34.2 ml/L) is larger than either He (15.8 ml/L) or N_2 (8.6 ml/L)[37]. Researchers have also described stronger attractive forces between silylated surfaces in Ar-saturated

water compared to air saturated water[38]. Even though the force is related to the solubility of the dissolved gas, as generalized from Figure 6.3a, Figure 6.3b and Figure 6.4b, this may not be the only determinant. As an example, for CO_2 (Figure 6.4a), whose solubility is similar to Ar (Figure 6.4b), the measured force was weaker in comparison to air.

The influence of dissolved gas on the interaction force between hydrophobic polyethylene surfaces was systematically studied by Nalaskowski *et al.*[8]. As reported, more step-like irregularities appeared in the force curves for argon and butane—whose solubility is higher—in comparison to the analogous force curves for helium and nitrogen. As the first derivative of free energy, steps on the force curves indicate a rapid alteration of free energy, which is related to phase transition. Therefore, "submicrocavities" and "bridging of the surfaces" were assumed to precipitate measured long-range attraction. In contrast, the absence of steps on the force curves associated for Ar-, He-, N_2- or CO_2-equilibrated water in present work do not support "submicrocavities" or "bridging of the surfaces" as being the origin for measured forces. Yaminsky and Ninham[39] showed that attraction between hydrophobic surfaces is caused by phase transition or cavity formation between two surfaces. Higher concentrations of dissolved gas in a system are linked to the formation of cavities, which will affect both the range and magnitude of attractive force. However, solubility is not sufficient to explain the effect of dissolved gas on the attractive force as illustrated in Figure 6.4, since the analogous solubility of Ar and CO_2 did not give rise to similar strength of attractions. This finding does not support the relation between gas solubility and the formation of nanobubbles.

Therefore, the dissolved gas molecules (Ar, He, N_2 or CO_2) probably also promote the structuring of water as dissolved air molecules do, although the result of the present work is not enough to explain the different effect of various types of gas. Water molecules surrounding the hydrophobic solutes develop "frozen patches" [40] or 'clathrate cages' [41,42] in order to maintain the *H*-bond network. The smooth long-range attractive force is probably attributed to the structured water in the form of clathrate which is stabilized by the dissolved gas.

6.5 Conclusion

For this study, the surface forces between thiolated gold surfaces in degassed water and air-equilibrated water were measured. Although surface force was found to decrease with the degassing of water, long-range attractive forces were still evident after degassing. In other words, dissolved air is not essential for the presence of attractive forces. The absence of steps on the force curves did not support bridging of nanobubbles as the origin of the measured force. Another finding from this research is that the forces are related with the hydrophobicity in both degassed water and in air-equilibrated water. As a result, the measured hydrophobic force is probably attributed to the structuring of water induced by hydrophobic surfaces[1].

Furthermore, the dependence of hydrophobic force on the type of dissolved gas tends to be related to the solubility of the gas. For example, the incorporation of helium, nitrogen —gases with similar solubility parameters—give rise to similar long-range attractive forces. Despite this finding, significant force differences measured in carbon dioxide-equilibrated water and argon-equilibrated water as identified in this research cannot be explained by the solubility of these gases. However, as confirmed by analyses of obtained force curves without presence of discontinuities, all the utilized dissolved gases are not likely to be associated with nanobubbles or cavities. This study also showed that gas molecules may strengthen the stability of clathrate in structured water films so as to promote long-range hydrophobic force.

6.6 References

(1) Wang, J.; Yoon, R.-H.; Eriksson, J. C. *J. Colloid Interface Sci.* **2011**, *364*, 257.
(2) Maeda, N.; Rosenberg, K. J.; Israelachvili, J. N.; Pashley, R. M. *Langmuir* **2004**, *20*, 3129.
(3) Meagher, L.; Craig, V. S. J. *Langmuir* **1994**, *10*, 2736.
(4) Meyer, E. E.; Lin, Q.; Israelachvili, J. N. *Langmuir* **2005**, *21*, 256.
(5) Mahnke, J.; Stearnes, J.; Hayes, R. A.; Fornasiero, D.; Ralston, J. *Phys. Chem. Chem. Phys.* **1999**, *1*, 2793.
(6) Leung, K.; Luzar, A.; Bratko, D. *Phys. Rev. Lett.* **2003**, *90*, 065502.
(7) Craig, V. S. J.; Ninham, B. W.; Pashley, R. M. *Langmuir* **1999**, *15*, 1562.
(8) Nalaskowski, J.; Hupka, J.; Miller, J. D. *Physicochem. Probl. Miner. Process.* **1999**, *33*, 129.
(9) Parker, J. L.; Claesson, P. M.; Attard, P. *J. Phys. Chem.* **1994**, *98*, 8468.
(10) Hampton, M. A.; Donose, B. C.; Nguyen, A. V. *J. Colloid Interface Sci.* **2008**, *325*, 267.
(11) Zhang, J. H.; Yoon, R. H.; Mao, M.; Ducker, W. A. *Langmuir* **2005**, *21*, 5831.
(12) Meyer, E. E.; Lin, Q.; Israelachvili, J. N. *Langmuir* **2004**, *21*, 256.
(13) Wang, J. L.; Yoon, R. H. *Langmuir* **2008**, *24*, 7889.
(14) Ishida, N.; Inoue, T.; Miyahara, M.; Higashitani, K. *Langmuir* **2000**, *16*, 6377.
(15) Lou, S. T.; Ouyang, Z. Q.; Zhang, Y.; Li, X. J.; Hu, J.; Li, M. Q.; Yang, F. J. *J Vac Sci Technol B* **2000**, *18*, 2573.
(16) Yoon, R. H.; Flinn, D. H.; Rabinovich, Y. I. *J. Colloid Interface Sci.* **1997**, *185*, 363.
(17) Raiteri, R.; Preuss, M.; Grattarola, M.; Butt, H.-J. *Colloids Surf., A* **1998**, *136*, 191.
(18) Stevens, H.; Considine, R. F.; Drummond, C. J.; Hayes, R. A.; Attard, P. *Langmuir* **2005**, *21*, 6399.
(19) Pashley, R. M.; Rzechowicz, M.; Pashley, L. R.; Francis, M. J. *J. Phys. Chem. B* **2005**, *109*, 1231.
(20) Wang, J.; Yoon, R.-H. *ECS Trans.* **2010**, *28*, 3.
(21) Considine, R. F.; Hayes, R. A.; Horn, R. G. *Langmuir* **1999**, *15*, 1657.
(22) Ederth, T.; Claesson, P.; Liedberg, B. *Langmuir* **1998**, *14*, 4782.
(23) Ishida, N.; Sakamoto, M.; Miyahara, M.; Higashitani, K. *Langmuir* **2000**, *16*, 5681.
(24) Zhang, X.; Kumar, A.; Scales, P. J. *Langmuir* **2011**, *27*, 2484.
(25) Sakamoto, M.; Kanda, Y.; Miyahara, M.; Higashitani, K. *Langmuir* **2002**, *18*, 5713.
(26) Ederth, T.; Liedberg, B. *Langmuir* **2000**, *16*, 2177.
(27) Ederth, T. *J. Phys. Chem. B* **2000**, *104*, 9704.
(28) Ryan, W. L.; Hemmingsen, E. A. *J. Colloid Interface Sci.* **1993**, *157*, 312.
(29) Ishida, N.; Kusaka, Y.; Ushijima, H. *Langmuir* **2012**.
(30) Meyer, E. E.; Rosenberg, K. J.; Israelachvili, J. *Proc. Natl. Acad. Sci. U. S. A.* **2006**, *103*, 15739.
(31) Wood, J.; Sharma, R. *Langmuir* **1995**, *11*, 4797.
(32) Ohnishi, S.; Yaminsky, V. V.; Christenson, H. K. *Langmuir* **2000**, *16*, 8360.
(33) Parker, J. L.; Claesson, P. M.; Wang, J. H.; Yasuda, H. K. *Langmuir* **1994**, *10*, 2766.
(34) Du, Q.; Freysz, E.; Shen, Y. R. *Science* **1994**, *264*, 826.
(35) Li, Z.; Yoon, R.-H. *J. Colloid Interface Sci.* **2012**.
(36) Li, Z.; Yoon, R.-H. *Miner. Eng.* **2012**.
(37) *CRC Handbook of Chemistry and Physics*; CRC Press, 1992.
(38) Rabinovich, Y. I.; Yoon, R. H. *Colloids Surf., A* **1994**, *93*, 263.
(39) Yaminsky, V. V.; Ninham, B. W. *Langmuir* **1993**, *9*, 3618.
(40) Frank, H. S.; Evans, M. W. *J. Chem. Phys.* **1945**, 507.
(41) Israelachvili, J. N. *Intermolecular and Surface Forces*; 3rd ed.; Academic Press: Burlington, 2011.
(42) Head-Gordon, T. *Proceedings of the National Academy of Sciences* **1995**, *92*, 8308.

Table 6.1 Water Contact Angles of the Gold Surfaces Treated in a 10^{-5} M thiol in ethanol Solution

Thiol	Contact Time (min)	Contact Angle (°)			Contact Angle Hysteresis (°)
		θ_a	θ_r	θ_e	
C_2SH	55	84	69	80	15
C_4SH	17	96	86	92	10
$C_{12}SH$	23	105	98	102	7
$C_{16}SH$	45	109	102.5	107	6.5

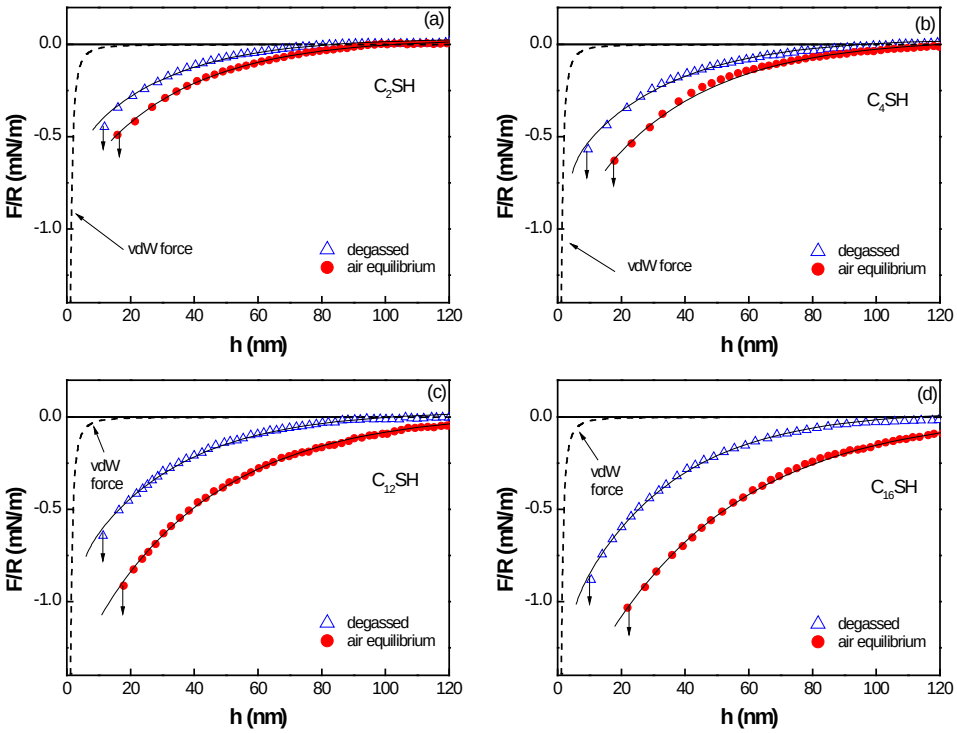

Figure 6.1 AFM force measurement conducted between C_2SH (a), C_4SH (b), $C_{12}SH$ (c) and $C_{16}SH$ (d) coated gold surfaces in degassed and air equilibrated water. The solid lines represent the extended DLVO fitting with a single exponential force term (eq. 6.1), sphere and triangle dots represent the experimental data. The dashed line represents the calculated van der Waals interaction (Hamaker constant for gold in water: $A_{131}=1.2\times10^{-20}$ J)

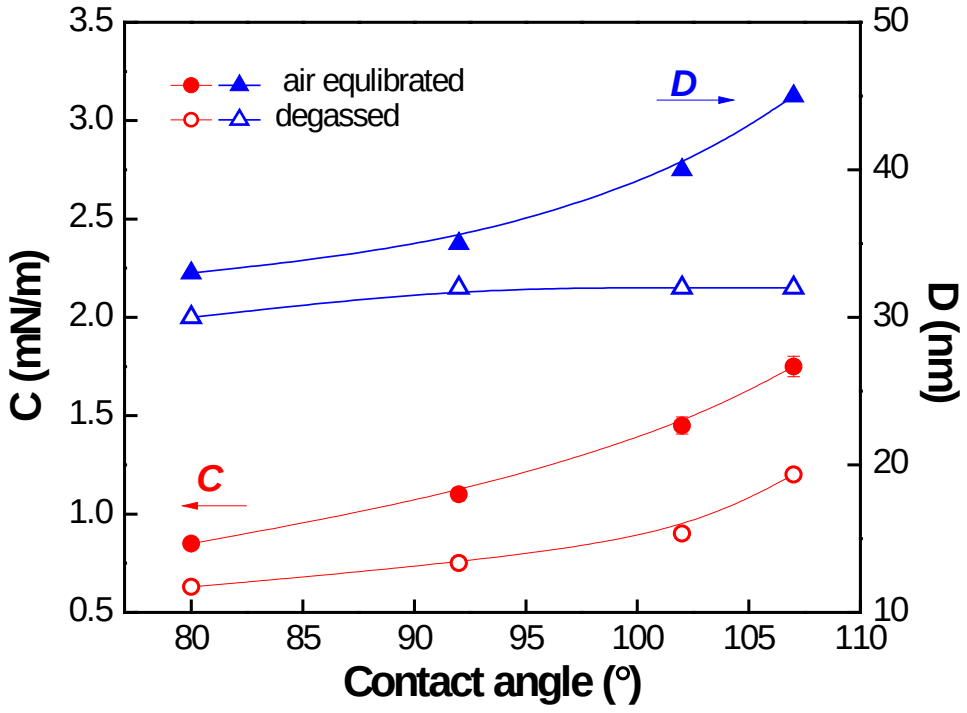

Figure 6.2 Fitting parameters from eq. 6.1 for hydrophobic forces shown in Figure 6.1, the parameters are shown versus the contact angles of the hydrophobic surfaces. Solid symbols represent the parameters from air equilibrated water, while the empty ones are for the parameters in degassed water.

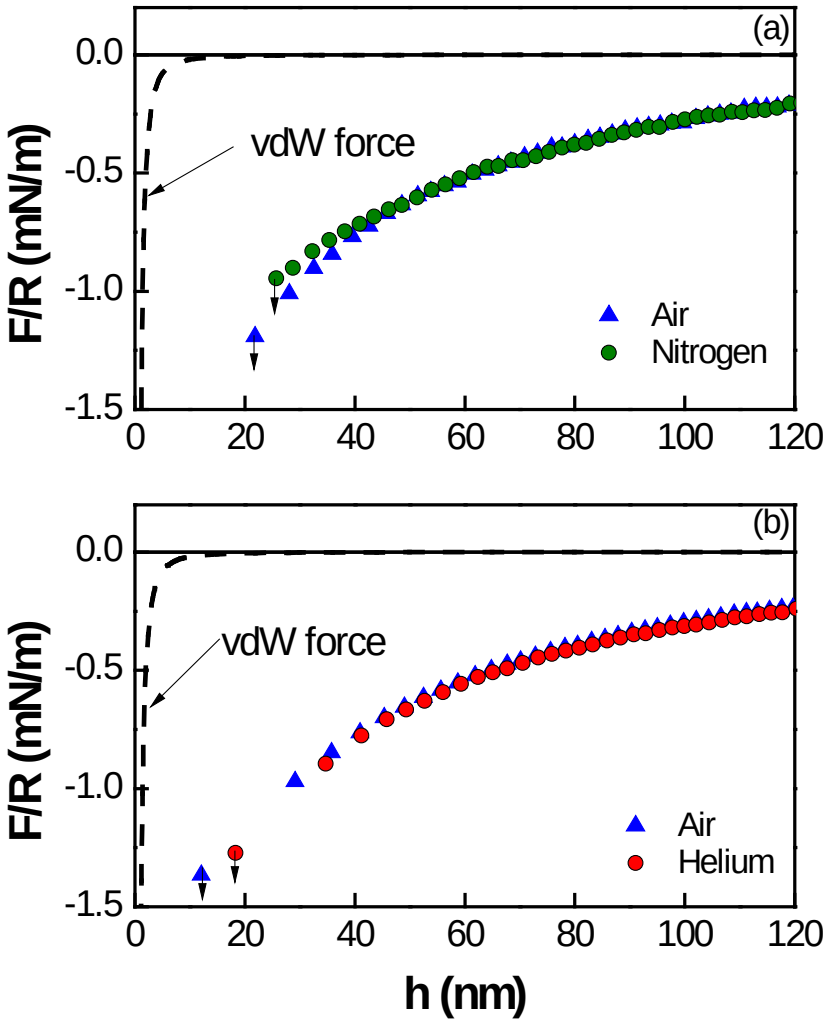

Figure 6.3 AFM force measured between xanthate coated gold surfaces in the nitrogen (a) or helium (b) equilibrated water compared with that in air equilibrated water.

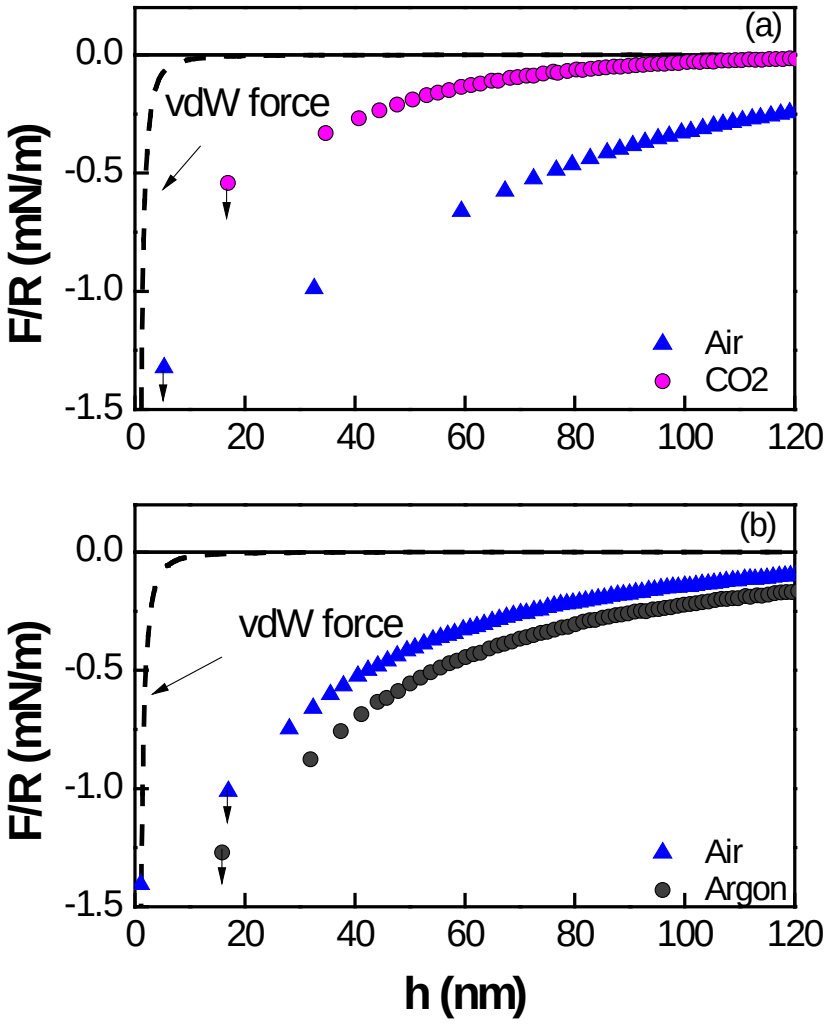

Figure 6.4 AFM force measured between xanthate coated gold surfaces in the carbon dioxide (a) or argon (b) equilibrated water compared with that in air equilibrated water.

Chapter 7

Thermodynamics of Interaction between Alkanethiol (C_nSH)-Coated Gold Surfaces in Ethanol

7.1 Abstract

It has been reported that the hydrophobic forces measured between gold surfaces in water decreased upon addition of ethanol, reaching a minimum at ethanol mole fractions in the range of 0.15–0.21[1]. At higher concentrations, the hydrophobic force began to increase, reaching a maximum close to that obtained in pure water. The initial decrease in hydrophobic force with increasing ethanol addition was attributed to the disruption of H-bonded water clusters, while the subsequent increase at higher concentrations was attributed to the formation of H-bonded ethanol structures.

In the present work, AFM force measurements were conducted in pure ethanol using gold surfaces hydrophobized with alkanethiols (C_nSH) with n = 2-16. The measurements were carried out at temperatures in the range of 5 to 35 ^oC to derive thermodynamic information. With a given alkanethiol and at a given temperature, both the excess enthalpies (ΔH^f) and entropies (ΔS^f) of the thin liquid films (TLFs) of ethanol become more negative with decreasing film thickness (h). Further, the changes in excess Gibbs free energies of the film (ΔG^f) are negative as $|\Delta H^f| > |T\Delta S^f|$. These findings suggest that the long-range attractions observed in the present work may be due to the formation of H-bonded ethanol clusters, with the $T\Delta S^f$ term representing a thermodynamic cost for building the structures. It has been found also that the long-range attraction becomes stronger and ΔG^f becomes more negative with increasing chain length and hence water contact angles (θ_e).

The results obtained in the present work are similar to those obtained with the TLFs of water confined between silica surfaces hydrophobized with octadecyltrichlorosilane (OTS)[2]. It appears that the long-range attractions observed in water and ethanol are the consequences of the H-bonding liquids confined between hydrophobic surfaces forming clusters to minimize free energies.

7.2 Introduction

Water confined between two hydrophobic surfaces appears to be structured differently in comparison to bulk water[3], which has prompted researchers to investigate the unique molecular structures existing in interfacial fluid molecules[4]. Well-ordered structures in water films confined by hydrophobic graphite slabs have been identified by classical molecular dynamic simulations[5]. Thin liquid films (TLFs) of water confined by two thiolated gold surfaces were found to be better-ordered at lower temperatures, *or* as the film thickness became smaller[6], which was confirmed by the lower excess film entropy under the same experimental conditions. Such well-ordered water molecules are believed to exist in the form of partial clathrates[6].

The ordering of water may be related to the non-DLVO force known as "structural force"[7], which is negative when two confining surfaces are hydrophobic[8]. Eriksson *et al.*[9] utilized a mean-field theory with square-gradient assumption as a basis for explaining attractive forces measured between hydrophobic surfaces. These authors attributed the attractive hydrophobic forces to the *H*-bond-propagated molecular ordering effects[9]. Other investigators conducted molecular dynamic simulations to investigate the structural change of water in the vicinity of hydrophobic surfaces,[10-13] with the results showing that the structuring is limited only to several layers of water molecules. On the other hand, thermodynamic analysis of macroscopic hydrophobic interactions provide an alternative means to explore the possibility that hydrophobic force originate from structuring of water in the TLFs[6].

The structural component of disjoining pressure plays a significant role not only in the films of water but also in the films of other polar liquids. For example, structural forces have been identified in the symmetrical films of water and alcohols[14-16]. Research has shown that the ordering of water can be mediated by hydrogen bonds[9]. The mixture of water and another type of *H*-bonding liquid, *e.g.*, ethanol, also undergoes a structural change as indicated by the unexpected low increase of entropy during mixing[17]. Structuring of the ethanol/water mixture has been analyzed by means of spectroscopic, X-ray diffraction, or mass spectrometric investigations[18-20]. As these studies have shown, when the mole fraction of a ethanol/water mixture was less than ~0.2, water was precluded from the thin film leaving only ethanol in the TLFs confined by hydrophobic surfaces, as indicated by the change in the film excess of ethanol (Γ_2)[1]. As the mole fraction of ethanol was increased, H-bonded clusters of ethanol began to be formed, during the course of which water is excluded from the TLFs[1,21]. Wang et al.[1] showed that the long-range attractive forces measured between hydrophobic surfaces in pure ethanol is due to the cluster formation[1].

In fact, the structural component associated with the disjoining pressure for thin films of water or alcohol has a similar "correlation length," which is a parameter resembled to the "decay length" in single exponential force law—as has been found between surfaces of rutile[8]. Given that incremental increases in temperature is known to be harmful to the stability of *H*-bond networks, the unique properties of water films were noted to disappear when the temperature was increased to 65°C[22]. To further explore the notion of whether hydrophobic force is of structural origin mediated by *H*-bonds, we measured the surface force in another *H*-bonding liquid - ethanol – confined between thiolated gold surfaces at various temperatures. Since thermodynamic analysis has been found to provide a more complete information on the structuring of water films[6], this method was used as previously described to analyze the TLFs of ethanol in the present work.

7.3 Thin Liquid Film Thermodynamics

The following is an analogue of the Gibbs-Duhem equation for an interface,

$$SdT - VdP + Ad\gamma + \sum_i n_i d\mu_i = 0 \qquad [7.1]$$

where S, V, A, and γ, are entropy, volume, interfacial area, and interfacial tension, respectively, while n_i and μ_i are the number and chemical potential of species i under consideration.

For a thin liquid film (TLF) of thickness h confined between two surfaces (or interfaces), it would be necessary to consider the interaction energy (Πdh) between two surfaces, where Π is the disjoining pressure. Further, it would be necessary better to consider thermodynamic properties of film rather than those of an interface. One can then rewrite Eq. [7.1] as follows,

$$d\gamma^f = -S^{f,ex}/A\, dT + V^{f,ex}/A\, dP - \Pi dh - \sum_i \Gamma_i^{f,ex} d\mu_i \qquad [7.2]$$

where γ^f is the film tension in units of Jm^{-2}, $S^{f,ex}$, $V^{f,ex}$ and $\Gamma_i^{f,ex}$ are the excess properties relative to those of the bulk liquid. For an aqueous solution of a single solute[23],

$$S^{f,ex}/A = S^f/A - \Gamma_w^f s_w^f - \Gamma_s^f s_s^f \qquad [7.3]$$

$$V^{f,ex}/A = h - \Gamma_w^f s_w^f - \Gamma_s^f s_s^f \qquad [7.4]$$

and

$$\Gamma_s^{f,ex} = \Gamma_s^f - \Gamma_w^f c_s/c_w \qquad [7.5]$$

In pure solvent and in dilute solutions, the second and third terms of Eq. [7.3]-[7.5] can be ignored, in which case $S^{f,ex}/A \cong S^f/A$, $V^{f,ex}/A \cong h$, and $\Gamma_s^{f,ex} \cong \Gamma_s^f$. For simplicity's sake, we may represent $S^{f,ex}/A$ as S^f in the present communication

When a liquid film thins from h = ∞ to a thickness h, Eq. [7.2] may be rewritten as

$$d\Delta\gamma^f = -\Delta S^f dT + hdP - \Pi dh - \sum_i \Delta\Gamma_i \mu_i \qquad [7.6]$$

in which $\Delta S^f = S^f - S^{f,\infty}$ and

$$\mu_i = \mu_i^{\,o} + RT\ln a_i \qquad [7.7]$$

where a_i is the activity of species i.

For an aqueous solution of a single solute (surfactant), Eq. [7.6] may be rewritten as

$$d\Delta\gamma^f = -\Delta S^f dT + hdP - \Pi dh - \Delta\Gamma_s d\mu_s \qquad [7.8]$$

Differentiating Eq. [7.7]

$$d\mu_s = RTd\ln a_s = \frac{\partial\mu_s}{\partial\ln a_s} d\ln a_s \qquad [7.9]$$

Substituting Eq. [7.9] into Eq. [7.6],

$$\begin{aligned} d\Delta\gamma^f &= -\Delta S^f dT + hdP - \Pi dh - \Delta\Gamma_s RT d\ln a_s \\ &= -\Delta S^f dT + hdP - \Pi dh - \Delta\Gamma_s \frac{\partial\mu_s}{\partial \ln a_s} d\ln a_s \end{aligned} \qquad [7.10]$$

which can be used to obtain changes in film tension ($\Delta\gamma^f$) as functions of T, P, h, Γ_s, and surfactant activity (a_s).

One can then use the Derjaguin approximation to relate the energy changes ($\Delta\gamma^f$) with the changes in the surface forces (F) measured as follows,

$$\begin{aligned} \Delta\gamma^f &= \gamma_h^f - \gamma_\infty^f = \Delta G^f \\ &= -\int_\infty^h \Pi dh = -\int_\infty^h (\Pi_e + \Pi_d + \Pi_h) dh \\ &= \frac{F}{2\pi R} \end{aligned} \qquad [7.11]$$

where Π_e, Π_d, and Π_h represent the disjoining pressures due to electrostatic, van der Waals and hydrophobic forces, respectively, and R is the radius of curvature of the macroscopic surfaces (between sphere and plate or between two curves surfaces) used in surface force measurements.

The surface forces measured in experiment are often represented by a single-exponential force law:

$$\frac{F}{R} = -C \exp\left(-\frac{h}{D}\right) \qquad [7.12]$$

Substituting Eq. [7.12] into Eq. [7.11],

$$\begin{aligned} \Delta\gamma^f &= \frac{F}{2\pi R} = -\frac{C}{2\pi} \exp\left(-\frac{h}{D}\right) \\ &= \Delta G^f \end{aligned} \qquad [7.13]$$

and differentiating Eqs. [7.13],

$$\begin{aligned} \Delta S^f &= -\left(\frac{\partial \Delta G^f}{\partial T}\right)_{P,h,a_i} \\ &= -\left(\frac{\partial (F/2\pi R)}{\partial T}\right)_{P,h,a_i} \\ &= -\frac{F}{2\pi R}\left(\frac{d\,ln\,C}{dT} + \frac{h}{D}\frac{d\,ln\,D}{dT}\right) \end{aligned} \qquad [7.14]$$

which gives changes in excess entropy from the surface force data obtained in experiment.

From the values of excess entropy and excess free energy data, one can also obtain the enthalpy change using the following relation,

$$\Delta H^f = \Delta G^f + T\Delta S^f \qquad [7.15]$$

The thermodynamic relations derived above may be useful for understanding the constraints involved in determining the thermodynamic functions for macroscopic interactions from experimental surface force data.

7.4 Experimental

7.4.1 Materials

Gold-coated substrates were obtained by deposition of gold onto silicon surfaces using the Electron Beam Physical Vapor Deposition system (EPPVD), Model-250. The thickness of the gold layer was 50 nm with a thin layer of chromium (5 nm) underneath to reinforce the adhesion of gold to the silicon surface. Gold spheres were produced as described by Raiteri *et al*.[24]. In this method, gold wires (radius: 0.0127 mm, 99.9%, Alfa Aesar) connected were short circuited at 120V AC to melt thewires and produce gold spheres of various radii. The spheres with radii of ~10 μm were selected for AFM surface force measurements. In each measurement, a gold sphere was glued on the tip of a cantilever with spring constant of ~0.48 N/m. The cantilever was calibrated by using the thermal tune function[25] of the AFM used in the force measurement, while its deflections were monitored by means of the AFM Nanoscope V 7.3 software. The diameter of the sphere was measured by means of an optical microscope.

Gold-coated silicon plates were cleaned in a boiling piranha solution, which was a mixture of sulfuric acid (H_2SO_4, 98%, VMR International) and hydrogen peroxide (H_2O_2, 29.0-32.0%, Alfa Aesar). After 20 minutes of boiling, the plates were removed by a pair of forceps and placed in a beaker containing ultrapure water and subjected to an ultrasonic vibration for 5 minutes. The plates were removed from the water, cleaned repeatedly with ultrapure water, and dried in a nitrogen stream.

The gold sphere were attached to cantilevers by means of a resin (EPON 1004F), which is insoluble in ethanol. However, the resin breaks down in a boiling piranha solution. Therefore, the sphere-cantilever assembly was cleaned by a UV irradiation at a wavelength of 254 nm for 1 hr to remove organic contaminants.

Ultrapure water with a resistivity of 18.2 MΩ·cm at 25°C was produced using the Millipore water purification system. All of the hydrophobizing agents, which included ethanethiol (C_2SH, 98%, TCI America), 1-butanethiol (C_4SH, 97%, TCI America), 1-dodecanethiol ($C_{12}SH$, 98%, TCI America) and 1-hexadecanethiol ($C_{16}SH$, 97%, TCI America) were dissolved in ethanol (200 proof, >99.5% pure, Decon labs, Inc.) before use. All of the surface force measurements were conducted in ethanol.

7.4.2 Hydrophobization of Gold Surfaces

After the cleaning procedures described above, the gold-coated silicone plates and the sphere-cantilever assembly were washed thoroughly with ethanol and then subjected to surface hydrophobization. For a given set of force measurements, a pair of a gold-coated silicon plate and a gold sphere was immersed in a thiol-in-ethanol solution of known concentration simultaneously for a given period of time, so that both the plate and sphere have an identical hydrophobicity. After a given immersion time, the macroscopic surfaces were washed thoroughly with pure ethanol to remove residual thiol. In the present

work, the surface hydrophobicity was controlled by using i) *n*-alkane thiols (C_nSH) of different chain lengths with n = 2, 4, 12 and 16, ii) thiol-in-ethanol solutions of different concentrations, and iii) different immersion times in a given solution.

7.4.3 AFM Forces Measurement at Various Temperatures

The surface forces acting between thiolated gold plate and sphere were measured in pure ethanol using a Nanoscope V Atomic Force Microscope (AFM). Starting from 5°C, the temperature of the ethanol in the AFM liquid cell was then ramped up to 15, 25 and 35°C sequentially using the heater/cooler accessory placed under a liquid cell. A Digital Instruments Thermal Applications Controller (TAC) was utilized to set and control the temperatures. All of the force measurements were carried out using the colloidal probe technique as described previously[26]. Measured forces (F) were normalized by the radius of gold sphere (R) and plotted *vs*. the closest separation distance (h) between the sphere and plate.

7.5 Results and Discussion

Thiols chemisorb on gold and give rise to robust hydrophobic surfaces that are ideally suited for surface force measurements. Chemisorbing reagents would not be laterally mobile enough to provide a mechanism of charge correlation, which is necessary for the charged patch model of Miklavic *et al.*[27] to explain the long-range attractions between hydrophobized surfaces. Further, it is not likely that thiol adsorption can reverse the surface charge of gold and, therefore, would not create oppositely charged patches.

When gold surfaces are immersed in a 10^{-3} M $C_{16}SH$-in-ethanol solution for a long period of time (>15 hrs), very hydrophobic surfaces are obtained with advancing water contact angles (θ_w) in the neighborhood of 110^{o}[26,28]. The hydrophobic surfaces obtained under such conditions showed discontinuities (or steps) in the (F/R) *vs*. h curves, which lead to a conclusion that long-range attractions are due to cavitation or the preexisting air bubbles on the surface[28]. It has been shown, however, that the steps disappear when gold surfaces are hydrophobized at a low thiol concentration and/or at a short immersion time[26].

In the present work, gold surfaces were hydrophobized at low C_nSH concentrations (10^{-5} M) to minimize the possibility that cavities and/or air bubbles affect the measurement. The water contact angles of the hydrophobized surfaces varied depending on the chain lengths and the immersion times employed, as shown in Table 1. As shown, the contact angles increased with increasing chain lengths. With C_2SH, a 60 min immersion time was necessary to obtain an equilibrium contact angle (θ_e) of 82^{o}. Note also that the contact angle hysteresis decreased with increasing chain lengths, indicating that the surface coatings became smoother with increasing chain length.

Figure 7.1 shows the results of the AFM force measurements conducted with C_nSH-coated gold surfaces at different temperatures in the range of 5 to 35°C. In all cases, the force *vs*. distance curves were smooth, suggesting that the long-range attractions were not due to bubbles and/or cavities. At temperatures above 40^{o}C, however, bubbles nucleated on hydrophobic surfaces. Therefore, no force measurements were conducted at temperatures above 35^{o}C. It is well known that ethanol has a much higher solubility for inert gases than water. As temperature rises, gas solubilites decrease and bubbles nucleate on hydrophobic surfaces.

The results obtained with all of the C_nSH-coated gold surfaces showed attractive forces that were substantially stronger and longer-ranged than the van der Waals force. In the present work, the van der Waals force was represented by a Hamaker constant (A_{131}) of 0.94×10^{-20} J as obtained using the combining rule,

$$A_{131} = \left(\sqrt{A_{11}} - \sqrt{A_{33}}\right)^2 \qquad [7.16]$$

where A_{11} = 9.11x10^{-20} J and A_{33} = 4.2x10^{-20} J are the Hamaker constants of gold and ethanol, resepectively, in vacuum. The value of A_{11} was back-calculated from the value of A_{131} = 1.2×10^{-20} J that was obtained from direct force measurement and from the methylene iodide contact angle method[29]. The value of A_{11} was much lower than those (25-40×10^{-20} J) from the Lifshitz theory[30]. The results presented in Figure 7.1 show that the surface forces measured in the present work were substantially stronger than the van der Waals force. Therefore, the experimental data have been fitted to the extended DLVO theory, which includes contributions from the hydrophobic force. In this exercise, double-layer forces were calculated using the value of the ζ-potential (-56.2 mV) of gold nanoparticles measured in ethanol[31] as the surface potential (ψ_o) of the C_nSH-coated gold surfaces in ethanol. The hydrophobic force was represented by a single exponential force law (Eq. [7.13]).

Figure 7.2 shows the changes in *C* and *D* parameters with temperature for the experimental force data obtained using the C_nSH-coated gold surfaces. As shown, both *C* and *D* parameters increase with decreasing temperature, indicating that hydrophobic forces increase with decreasing temperature. At a given temperature, both parameters increase with increasing chain length of the hydrophobizing agents (C_nSH) and hence the water contact angles (see Table 7.1). Note that *C vs.* temperature (*t*) plot for the $C_{16}SH$-coated surfaces shows a higher slope, indicating that C becomes more sensitive to *t* in the thin liquid film confined between more hydrophobic surfaces. However, the slopes of the *D vs. t* plots are more or less constant for all of the hydrophobic surfaces studied in the present work. These findings show that hydrophobic forces are closely related to the hydrophobicity of the confining surfaces, as has also been shown in previous studies[32-34].

Based on the data presented in Figure 7.2, the changes in excess film tension ($\Delta\gamma^f$), or Gibbs free energy (ΔG^f), have been calculated using Eq. [7.13] and are plotted *vs.* film thickness (h) in Figure 7.3. The free energy change is less than zero and becomes increasingly negative with decreasing film thickness (h).

The data presented in Figure 7.2 have also been used to calculate the excess film entropies (ΔS^f) using Eq. [7.14] and are plotted *vs.* h in Figure 7.4. The entropy changes are negative and become more negative with decreasing h and decreasing temperature.

Based on the values of ΔG^f and ΔS^f presented in Figures 7.3 and 7.4, respectively, the values of ΔH^f have been obtained using Eq. [7.15] and are plotted in Figure 7.5 vs. h. The results show that the enthalpy changes become more negative with decreasing h and temperature.

Figure 7.6 shows the changes in ΔG^f, $T\Delta S^f$, and ΔH^f at 25^{o}C for the interaction between $C_{16}SH$-coated gold sphere and plate in pure ethanol. As shown, ΔH^f is more negative than $T\Delta S^f$, indicating that the macroscopic interaction is driven by enthalpy change. When both ΔS^f and ΔH^f are negative as shown in Figures 7.4 and 7.5, respectively, it is necessary that $|\Delta H^f| > |T\Delta S^f|$ for $\Delta G^f < 0$. That is, two macroscopic surfaces are attracted to each other when the change in excess film enthalpy is more negative than the temperature times the change in excess film entropy.

It is well known that hydrophobic interaction at molecular scale, *e.g.*, self-assembly of hydrocarbon chains, is driven by entropy increase. Water molecules form low-entropy cages around hydrocarbon chains, which can be shed of when they self-assemble, resulting in entropy increase. Water molecules can surround hydrocarbon chains without compromising the angles between two H-bonds due to the high curvature of the hydrocarbon chains. Frank and Evans[35] showed actually that the water

molecules forming the lo-entropy cages actually form stronger H-bonds due to the cooperative bonding effect.

The results presented in Figure 7.5 show, on the contrary, that interaction between macroscopic hydrophobic surfaces in ethanol entails decrease in entropy. At the same time, the interaction entails decrease in enthalpy, which may be attributed to the formation of H-bonded ethanol structures in the thin liquid films (TLFs) of ethanol confined by hydrophobic surfaces. Since the hydrophobic surfaces cannot support the H-boding of ethanol, the ethanol molecules should be of high free energy state, which in turn increase the propensity of ethanol to form H-bonded structures. It is well known that ethanol forms chain structures; however, certain fraction of ethanol molecules forms two-dimensional structures. When they are confined in between hydrophobic surfaces, it is possible that larger H-bonded clusters may be formed owing to the high free energy, which should cause a decrease in enthalpy. A thermodynamic cost for building the larger and more numerous clusters will be the decrease entropy.

Figures 7.7-7.9 show the results obtained with gold surfaces hydrophobized with C_2SH, C_4SH, $C_{12}SH$ and $C_{16}SH$ at 25^{o}C. The equilibrium contact angles (θ_e) were 82°, 92°, 102° and 107°, respectively. As shown in Figure 7.7, ΔH^f became more negative with increasing chain length and θ_e. Likewise, Figure 7.8 shows that ΔS^f becomes more negative with increasing chain length and θ_e. These findings suggest that the higher the hydrophobicity, the more negative the changes in enthalpy and entropy. The higher the hydrophobicity, the less likely H-bonds can form with the surface. At the same time, the non-H-bonded ethanol molecules would have higher propensity to form structures. As a consequence, ΔG^f becomes increasingly negative as shown in Figure 7.9.

7.6 Conclusion

AFM surface force measurements have been conducted using gold surfaces hydrophobized with alkanethiols (C_nSH) of n = 2-16. The measurements were conducted in ethanol, a well-known H-bonding liquid. The results obtained are similar to those measured in pure water in that long-range attractive forces were measured in both. The attractive force curves measured in the present work showed no discernible discontinuities, excluding the possibility that the long-range attractions observed in ethanol were caused by bubbles or cavities.

Thermodynamic analysis of the AFM force data obtained at several different temperatures showed that both of the excess film entropy (ΔS^f) and enthalpy (ΔH^f) became increasingly negative as film thickness became smaller, suggesting that the long-range attractions are due to the increased formation of H-bonded structures in the TLFs of ethanol. That the long-range attractions increase with decreasing temperature suggests that the structuring become easier at lower temperatures. The decrease in excess film enthalpy is an indication for the increased formation of H-bonded structures, while the decrease in entropy is the thermodynamics cost for building the structures. It appears that the long-range attractions observed in both ethanol and water are the consequences of the H-bonding liquids confined between hydrophobic surfaces forming clusters to minimize free energy.

7.7 References

(1) Wang, J.; Li, Z.; Yoon, R.-H.; Eriksson, J. C. *J. Colloid Interface Sci.* **2012**, *379*, 114.
(2) Li, Z.; Yoon, R.-H. *J. Colloid Interface Sci.* **2012**.
(3) Derjaguin, B. V.; Churaev, N. V. *Langmuir* **1987**, *3*, 607.
(4) Tiani, D. J.; Yoo, H.; Mudalige, A.; Pemberton, J. E. *Langmuir* **2008**, *24*, 13483.
(5) Hirunsit, P.; Balbuena, P. B. *J. Phys. Chem. C* **2007**, *111*, 1709.
(6) Wang, J.; Yoon, R.-H.; Eriksson, J. C. *J. Colloid Interface Sci.* **2011**, *364*, 257.

(7) Derjaguin, B. V.; Kusakov, M. M. *Izv. Akad. Nauk SSSR, Ser. Khim.* **1936**, *5*, 741.
(8) Churaev, N. V.; Derjaguin, B. V. *J. Colloid Interface Sci.* **1985**, *103*, 542.
(9) Eriksson, J. C.; Ljunggren, S.; Claesson, P. M. *J. Chem. Soc., Faraday Trans. II* **1989**, *85*, 163.
(10) Lee, C. Y.; Mccammon, J. A.; Rossky, P. J. *J. Chem. Phys.* **1984**, *80*, 4448.
(11) Sakurai, M.; Tamagawa, H.; Ariga, K.; Kunitake, T.; Inoue, Y. *Chem. Phys. Lett.* **1998**, *289*, 567.
(12) Fa, K. Q.; Nguyen, A. V.; Miller, J. D. *J. Phys. Chem. B* **2005**, *109*, 13112.
(13) Layfield, J. P.; Troya, D. *J. Phys. Chem. B* **2011**, *115*, 4662.
(14) Rabinovich, Y. I.; Derjaguin, B. V.; Churaev, N. V. *Adv. Colloid Interface Sci.* **1982**, *16*, 63.
(15) Israelachvili, J. N.; Adams, G. E. *Journal of the Chemical Society, Faraday Transactions 1: Physical Chemistry in Condensed Phases* **1978**, *74*, 975.
(16) Peschel, G.; Belouschek, P.; Müller, M. M.; Müller, M. R.; König, R. *Colloid Polym. Sci.* **1982**, *260*, 444.
(17) Franks, F.; Desnoyers, J. E. In *Water Science Reviews*; Franks, F., Ed.; Cambridge University Press: Cambridge, 1985; Vol. 1, p 171.
(18) Nishi, N.; Takahashi, S.; Matsumoto, M.; Tanaka, A.; Muraya, K.; Takamuku, T.; Yamaguchi, T. *J. Phys. Chem.* **1995**, *99*, 462.
(19) Wakisaka, A.; Komatsu, S.; Usui, Y. *J. Mol. Liq.* **2001**, *90*, 175.
(20) Egashira, K.; Nishi, N. *The Journal of Physical Chemistry B* **1998**, *102*, 4054.
(21) Noskov, S. Y.; Lamoureux, G.; Roux, B. *J. Phys. Chem. B* **2005**, *109*, 6705.
(22) Derjaguin, B. V.; Churaev, N. V. *J. Colloid Interface Sci.* **1974**, *49*, 249.
(23) Eriksson, J. C.; Yoon, R.-H. In *Colloid Stability: The Role of Surface Forces*; Tadros, T. F., Ed.; WILEY-VCH Verlag GmbH & Co. KGaA: Weinheim, Germany, 2006; Vol. 1, p 99.
(24) Raiteri, R.; Preuss, M.; Grattarola, M.; Butt, H.-J. *Colloids Surf., A* **1998**, *136*, 191.
(25) Serry, F. M. 2010.
(26) Wang, J. L.; Yoon, R. H. *Langmuir* **2008**, *24*, 7889.
(27) Miklavic, S. J.; Chan, D. Y. C.; White, L. R.; Healy, T. W. *J. Phys. Chem.* **1994**, *98*, 9022.
(28) Ederth, T.; Claesson, P.; Liedberg, B. *Langmuir* **1998**, *14*, 4782.
(29) Wang, J., Virginia Polytecnic Institute and State University, 2008.
(30) Israelachvili, J. N. *Intermolecular and Surface Forces*; 3rd ed.; Academic Press: Burlington, 2010.
(31) Tien, D. C.; Tseng, K. H.; Liao, C. Y.; Huang, J.-C.; Tsung, T. T. In *International MultiConference of Engineers and Computer Scientists* Hong Kong, 2008; Vol. II.
(32) Yoon, R. H.; Flinn, D. H.; Rabinovich, Y. I. *J. Colloid Interface Sci.* **1997**, *185*, 363.
(33) Yoon, R. H.; Ravishankar, S. A. *J. Colloid Interface Sci.* **1996**, *179*, 403.
(34) Rabinovich, Y. I.; Yoon, R. H. *Langmuir* **1994**, *10*, 1903.
(35) Frank, H. S.; Evans, M. W. *J. Chem. Phys.* **1945**, 507.

Table 7.1 Water Contact Angles of the Gold Surfaces Treated in a 10^{-5} M thiol in ethanol Solutions

Thiol	Immersion Time (min)	Contact Angle (°)			Contact Angle Hysteresis (°)
		θ_a	θ_r	θ_e	
C_2SH	60	85.5	70.0	82.0	15.5
C_4SH	17	96.0	86.0	92.0	10.0
$C_{12}SH$	23	105.0	98.0	102.0	7.0
$C_{16}SH$	45	109.0	102.5	107.0	6.5

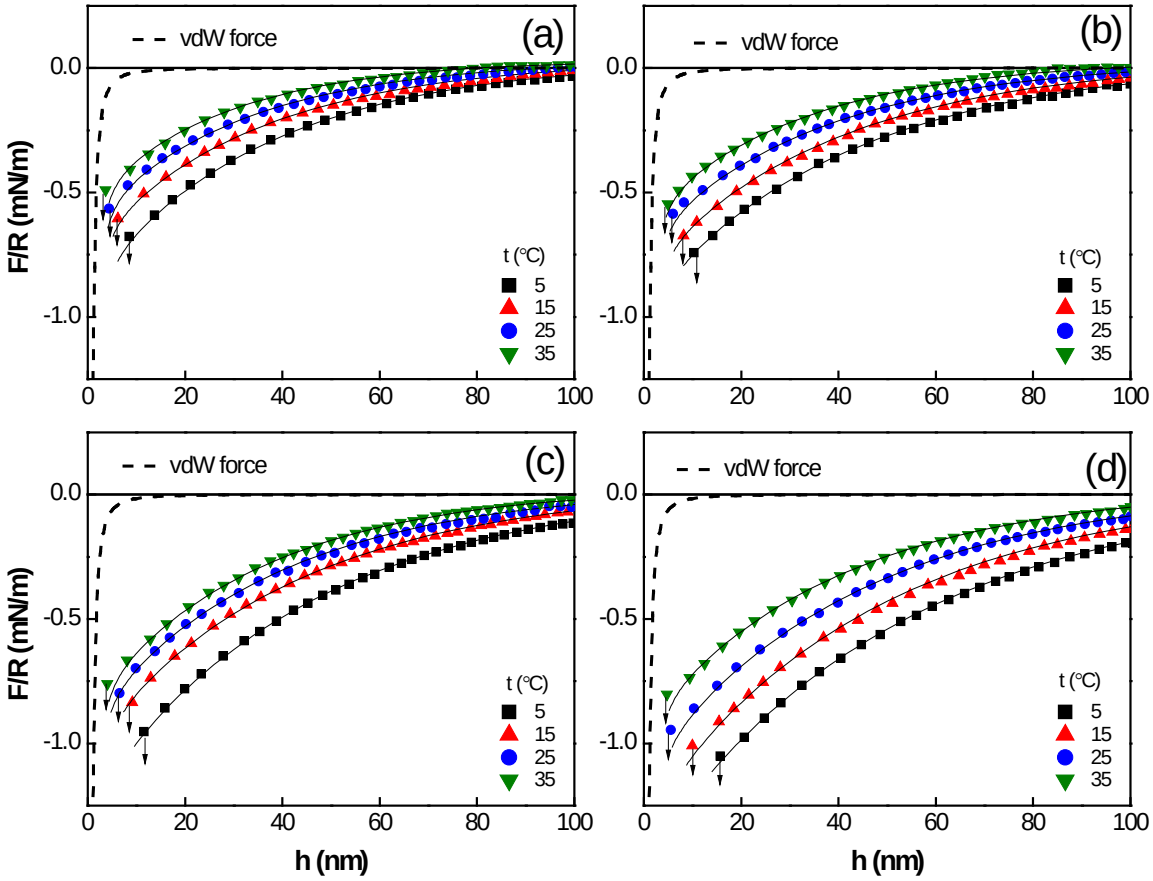

Figure 7.1 Surface forces (F) measured in ethanol at various temperatures normalized by the radius (R) of spheres *vs*. the separation distance (h) between the plate and sphere. The surfaces were treated in C_2SH (a), C_4SH (b), $C_{12}SH$ (c) and $C_{16}SH$ (d) solutions respectively. The dashed line represents the van der Waals force calculated with a Hamaker constant of 0.94×10^{-20} J. The experimental data plotted as symbol lines were fitted by extended DLVO theory (solid lines).

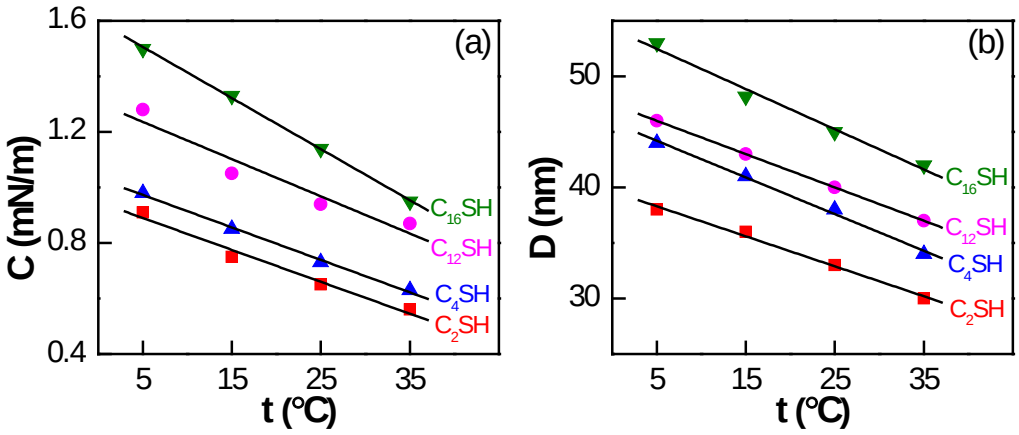

Figure 7.2 *C* (a) *vs*. t and *D* (b) *vs*. *t* plots as a function of the chain length of alkanethiols. The Fitting parameters *C* and *D* for the hydrophobic force represented by Eq. [7.12] were obtained by fitting the experimental data (Figure 7.1) with an extended DLVO theory.

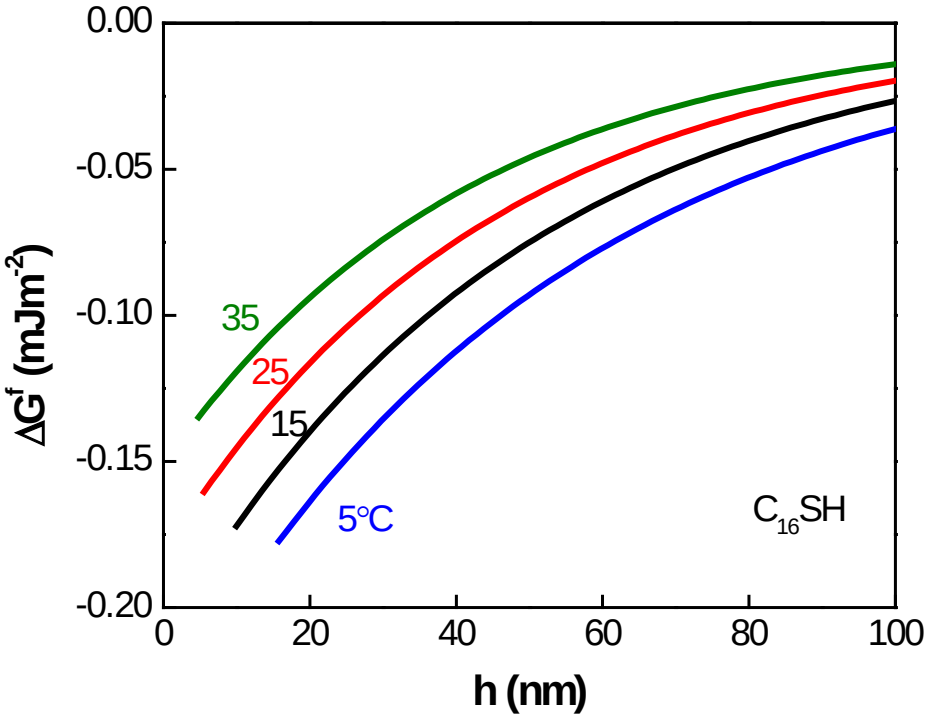

Figure 7.3 The change of Gibbs free energy of the thin ethanol film confined between two $C_{16}SH$-coated gold surfaces *vs*. the film thickness (*h*) at various temperatures.

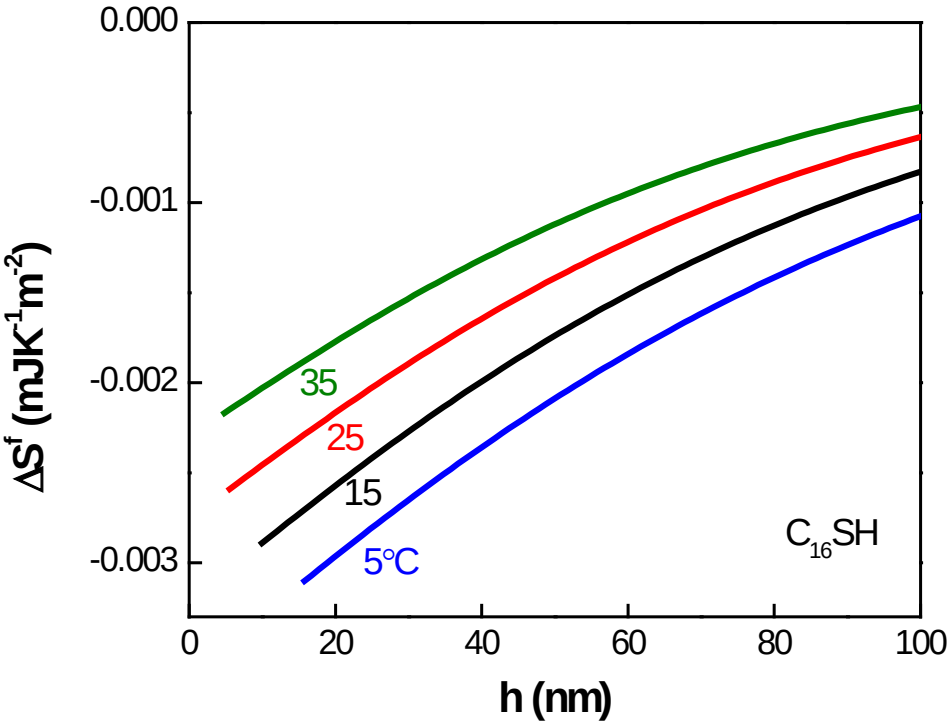

Figure 7.4 Change of excess film entropy (ΔS^f) in the thin films of ethanol confined by $C_{16}SH$-coated gold surfaces *vs*. film thickness (h) at different temperatures of the medium.

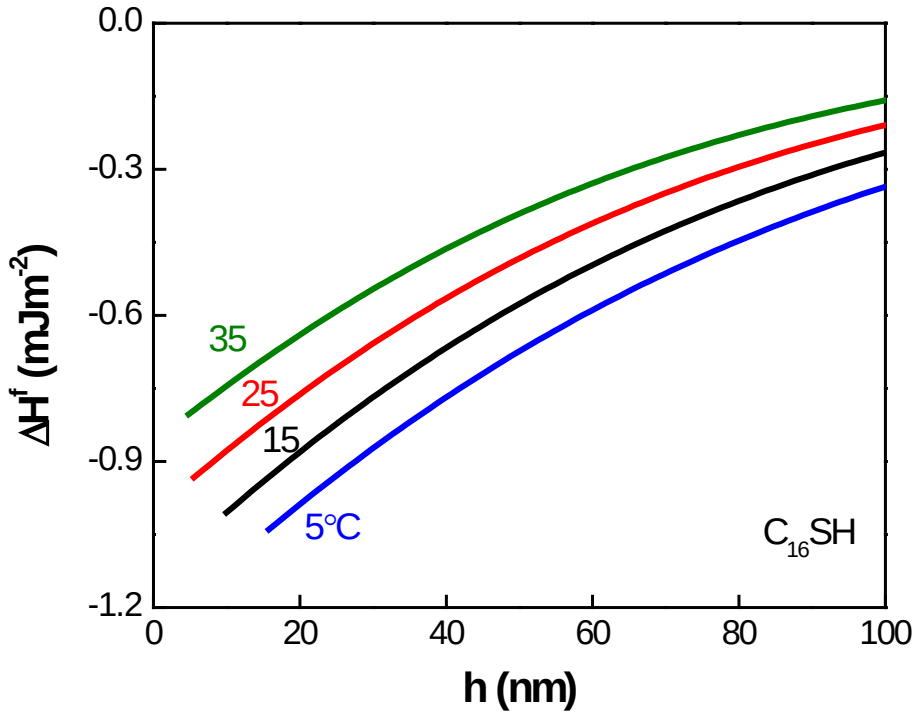

Figure 7.5 The change in the excess film enthalpy (ΔH^f) of the ethanol film confined between two $C_{16}SH$- coated gold surfaces *vs*. the film thickness (h) at various temperatures.

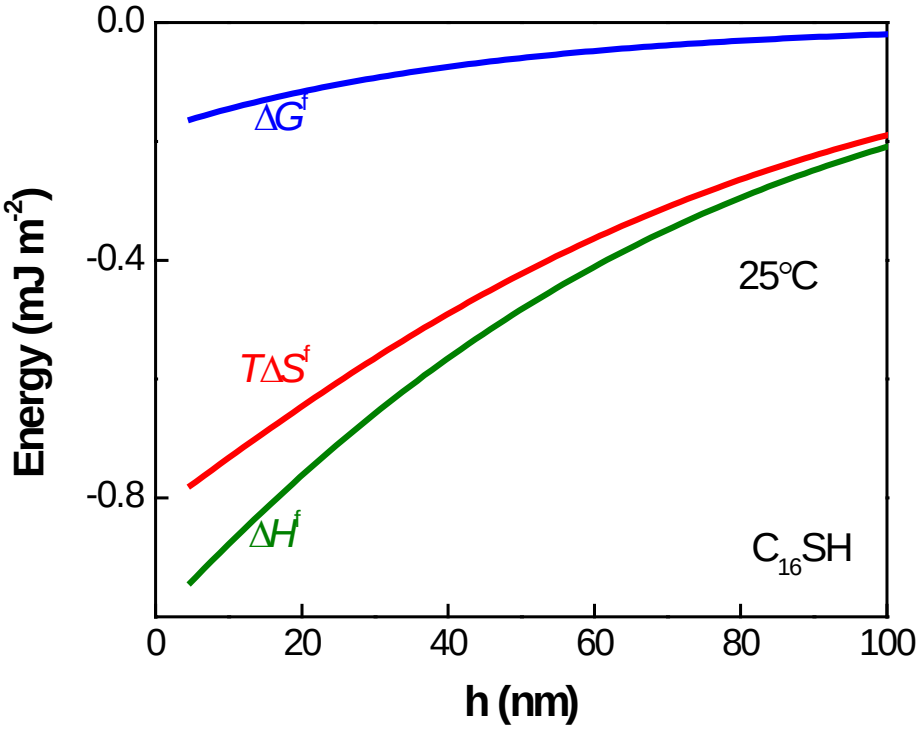

Figure 7.6 Changes in the excess thermodynamic properties at 25°C for the thin ethanol films between hydrophobic gold surfaces treated by $C_{16}SH$.

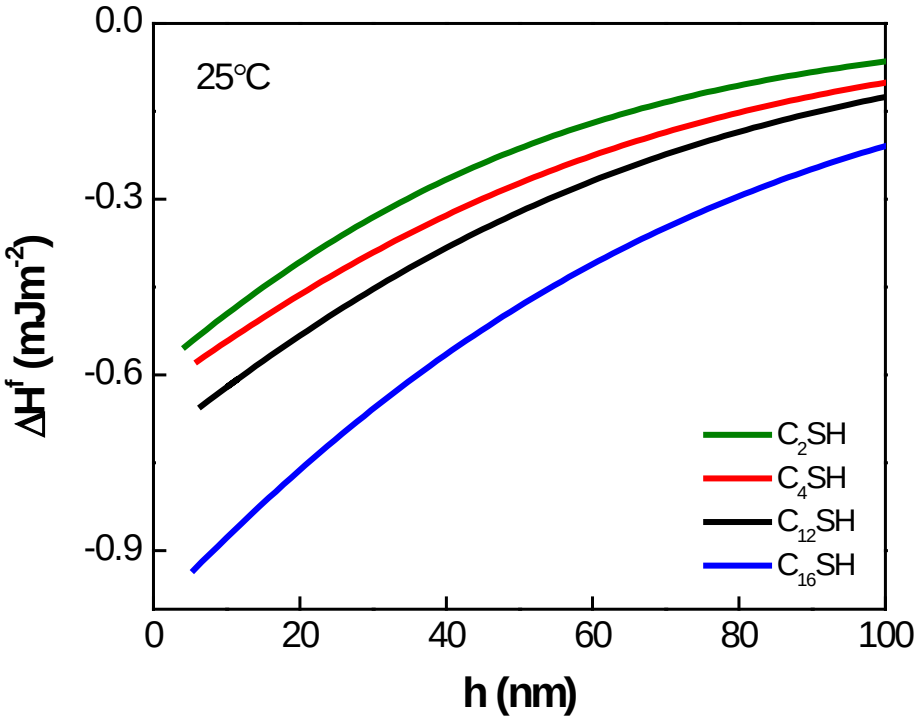

Figure 7.7 The change of excess film enthalpy (ΔH^f) at 25°C for the thin ethanol film confined between two hydrophobic gold surfaces modified by C_2SH, C_4SH, $C_{12}SH$ and $C_{16}SH$ respectively to have water contact angle (θ_w) of 82°, 92°, 102° and 107° as shown from top to bottom.

.

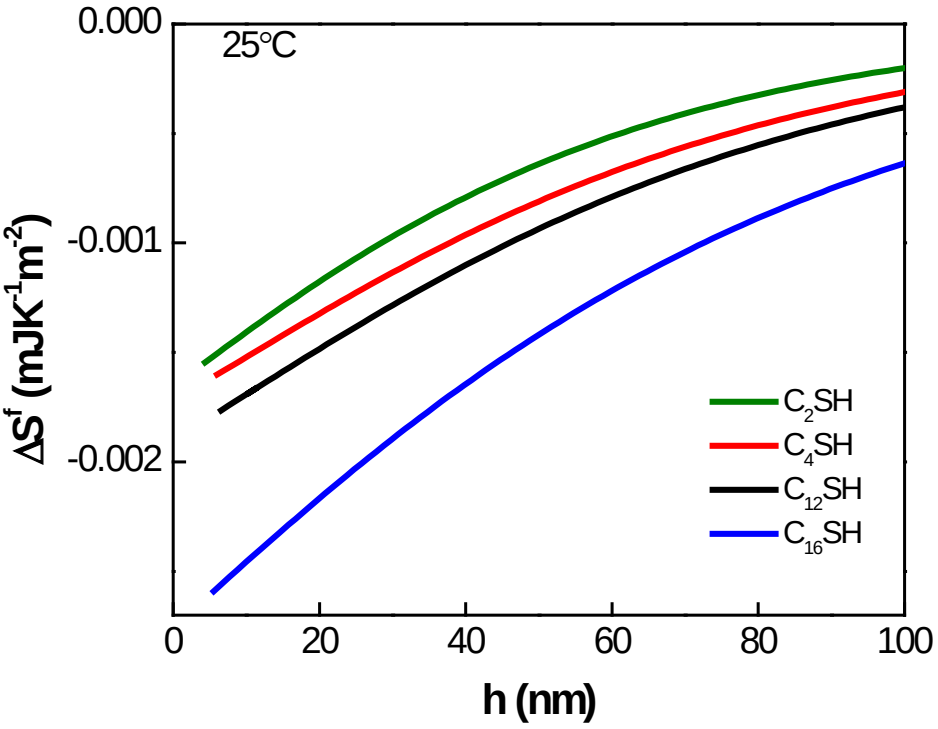

Figure 7.8 Changes in excess film entropy (ΔS^f) at 25°C in the thin ethanol film confined between different sets of hydrophobic gold surfaces. The surfaces were prepared by being immersed in C_2SH, C_4SH, $C_{12}SH$ and $C_{16}SH$ -in-ethanol solutions respectively to have water contact angle (θ_w) of 82°, 92°, 102° and 107° as shown from top to bottom.

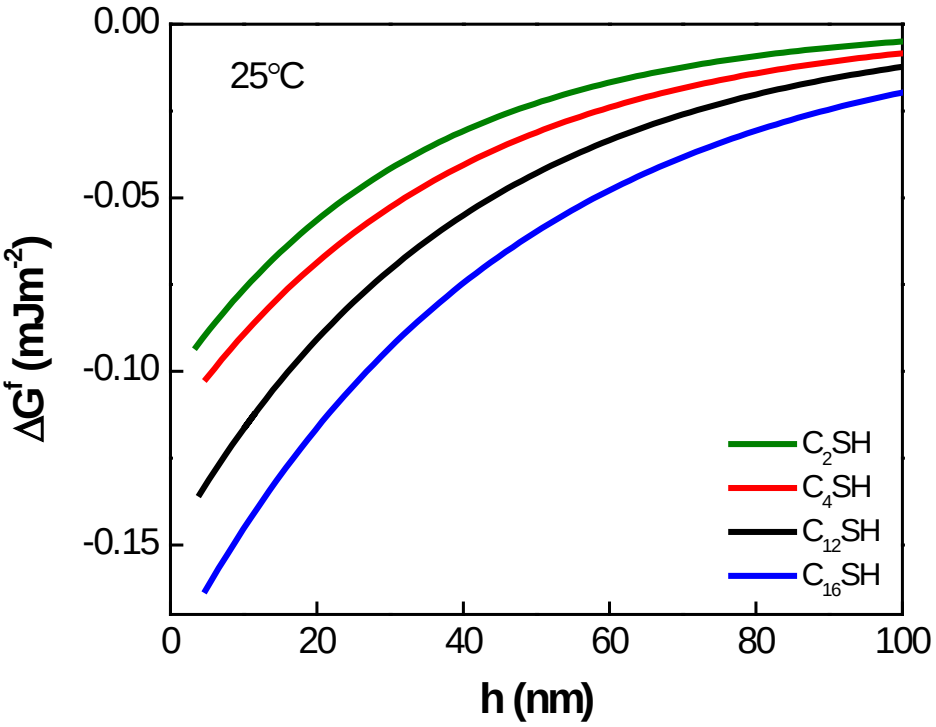

Figure 7.9 The change of Gibbs free energy (ΔG^f) at 25°C for the thin ethanol film confined between two hydrophobic gold surfaces modified by C_2SH, C_4SH, $C_{12}SH$ and $C_{16}SH$ respectively to have water contact angle (θ_w) of 82°, 92°, 102° and 107° as shown from top to bottom.

CHAPTER 8

Conclusions

1. Hydrophobic force *vs*. distance curves show no steps, indicating that bubbles and cavities are not responsible for the long-range forces observed in the present work.

2. The hydrophobic interaction at macroscopic scale entails decreases in both film entropy and enthalpy. Under this condition, the macroscopic interaction is driven by enthalpy change, i.e., $\left|\Delta H^{f}\right| > \left|T\Delta S^{f}\right|$, which is contrary to molecular-scale hydrophobic interactions. The enthalpy change is due to the formation of *H*-bonded structures, possibly partial clathrates or low-density liquid (LDL) species.

3. In the presence of dissolved gases, hydrophobic forces become stronger. Gas molecules may promote structuring *via* the van der Waals interaction between the guest and host molecules in the same manner as in gas hydrate formation. Hydrophobic force increases in different gases in the order of $CO_2 < He < N_2 < Ag$.

4. Hydrophobic force decreases in the presence of electrolytes: possibly due to breakage of *H*-bonded structures.

5. Strong attractive forces are present in the thin liquid films (TLFs) of pure ethanol confined between hydrophobic surfaces. The attractive forces increase with increasing the water contact angles of the confining surfaces. This finding suggests that the ethanol molecules in the vicinity of hydrophobic surfaces form *H*-bonded structures as a means to minimize free energy.

6. The hydrophobic forces observed in *H*-bonding liquids (*i.e*, water, ethanol, and methanol) are the consequences of forming structures amongst themselves as a means to minimize free energy. In this regard, the hydrophobic force may be regarded a thermodynamic force.